105p

SEL-63-110

THE DISTRIBUTION OF IONS AND ELECTRONS IN THE EARTH'S EXOSPHERE

N64-20008

CAT. 12 Code 1

NASA CR53689

by

J. J. Angerami and *J. O. Thomas

UNPUBLISHED PRELIMINARY DATA

December 1963

Technical Report No. 4

Prepared under
National Aeronautics and Space Administration
Grant NsG 30-60
and

Technical Report No. 3412-3

Prepared under
Air Force Office of Scientific Research
Grant AF-AFOSR-62-370

*Dr. J. O. Thomas is now at the National Aeronautics and Space Administration, Ames Research Center, Moffett Field, California.

Radioscience Laboratory
Stanford Electronics Laboratories
Stanford University Stanford, California

R0 #5

ABSTRACT

20008 A

The factors which govern the distribution of electrons and ions in the earth's exosphere are discussed. The theory takes into account the effect of the electric field which arises from charge separation, the centrifugal force arising from the rotation of the earth and the effect of the earth's gravitational field. It is assumed that the charged particles are constrained to move only along the direction of the earth's magnetic lines of force. The modifications that result in the electron and ion distributions when a temperature variation is assumed along a line of force are also considered.

The results predicted by the theory are compared with actual experimental observations of the exospheric plasma which have been obtained in recent years using whistlers and using topside ionograms made by the Alouette satellite.

Author

CONTENTS

TABLES

FIGURES

NOTE: Figures 1 - 7 are included in the text.
Figures 8 - 22 are presented at the back of the report.

NOTE: Figs. 8 - 22 are presented at the end of the report.

Fig. 8. Variation of the ion composition at 500 km with the temperature at that level (Bauer 1963).

Fig. 9a. Relative electron and ion densities as a function of the geopotential height, z, for an isothermal exosphere. The form of the distributions depends strongly on the assumed base level composition and the assumed temperature as may be seen by comparing the above with the subsequent figures.

Fig. 9b. Relative electron and ion densities as a function of the geopotential height, z, for an isothermal exosphere. Comparison with Fig. 9c indicates the effect on the distributions of changing the temperature only.

Fig. 9c. Relative electron and ion densities as a function of the geopotential height, z, for an isothermal exosphere. Comparison with Fig. 9b indicates the effect on the distributions of changing the temperature only. Comparison with Fig. 9d reveals the effect of changing the base composition only.

Fig. 9d. Relative electron and ion densities as a function of the geopotential height, z, for an isothermal exosphere. Comparison with Fig. 9c reveals the effect of changing the base composition only.

Fig. 9e. Relative electron and ion densities as a function of the geopotential height, z, for an isothermal exosphere with a relatively high temperature.

Fig. 10. Summary of the results of Figs. 9a - e for the relative electron density distributions in the exosphere over a wide range of conditions.

Fig. 11. The variation with temperature of the levels at which the ions indicated have equal abundances. The broken lines correspond to the cases when the composition at the base level depends on the temperature there (through equations (65)). The continuous lines correspond to the cases when the composition at the base level is independent of temperature (Composition 1). These results are in agreement with those presented earlier by Bauer (1962).

Fig. 12a. To illustrate, for an isothermal exosphere, the relative electron density distributions along a field line with feet (at 500 km above the earth) at geomagnetic latitude 45° (see Tables 1 and 2).

Fig. 12b. To illustrate, for an isothermal exosphere, the relative electron density distributions along a field line with feet (at 500 km above the earth) at geomagnetic latitude 55° (see Tables 1 and 2). The broken lines indicate the distributions which would have been obtained if the centrifugal force had been neglected.

Fig. 12c. To illustrate, for an isothermal exosphere, the relative electron density distributions along a field line with feet (at 500 km above the earth) at geomagnetic latitude 65° (see Tables 1 and 2). The broken lines indicate the distributions which would have been obtained if the centrifugal force had been neglected.

Fig. 13. Schematic diagram to illustrate the variation of temperature along a line of force. $T_1(s)$ is used for the temperature distributions in the northern (winter) hemisphere and $T_2(s)$ for the southern (summer) hemisphere.

Fig. 14a. To illustrate, for a non-isothermal exosphere (see Fig. 13), the relative electron density distribution along a field line with feet (at 500 km above the earth) at geomagnetic latitude 35° (see Tables 1 and 2).

Fig. 14b. To illustrate, for a non-isothermal exosphere (see Fig. 13), the relative electron density distribution along a field line with feet (at 500 km above the earth) at geomagnetic latitude 45° (see Tables 1 and 2).

Fig. 14c. To illustrate, for a non-isothermal exosphere (see Fig. 13), the relative electron density distribution along a field line with feet (at 500 km above the earth) at geomagnetic latitude 55° (see Tables 1 and 2). The broken lines indicate the distributions which would have been obtained if the centrifugal force had been neglected.

Fig. 14d. To illustrate, for a non-isothermal exosphere (see Fig. 13), the relative electron density distribution along a field line with feet (at 500 km above the earth) at geomagnetic latitude 65° (see Tables 1 and 2). The broken lines indicate the distributions which would have been obtained if the centrifugal force had been neglected.

Fig. 15a. The predicted ratio of the electron density in winter to that at the same location and altitude in summer for a number of different altitudes. Composition 1 (see Table 1) is used at 500 km, as was done previously. The assumed temperature distribution is illustrated in Fig. 13.

Fig. 15b. The predicted ratio of the electron density in winter to that at the same location and altitude in summer for a number of different altitudes. Compositions 1 and 2f (see Table 1) are used at 500 km, as was done previously. The assumed temperature distribution is illustrated in Fig. 13.

Fig. 16a. Equatorial N(h) profile. The electron density at 1000 km was assumed to be 10^4/cc (see Tables 1 and 2). The temperature distributions along a field line are given by equation (66) and are illustrated schematically in Fig. 13.

Fig. 16b. N(h) profile at geomagnetic latitude 30°. The electron density at 1000 km was assumed to be 10^4/cc (see Tables 1 and 2). The temperature distributions along a field line are given by equation (66) and are illustrated schematically in Fig. 13.

Fig. 16c. N(h) profile at geomagnetic latitude 60°. The electron density at 1000 km was assumed to be 10^4/cc (see Tables 1 and 2). The temperature distributions along a field line are given by equation (66) and are illustrated schematically in Fig. 13.

Fig. 17. The average quiet day electron density at 1000 km (based on the results of Thomas and Sader 1963). The continuous lines are observed values and the broken lines are extrapolations which are roughly consistent with equatorial Alouette data.

Fig. 20. Comparison of experimental and theoretical exospheric N(h) profiles in the equatorial plane. The curves a - g are those described in Fig. 19a. The diagonally shaded area defines approximately the region within which the experimental profiles of Fig. 19b are observed to lie. The vertical shading near 1000 km indicates the approximate region in which the Alouette observations for 1000 km lie.

Fig. 21. Comparison of theory and experiment. The theoretical curve was computed assuming a constant exospheric temperature of 1000°K and ionic Composition 1 (Table 1) at the base level. The electron density at 1000 km was taken to be that given by Alouette for summer night conditions (Fig. 17).

Fig. 22. Observed and predicted ratios of the electron density at 1000 km at conjugate points in the winter and summer hemispheres. The middle line giving the observed average quiet day ratios is based on summer and winter Alouette observations at Stanford. The ratio is approximately 0.5 over the latitude range considered. The theoretically predicted ratios are in reasonably good agreement.

NOMENCLATURE

NOTE: The suffixes e and i are used to denote electrons and ions respectively, and the suffix o is used to denote values measured at the base level usually taken to be 500 kilometers above the earth.

η	electron density at 500 km relative to O^+ density at that level
η_i	ion density at 500 km relative to O^+ density at that level
h	altitude
H_i	scale height of non-ionized ion, at 500 km
m_e	electron mass
m_i	ion mass
m_+	temperature-weighted ion mass average
n_e or N	electron density
n_{eo}	electron density at the base level
n_i	ion density; i = 1,2,3, for O^+, He^+ and H^+ respectively
n_{io}	ion density at the base level
R_{eo}	ratio of electron densities at 500 km above the earth at conjugate points in the two hemispheres
$s(\theta_o,\theta)$	the distance measured along a line of force from its foot (at 500 km) to the point (θ_o,θ) on the field line
$s'(\theta_o,\theta')$	the distance measured along a line of force from its foot (at 500 km) to the point (θ_o,θ'). It is used as an upper limit of integration
$s_M(\theta_o)$	the distance measured along a field line from the geomagnetic equatorial plane to a point on the base level at latitude θ_o

T	electron or ion temperatures when they are assumed the same in an isothermal exosphere
T_e	electron temperature
T_{eo}	electron temperature at 500 km
T_i	ion temperature
T_{io}	ion temperature at 500 km
T_o	electron or ion temperature at 500 km, when they are assumed equal
$T(s)$	electron or ion temperatures, when they are assumed equal
θ	geomagnetic latitude of a point on a field line
θ_o	geomagnetic latitude of a field line at 500 km above the earth's surface
θ'	geomagnetic latitude of a point on a field line, when this point is the upper limit of an integration
(θ_o,θ)	coordinates of a point on a magnetic field line in terms of the latitude, θ, of the point and the latitude θ_o, of the foot (at 500 km) of the particular field line concerned
$z(\theta_o,\theta')$	temperature modified geopotential height, corresponding to the point (θ_o,θ'). For an isothermal exosphere, z is sometimes referred to as the geopotential height

I. INTRODUCTION

A great deal of experimental data on the distribution of ions and electrons in the upper parts of the earth's ionosphere are becoming increasingly available as the new techniques required to investigate the physical properties of the exosphere at these heights are developed. An excellent brief report on activities in this field has been given by Bordeau (1963) and the main references to experimental work are quoted in that paper.

In this report, an account is given of theoretical considerations which govern the distribution of electrons and ions above 500 km in this region of space. These distributions are derived on the assumptions that the charged particles are constrained to move only along the direction of the earth's magnetic lines of force under the action of the earth's gravitational field and of the centrifugal force arising from the rotation of the earth. The effect of the electric field, E, which arises from the charge separation that occurs [Mange (1960)] resulting from the tendency of electrons to rise with respect to the heavier positive ions is also taken into account. The modifications that result in the electron and ion distributions when a temperature variation along a line of force is assumed, such that there are relatively large temperature differences between the northern and southern hemispheres in the vicinity of the peak of the F region, are also considered. Special attention is given to the distributions that result when computed along a line of force, and the resulting differences in vertical profiles observed at different latitudes are discussed. It is found useful and convenient to present the predicted ratios of electron density at a given level in the northern hemisphere to that obtained at the corresponding conjugate point in the southern hemisphere. The theory predicts that, under certain circumstances, this ratio, when plotted against geomagnetic latitude, exhibits two maxima, one in very

low latitudes and the other at high latitudes. The relative magnitudes and positions of these maxima depend to a certain extent on the precise assumptions that are made about the relative densities of the constituents at the base of the exosphere and on the assumed temperature distributions.

In Section III, the solution of the problem outlined in Section II is presented. In Section IV, the results of the theory to be expected on certain reasonable assumptions about the physical properties of the exosphere are given. Also in this section, the predictions of the theory are compared with the results of a number of other workers who have considered this problem from a theoretical point of view and the main differences are outlined. In particular, reference is made to the calculations of Johnson (1960), Bates and Patterson (1961), Hanson (1962), Bauer (1962, 1963), Rothwell (1962), Gliddon (1963), and Hanson and Patterson (1963). Also in Section IV, the results predicted by the theory presented in the report are compared with actual experimental observations which have been made in recent years. In particular, a comparison is made with the results presented by workers who have considered data obtained from the Alouette satellite (see, for example, King (1963), Thomas and Sader (1963) and references quoted therein). The main conclusions are described and summarized in the last section.

II. THE PROBLEM AND THE ASSUMPTIONS

The electrons and ions in the earth's exosphere are acted upon by a number of important forces. These include the gravitational attraction toward the earth, the centrifugal force due to the rotation of the earth about its geographic axis, and the force due to the electric field, E, resulting from the tendency of electrons to rise with respect to the heavier positive ions (Mange 1960). In this region of space, the particles are in diffusive equilibrium and obey Dalton's law of partial pressures so that each constituent has a partial pressure corresponding to that which it would have if it were the only constituent present. The distribution of

electrons and ions which would arise under the circumstances outlined immediately above will be modified if there is a gradient of temperature along a line of force. The resulting effects are discussed in detail below. The main assumptions are as follows:

1. The upper atmosphere, above 500 km, consists of neutral particles together with a neutral mixture of singly charged positive ions and electrons only, and these are in diffusive equilibrium. The positive ions are O^+, He^+ and H^+.
2. The partial pressure for each species is balanced by the earth's gravitational and centrifugal forces and the electric field arising from charge separation.
3. The charged particles are constrained to move only along the lines of force so that the distributions along different lines of force are quite independent of each other.
4. No electrons are produced by the action of the sun's ionizing radiations above 500 km.
5. The rate at which electrons recombine is so small in comparison with other effects that the loss of electrons from this cause can be neglected in the calculations.
6. The axis of rotation of the earth coincides with the magnetic dipole axis.
7. A difference of temperature can exist between the northern and southern hemispheres. The ratio T_S/T_N of the temperatures in the southern and northern hemispheres respectively is not greater than 1.5, consistent with satellite drag observations [King-Hele and Walker (1960)].
8. The relative densities of O^+, He^+ and H^+ are known at the reference level at 500 km.

The calculations described in the subsequent paragraphs are aimed at deriving the resulting electron distributions along a line of force.

III. THEORETICAL FORMULATION OF THE SOLUTION

A. FORCE ON UNIT MASS

The total force $\vec{g}$ acting on a unit mass at a point A, represented by the coordinates (r, θ), (θ_o, θ) or (θ_o, s) (Fig. 1), is given by

$$\vec{g}(r,\theta) = \vec{f}_g(r,\theta) + \vec{f}_c(r,\theta)$$
$$= -\vec{u}_r\, g_o \frac{r_o^2}{r^2} + \vec{u}_x\, \Omega^2 r \cos\theta \qquad (1)$$

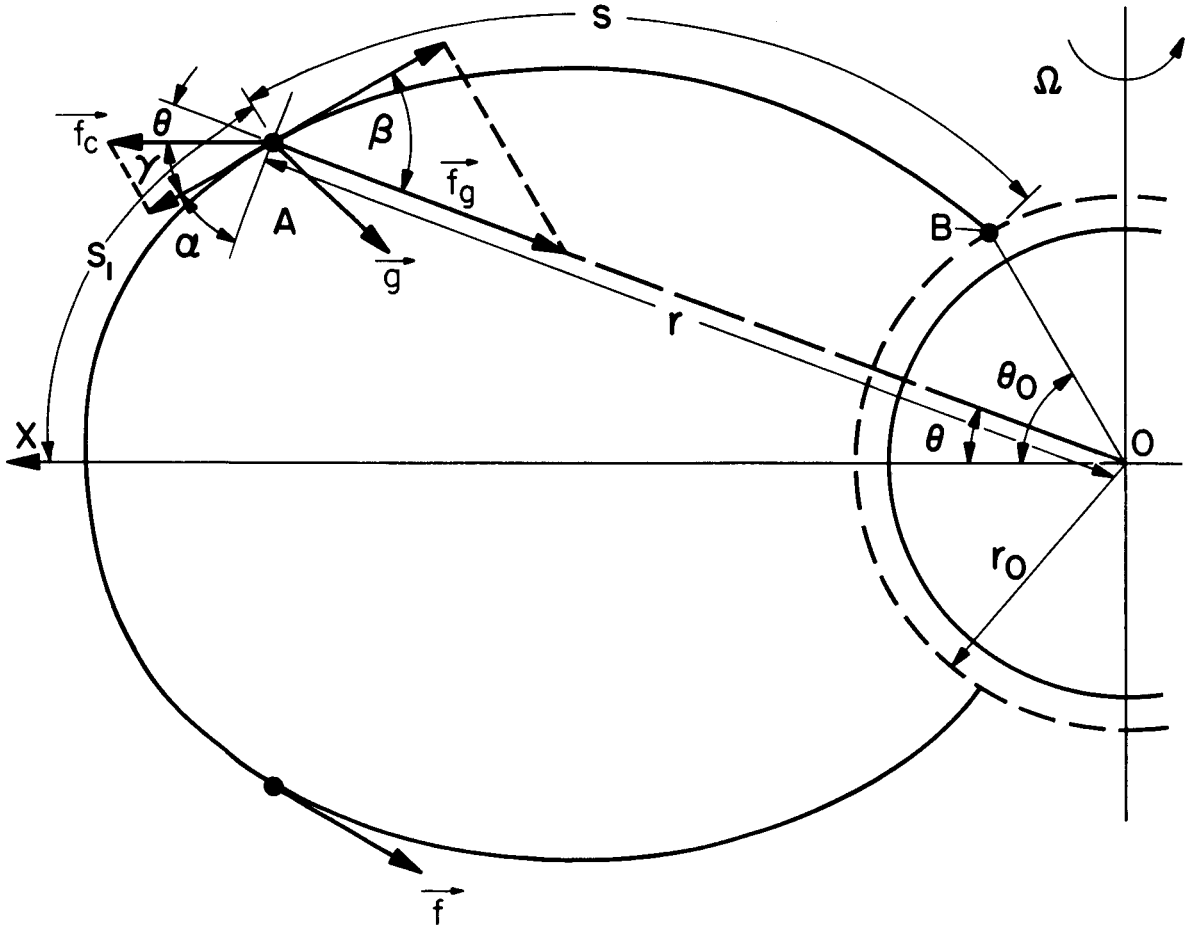

FIG. 1. GRAVITATIONAL AND CENTRIFUGAL FORCES ($\vec{f}_g$ and $\vec{f}_c$) ACTING ON UNIT MASS LOCATED AT THE POINT A DEFINED BY ONE OF THE COORDINATE PAIRS (r,θ), (θ_o,θ) OR (θ_o,s).

where $\vec{g}_o$ is the total force on a unit mass at the reference level r_o at the poles, Ω is the angular velocity of rotation of the earth about the geographic axis, $\vec{f}_g$ and $\vec{f}_c$ are the gravitational and centrifugal forces respectively, $\vec{u}_r$ and $\vec{u}_x$ are unit vectors in the directions of r and x, respectively, and the distance s is measured along a line of force (Fig. 1). It is clear that the force on the unit mass when it is over the poles acts toward the center of the earth, and that at some particular points which may be determined on each side of the earth in the equatorial plane, the forces $\vec{f}_g$ and $\vec{f}_c$ become equal and opposite. In fact, it is possible to define a curve where the magnitudes of the two forces (but not their directions, except on the equatorial plane) are equal.

Figure 2 shows the locus of points for which $\vec{f}_g$ and $\vec{f}_c$ are equal in magnitude (curves AB). The magnitudes of $\vec{f}_g$ and $\vec{f}_c$ and the resultant force $\vec{g}(r,\theta)$ on a unit mass are drawn to scale in Fig. 2 for different positions along a line of force through 70 degrees geomagnetic latitude. If it is assumed that charged particles can move only along the lines of force of the earth's magnetic field, then it becomes important to consider the way in which the resultant force $\vec{f}(r,\theta)$ obtained by considering only the resolved component of $\vec{g}(r,\theta)$ along the direction of the earth's lines of force varies in space (Fig. 2). The loci of points at which $\vec{f}(r,\theta)$ is zero are shown as the broken curves (CD) in Fig. 2. Referring to Fig. 1 and Eq. (1), it is clear that the algebraic value of this force f (written without the arrow) is given by

$$f(r,\theta) = g_o \frac{r_o^2}{r^2} \cos\beta - \Omega^2 r \cos\theta \cos\gamma \qquad (2)$$

From Fig. 1, it is seen that

$$\cos\beta = \sin\alpha = \frac{\tan\alpha}{\sqrt{1+\tan^2\alpha}} = \frac{2\tan\theta}{\sqrt{1+4\tan^2\theta}} = \frac{2}{\cos\theta}\,\frac{\sin\theta}{\sqrt{1+4\tan^2\theta}} \qquad (3a)$$

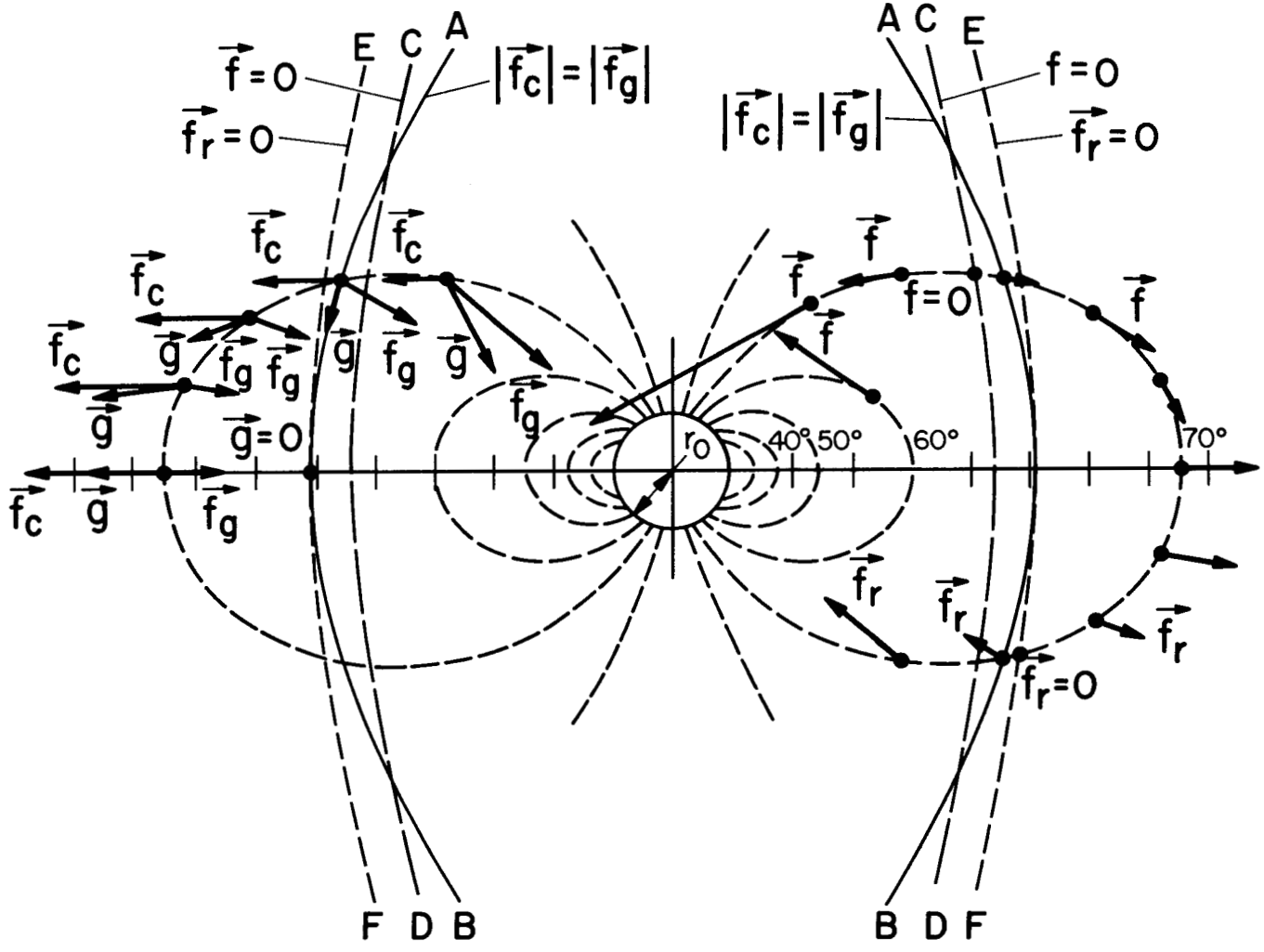

FIG. 2. THE RELATIVE MAGNITUDES OF THE GRAVITATIONAL AND CENTRIFUGAL FORCES AT DIFFERENT POINTS ALONG A LINE OF FORCE.

$$\cos\gamma = \sin(\alpha+\theta) = \sin\theta\cos\alpha + \sin\alpha\cos\theta$$

$$= \cos\alpha(\sin\theta + \tan\alpha\cos\theta)$$

$$= \frac{\sin\theta+\tan\alpha\cos\theta}{\sqrt{1+\tan^2\alpha}} = \frac{\sin\theta+2\tan\theta\cos\theta}{\sqrt{1+4\tan^2\theta}} = \frac{3\sin\theta}{\sqrt{1+4\tan^2\theta}} \qquad (3b)$$

where α is the magnetic dip at (r,θ), given by

$$\tan\alpha = 2\tan\theta$$

Substituting the above values in (2), changing the variables (r,θ) to (θ_o,θ) where θ_o is the geomagnetic latitude at the reference level r_o, and using (A1) of Appendix A:

$$f(\theta_o,\theta) = \frac{\sin\theta}{\sqrt{1+4\tan^2\theta}}\left(2g_o\cos^4\theta_o\,\frac{1}{\cos^5\theta} - \frac{3\Omega^2 r_o}{\cos^2\theta_o}\cos^3\theta\right) \qquad (4)$$

Equation (4) gives the resultant force resolved along the direction of the earth's magnetic field line, arising from the combined action of the earth's centrifugal and gravitational forces. It is clearly a function of the geomagnetic latitude θ_o at which the line of force under consideration crosses the reference level, and of the distance from the earth's surface to the point under consideration as represented by the coordinate θ, Fig. 1. As will be seen later, the precise way in which this force varies from point to point in space is extremely important for the physics of the exosphere.

B. DERIVATION OF EQUILIBRIUM DISTRIBUTIONS

There is strong evidence both on theoretical grounds [Nicolet (1961)] and on experimental grounds [e.g. Hanson (1962)] for supposing that the main ionized constituents of the upper atmosphere above the peak of the F2 layer are electrons, together with oxygen, helium and hydrogen ions in the

atomic state. In the analysis described below, it is assumed that these are the only ionized constituents and that no negative ions are present, so that the atmosphere consists of neutral particles and a neutral mixture of O^+, He^+, and H^+, and electrons in diffusive equilibrium. The ions will be referred to by subscripts i and electrons by subscripts e. It is assumed that the lines of force act as barriers across which charged particles cannot flow. It is instructive to consider the variation of partial pressure along a tube of force. We can then write

$$\left.\begin{aligned} dp_e &= -m_e n_e f\, ds - n_e eE ds \\ dp_i &= -m_i n_i f\, ds + n_i eE ds \end{aligned}\right\} \qquad (5)$$

where the field E (Fig. 3) arises from the small separation between charges due to the fact that electrons are lighter than the positive ions and, therefore, tend to move upwards [Mange (1960)].

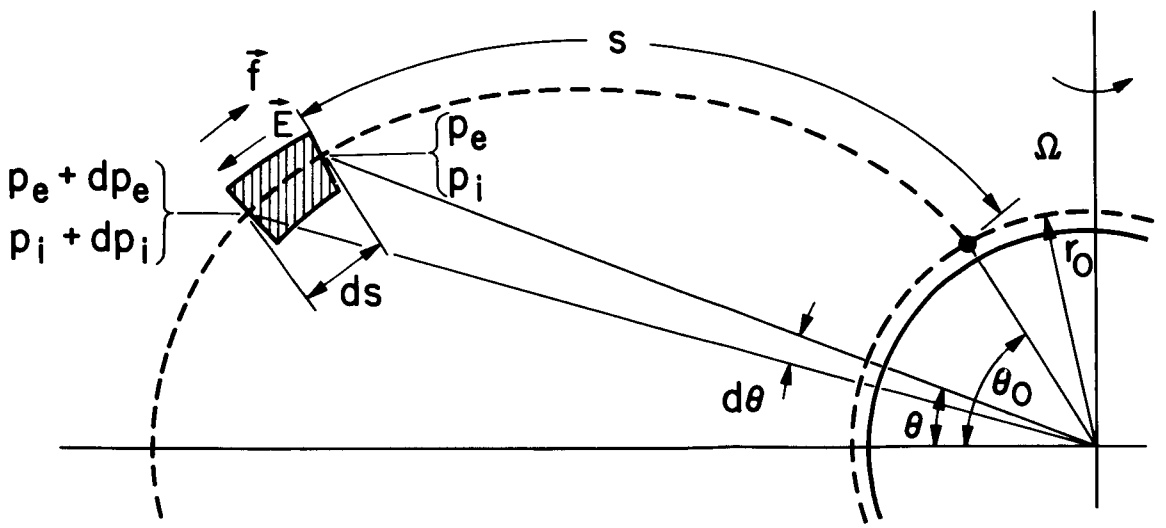

FIG. 3. TO ILLUSTRATE AN ELEMENT OF VOLUME TAKEN ALONG A LINE OF FORCE. The partial pressures of the ions and electrons, p_i and p_e, and the electric field E (Mange 1960) are also shown.

In these equations, m_e and m_i are the mass of the electron and of the ith ion, n_e and n_i are the electron and ith ion densities, e is the electronic charge, and p_e and p_i represent the partial pressures of the electrons and the ith ions, respectively. It is assumed (Fig. 3) that the pressure changes over a small volume contained within the tube of force by an amount dp over the distance ds measured along the line of force. The direction of the electric field E is as shown in Fig. 3. It should be noted that the gradient of partial pressure changes direction according to whether the point under consideration is inside or outside the lines marked CD in Fig. 2. From Dalton's law for the partial pressures of the constituents of a gas in diffusive equilibrium, we know that each constituent, in this case each ion species, and the electrons, has a partial pressure corresponding to that which it would have if it were the only constituent present. We may then write

$$\left.\begin{aligned} p_e &= n_e k T_e \\ p_i &= n_i k T_i \end{aligned}\right\} \qquad (6)$$

T_e and T_i refer to the electron and ion temperatures respectively, and in the subsequent theory it is assumed that these can be different. Since the atmosphere at every point is taken to be electrically neutral, we may write

$$n_e = \sum_i n_i \qquad (7)$$

which leads to

$$\frac{p_e}{T_e} = \sum_i \frac{p_i}{T_i} \qquad (8)$$

so that

$$\frac{dp_e}{T_e} = \sum_i \frac{dp_i}{T_i} \qquad (9)$$

From Eqs. (5) and (9) the electric field can be calculated:

$$-\frac{m_e n_e}{T_e} f ds - eE \frac{n_e}{T_e} ds = \sum_i -\frac{m_i n_i}{T_i} f ds + eE \sum_i \frac{n_i}{T_i} ds$$

$$eE = \frac{\sum_i \frac{m_i n_i}{T_i} - \frac{m_e n_e}{T_e}}{\frac{n_e}{T_e} + \sum_i \frac{n_i}{T_i}} \cdot f$$

$$eE = \frac{\sum_i \frac{T_e}{T_i} m_i n_i - m_e n_e}{n_e + \sum_i \frac{T_e}{T_i} n_i} \cdot f$$

Since $m_i \geq 1850\, m_e$ and $T_e/T_i \geq 1$ the last expression can be simplified to give

$$eE = \frac{\sum_i \frac{T_e}{T_i} n_i m_i}{n_e + \sum_i \frac{T_e}{T_i} n_i} \cdot f = \frac{m_+}{2} f \qquad (10)$$

where m_+ is the "temperature-weighted ion mass average"

$$m_+ = 2 \frac{\sum_i \frac{T_e}{T_i} n_i m_i}{n_e + \sum_i \frac{T_e}{T_i} n_i} \qquad (11)$$

Using (10) in (5):

$$\left.\begin{aligned} dp_e &= -n_e\left(m_e + \frac{m_+}{2}\right) f\, ds \\ dp_i &= -n_i\left(m_i - \frac{m_+}{2}\right) f\, ds \end{aligned}\right\} \qquad (12)$$

From (11), if $T_e/T_i \geq 1$ then

$$2 \frac{\sum_i n_i m_i}{\sum_i n_i} \geq m_+ \geq \frac{\sum_i n_i m_i}{\sum_i n_i}$$

and thus we may write (12) as

$$\left.\begin{aligned} dp_e &= - n_e \frac{m_+}{2} f \, ds \\ dp_i &= - n_i (m_i - \frac{m_+}{2}) f \, ds \end{aligned}\right\} \qquad (13)$$

From Eq. (6) we may then write

$$\left.\begin{aligned} dp_e &= kd(n_e T_e) \\ dp_i &= kd(n_i T_i) \end{aligned}\right\} \qquad (14)$$

and

$$\left.\begin{aligned} \frac{d(n_e T_e)}{n_e T_e} &= - \frac{m_+}{2kT_e} fds \\ \frac{d(n_i T_i)}{n_i T_i} &= - \frac{(m_i - \frac{m_+}{2})}{kT_i} fds \end{aligned}\right\} \qquad (15)$$

Equations (15) have a number of important consequences, which are discussed below. It should be noted that if a constant temperature is assumed along a line of force for both the electrons and ions, Equations (15) show that:

1. Since m_+ is always greater than zero, the electron density decreases with s and thus also with height.

2. If $m_i > m_+/2$, the ion density n_i decreases with s and thus with height. This condition is always satisfied by the heaviest constituent and also by a light constituent if it, or a still lighter one is strongly predominant (see Fig. 4, page 21).

3. If $m_i < m_+/2$, the ion density n_i increases with s and thus with height. This happens with a light constituent in the presence of a predominant heavier one.

4. If $m_i = m_+/2$, the ion density of constituent i (cannot be the heaviest) passes through a maximum.

These equations are basic and contain the essential information about the distribution of both electron and the ion densities with height. In order to solve them to obtain this distribution, however, it is necessary to make a number of changes of variable to simplify the mathematics. For convenience, distances along a line of force will be measured from a reference level at a distance r_o (Fig. 1) from the center of the earth. All quantities measured at this level will be indicated by the subscript zero. Integrating Eqs. (15) between the limits $s = 0$ and $s = s'$, the electron and ion densities at the distance s' from the reference level along the line of force are given by

$$\left.\begin{aligned} \frac{n_e(s')\,T_e(s')}{n_{eo}T_{eo}} &= \exp\left[-\int_o^{s'} \frac{m_+}{2kT_e}\,f\,ds\right] \\ \frac{n_i(s')\,T_i(s')}{n_{io}T_{io}} &= \exp\left[-\int_o^{s'} \frac{(m_i - \frac{m_+}{2})}{kT_i}\,f\,ds\right] \end{aligned}\right\} \qquad (16)$$

in which the ion and electron temperatures must be given as functions of s.

In the above integrals it is convenient to separate the effects of T and f, as follows:

$$\left.\begin{aligned} \int_o^{s'} \frac{m_+}{2kT_e}\,f\,ds &= \int_o^{s'} \frac{m_+ g_o}{2kT_{eo}} \left\{\frac{f}{g_o}\,\frac{T_{eo}}{T_e}\right\} ds \\ &= \frac{g_o}{2kT_{eo}} \int_o^{z_e} m_+ dz_e \end{aligned}\right\} \qquad (17)$$

$$\int_o^{s'} \frac{(m_i - \frac{m_+}{2})}{kT_i} f ds = \int_o^{s'} \frac{(m_i - \frac{m_+}{2}) g_o}{kT_{io}} \left\{ \frac{f}{g_o} \frac{T_{io}}{T_i} \right\} ds$$

$$= \frac{g_o}{kT_{io}} \int_o^{z_i} (m_i - \frac{m_+}{2}) dz_i \qquad (17) \text{ (Cont'd)}$$

In these equations, z_e and z_i are the "temperature-modified geopotential heights" for electrons and each ion species respectively and are defined by

$$dz_e = \frac{f}{g_o} \frac{T_{eo}}{T_e} ds$$

$$dz_i = \frac{f}{g_o} \frac{T_{io}}{T_i} ds \qquad (18)$$

from which we get, setting $z_e = z_i = 0$ at the reference level $s = 0$,

$$z_e = \int_{s=0}^{s=s'} \frac{f}{g_o} \frac{T_{eo}}{T_e(s)} ds$$

$$z_i = \int_{s=0}^{s=s'} \frac{f}{g_o} \frac{T_{io}}{T_i(s)} ds \qquad (19)$$

Thus, if $T_{eo}/T_e(s)$ is to be different from $T_{io}/T_i(s)$, then, at a point s', the quantities z_e and z_i have different values.

Equations (16) can now be written in terms of the temperature-modified geopotential heights z_e and z_i as:

$$n_e(s') = n_{eo} \frac{T_{eo}}{T_e(s')} \exp\left[- \frac{g_o}{2kT_{eo}} \int_o^{z_e} m_+ dz_e \right] \qquad (20)$$

$$\left.\begin{aligned} n_i(s') &= n_{io}\,\frac{T_{io}}{T_i(s')}\,\exp\left[-\frac{g_o}{kT_{io}}\int_o^{z_i}(m_i-\frac{m_+}{2})dz_i\right] \\ &= n_{io}\,\frac{T_{io}}{T_i(s')}\,\exp\left[-\frac{z_i}{H_i}\right]\cdot\exp\left[\frac{g_o}{2kT_{io}}\int_o^{z_i} m_+ dz_i\right] \end{aligned}\right\} \quad (20)\ (\text{Cont'd})$$

where

$$H_i = \frac{kT_{io}}{m_i g_o} \qquad (20a)$$

is the scale height of the non-ionized atomic species i, at the reference level.

In Eq. (20), $n_e(s')$ and $n_i(s')$ are given in terms of integrals in m_+ [given by Eq. (11), and still unknown] with respect to z_e and z_i. To eliminate m_+ a relationship must be established between z_e and z_i. Equations (19) show that this can be accomplished either by knowing T_{eo}/T_e and T_{io}/T_i as functions of s or by assuming

$$\frac{T_{eo}}{T_e(s)} = \frac{T_{io}}{T_i(s)} = t(s) \qquad (21)$$

This means that the electrons and all the ions have the same temperature variation with s, the distance along a line of force. If Eq. (21) applies, then we may write (19) as

$$z_e = z_i = z = \int_{s=o}^{s=s'} \frac{f(s)}{g_o}\,t(s)\,ds \qquad (22)$$

Thus, the electron and ion densities can be written in terms of the same z as:

$$\left.\begin{aligned} n_e(s') &= n_{eo}t(s')\,\exp\left[-\frac{g_o}{2kT_{eo}}\int_o^{z} m_+ dz\right] \end{aligned}\right\} \quad (23)$$

$$n_i(s') = n_{io}t(s') \exp\left[-\frac{z}{H_i}\right] \exp\left[\frac{g_o}{2kT_{io}} \int_o^z m_+ dz\right] \Bigg\} \quad (23)$$

Because of charge neutrality,

$$n_e(s') = \sum_i n_i = \sum_i \left\{ n_{io}t(s') \exp\left[-\frac{z}{H_i}\right] \exp\left[\frac{g_o}{2kT_{io}} \int_o^z m_+ dz\right] \right\} \quad (24)$$

The last exponential can be calculated from the first of Eqs. (23):

$$\exp\left[\frac{g_o}{2kT_{io}} \int_o^z m_+ dz\right] = \exp\left[\frac{T_{eo}}{T_{io}} \frac{g_o}{2kT_{eo}} \int_o^z m_+ dz\right]$$

$$= \left\{ \exp\left[\frac{g_o}{2kT_{eo}} \int_o^z m_+ dz\right] \right\}^{C_i} = \left\{ \frac{n_{eo}}{n_e(s')}\, t(s') \right\}^{C_i} \quad (25)$$

where

$$C_i = \frac{T_{eo}}{T_{io}} \quad (26)$$

Equation (24) becomes:

$$n_e(s') = \sum_i \left\{ n_{io}t(s') \exp\left(-\frac{z}{H_i}\right) \left[\frac{n_{eo}}{n_e(s')}\, t(s')\right]^{C_i} \right\}$$

or:

$$\frac{n_e(s')}{n_{eo}} = \frac{1}{n_{eo}} \sum_i \left\{ n_{io}t(s')^{1+C_i} \exp\left(-\frac{z}{H_i}\right) \left(\frac{n_{eo}}{n_e(s')}\right)^{C_i} \right\} \quad (27)$$

Normalizing the ion densities at the reference level to the value for the heaviest ion (O^+), we write

$$\eta = \frac{n_{eo}}{n_{1o}} = \sum_i \eta_i = \eta_1 + \eta_2 + \eta_3$$

where

$$\eta_1 = 1$$

$$\eta_2 = n_{2o}/n_{1o} \tag{28}$$

$$\eta_3 = n_{3o}/n_{1o}$$

so that η is the electron density divided by the oxygen ion density at the reference level.

Equation (27) becomes

$$\frac{n_e(s')}{n_{eo}} = \frac{1}{\eta} \sum_i \left\{ \eta_i t(s')^{1+C_i} \exp(-\frac{z}{H_i}) \left(\frac{n_{eo}}{n_e(s')}\right)^{C_i} \right\} \tag{29}$$

In this equation, the three first factors in the summation are known, and the equation must be solved for $(n_e(s')/n_{eo})$.

Suppose now that the ratios of ion temperature to electron temperature at the reference level are the same for all ions, that is:

$$C_i = \frac{T_{eo}}{T_{io}} = C \qquad i = 1, 2, 3 \tag{30}$$

Then Eq. (29) becomes

$$\left(\frac{n_e(s')}{n_{eo}}\right)^{1+C} = t(s')^{1+C} \frac{1}{\eta} \sum_i \left\{ \eta_i \exp(-\frac{z}{H_i}) \right\}$$

from which we get, finally, the electron density

$$\frac{n_e(s')}{n_{eo}} = \frac{T_{eo}}{T_e(s')} \left[\frac{1}{\eta} \sum_i \left\{ \eta_i \exp(-\frac{z}{H_i}) \right\} \right]^{\frac{1}{1+C}} \tag{31}$$

From the second of Eqs. (23) and (25) we get the ion densities:

$$\frac{n_i(s')}{n_{io}} = \left(\frac{T_{eo}}{T_e(s')}\right)^{C+1} \exp\left(-\frac{z}{H_i}\right) \left\{\frac{n_{eo}}{n_e(s')}\right\}^{C} \tag{32}$$

The ion density may also be referred to the electron density at the reference level by Eqs. (28) so that

$$\frac{n_i(s')}{n_{eo}} = \frac{\eta_i}{\eta} \left(\frac{T_{eo}}{T_e(s')}\right)^{C+1} \exp\left(-\frac{z}{H_i}\right) \left[\frac{n_{eo}}{n_e(s')}\right]^{C} \tag{33}$$

Or, using Eq. (31),

$$\frac{n_i(s')}{n_{eo}} = \frac{\eta_i}{\eta} \frac{T_{eo}}{T_e(s')} \exp\left(-\frac{z}{H_i}\right) \left[\frac{\eta}{\sum_i \eta_i \exp\left(-\frac{z}{H_i}\right)}\right]^{\frac{C}{1+C}} \tag{34}$$

The distribution of electrons and ions in the exosphere are given by the Eqs. (31) and (33) in terms of the variable z , the temperature-modified geopotential height defined by Eq. (22). These equations provide us with the information we require to give the distribution of electrons and ions along a line of force, and hence, vertical profiles. It is shown in Section V that these general solutions reduce to the equations given by Bauer (1962) for the particular cases he considers. The derived distribution Eqs. (31), (33), and (34) are discussed in detail below.

C. FORM OF SOLUTION FOR EQUILIBRIUM ION AND ELECTRON DENSITIES

For the case in which the ion and electron temperatures are equal at the reference level [and hence, elsewhere, by Eq. (21)], we have C=1 and Eq. (31) becomes

$$\frac{n_e(s')}{n_{eo}} = \frac{T_{eo}}{T_e(s')} \left[\frac{1}{\eta} \sum_i \left\{ \eta_i \exp\left(-\frac{z}{H_i}\right) \right\}\right]^{\frac{1}{2}} \tag{35}$$

If the electron temperature is, say, twice the ion temperature, C=2 and

$$\frac{n_e(s')}{n_{eo}} = \frac{T_{eo}}{T_e(s')} \left[\frac{1}{\eta}\Sigma_i \left\{\eta_i \exp - \frac{z}{H_i}\right\}\right]^{\frac{1}{3}}$$

It is clear that if such a difference between ion and electron temperatures occurs, then the electron densities may be changed by a factor of 10 at very high altitudes.

If the temperature along a line of force is constant so that $T_{eo}/T_e(s')=1$, then

$$\frac{n_e(s')}{n_{eo}} = \left[\frac{1}{\eta}\Sigma_i \left\{\eta_i \exp(- \frac{z}{H_i})\right\}\right]^{\frac{1}{2}} \qquad (36)$$

From Eq. (34) we have the ratio of densities of two ions:

$$\frac{n_i}{n_j} = \frac{\eta_i}{\eta_j} \exp\left(\frac{z}{H_j} - \frac{z}{H_i}\right)$$

$$= \frac{\eta_i}{\eta_j} \exp\left(z \frac{H_i - H_j}{H_i H_j}\right) \qquad (37)$$

The ion densities will be equal at a value of $z = z_{ij}$ defined by

$$z_{ij} = \frac{H_i H_j}{H_i - H_j} \ln \frac{\eta_j}{\eta_i} \qquad (38)$$

Since the subscripts 1, 2, and 3 refer, respectively, to O^+, He^+, and H^+, the scale heights are

$$\left.\begin{aligned} H_2 &= 4\, H_1 \\ H_3 &= 16\, H_1 \end{aligned}\right\} \qquad (39)$$

Hence, the values of z at which $n_1=n_2$, $n_1=n_3$, and $n_2=n_3$ are, respectively, from equations (38):

$$\left.\begin{aligned} z_{12}(O^+ \rightarrow He^+) &= -\frac{4}{3} H_1 \ln\eta_2, > 0 \text{ if } \eta_2 < 1 \\ z_{13}(O^+ \rightarrow H^+) &= -\frac{16}{15} H_1 \ln\eta_3, > 0 \text{ if } \eta_3 < 1 \\ z_{23}(He^+ \rightarrow H^+) &= -\frac{16}{3} H_1 \ln\frac{\eta_3}{\eta_2}, > 0 \text{ if } \eta_3 < \eta_2 \end{aligned}\right\} \quad (40)$$

Thus, two ions will have the same density at some height above the reference level if, at the reference level, the heavier one is more abundant. Also, from Eq. (37), at z larger than z_{ij}, the ion i will have higher density than the ion j if it is lighter. Due to this fact, the z_{ij}, defined by Eqs. (40) are called transition values of z, and these are indicated in the same equations.

It is interesting to consider the conditions for which the transition $He^+ \rightarrow H^+$ happens above the transition $O^+ \rightarrow He^+$. From Eqs. (40) this condition is

$$\eta_2 > \eta_3^{0.8} \quad (41)$$

The distribution of electron density as a function of z (31) may thus be written [using (39)]

$$\frac{n_e(s')}{n_{eo}} = \frac{T_{eo}}{T_e(s')} \left[\frac{\exp(-x) + \eta_2 \exp(-x/4) + \eta_3 \exp(-x/16)}{\eta}\right]^{\frac{1}{1+C}} \quad (42)$$

where

$$x = \frac{z}{H_1} \quad (43)$$

1. If the reference level is low enough so that the O^+ is strongly predominant there, then

$$\left.\begin{aligned} \eta_2 &<< 1 \\ \eta_3 &<< 1 \end{aligned}\right\} \qquad (44)$$

For low values of x the exponentials in (42) are close to unity, and we have

$$\frac{n_e(s')}{n_{eo}} \simeq \frac{T_{eo}}{T_e(s')} \exp\left(-\frac{x}{1+C}\right) \qquad (45)$$

Thus, apart from the factor $T_{eo}/T_e(s')$, the electron density varies exponentially in z, with scale height $(1+C)H_1$.

2. For large values of x the two first exponentials in (43) become much smaller than the third, so that they can be disregarded and

$$\frac{n_e(s')}{n_{eo}} \simeq \frac{T_{eo}}{T_e(s')}\left(\frac{\eta_3}{\eta}\right)^{\frac{1}{1+C}} \exp\left(-\frac{x}{16(1+C)}\right) \qquad (46)$$

Apart from the factor $T_{eo}/T_e(s')$, the electron density presents, as a function of z, an exponential behavior, with scale height $(1+C)\,H_3$, and an asymptotic value

$$\left(\frac{\eta_3}{\eta}\right)^{1/(1+C)}$$

for z=0.

For the case C=1, the electron and ion distributions calculated as a function of z from (31) and (33) respectively are shown in Fig. 4, for $T=1000^{\circ}K$, $\eta_2=0.02$ and $\eta_3=0.0016$ [Bauer (1963)]. The dependence of n_e and n_i on altitude is implicit in these curves of Fig. 4 through the dependence on z (see Fig. 5, p. 25). A discussion of the

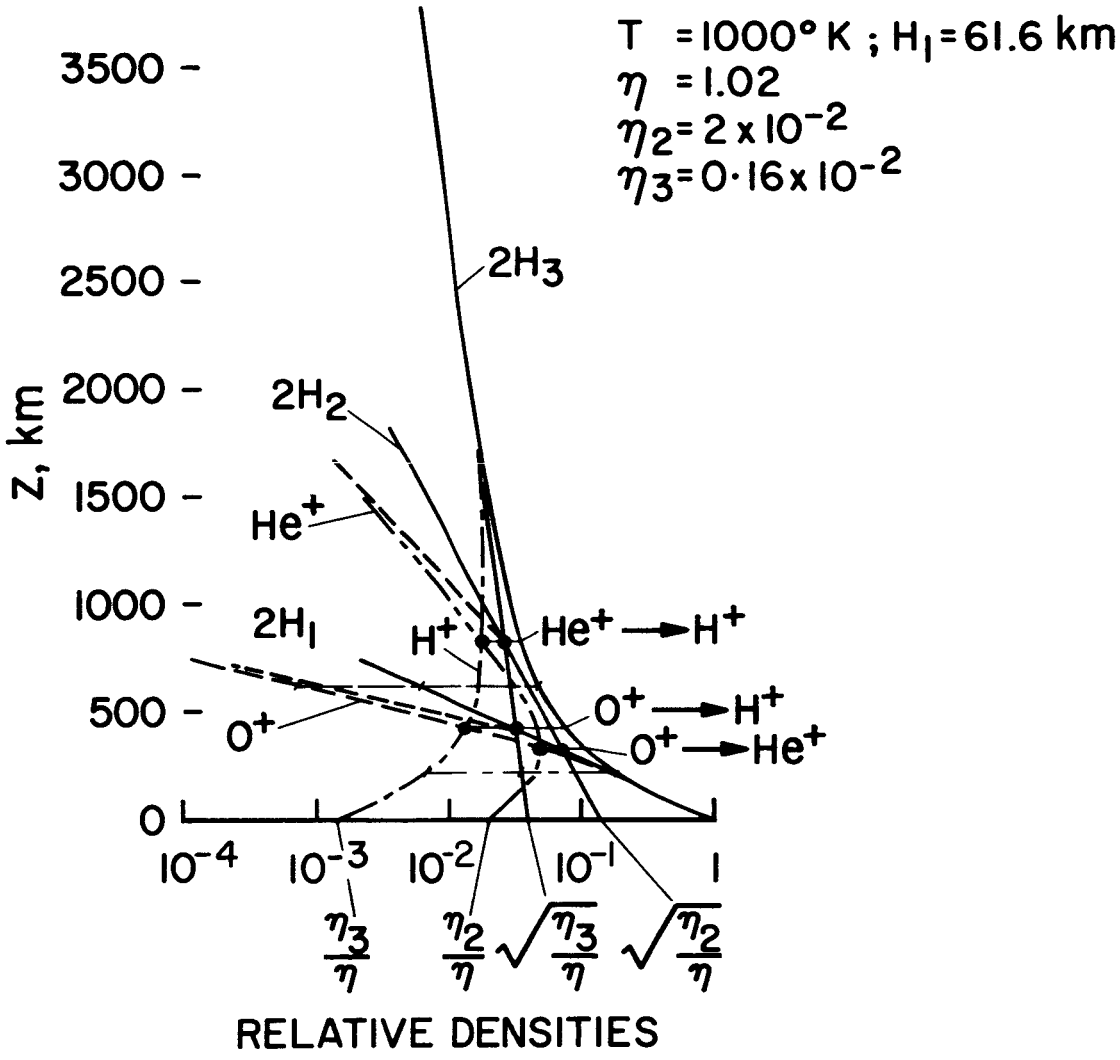

FIG. 4. DISTRIBUTION OF ELECTRON AND ION DENSITIES WITH THE TEMPERATURE-MODIFIED GEOPOTENTIAL HEIGHT, z, FOR THE CASE C = 1 AND CONSTANT TEMPERATURE T = 1000 °K.

resulting electron and ion density distributions as a function of height is deferred to Section IV. The curves of Fig. 4, however, are quite fundamental to an understanding of the processes involved in the theory of the exosphere and the curve for n_e as a function of z is the same as that given by Bauer (1963). The quantity z is, however, in the present work given a different meaning from that used by Bauer, since it contains a dependence on temperature and centrifugal force. The resulting differences predicted by the theory presented here compared with the results given by Bauer (1963) and others are discussed in Section V.

Using Eq. (33) it is seen that, for $C=1$,

$$\left(\frac{n_i(s')}{n_{eo}}\right)\left(\frac{n_e(s')}{n_{eo}}\right) = \frac{\eta_i}{\eta}\left(\frac{T_{eo}}{T_e(s')}\right)^2 \exp\left(-\frac{z}{H_i}\right)$$

$$= \left(\sqrt{\frac{\eta_i}{\eta}}\,\frac{T_{eo}}{T_e(s')}\,\exp\left(-\frac{z}{2H_i}\right)\right)^2$$

Hence, the geometrical mean of (n_i/n_{eo}) and (n_e/n_{eo}) is the quantity in parentheses. For an isothermal exosphere, this quantity happens to have a linear variation with z, when plotted on semi-log paper, with "scale height" $2H_i$ and passes through the point $\sqrt{\eta_i/\eta}$ at $z=0$.

This important property was used to obtain the ion densities from the electron density, in Fig. 4. More details are given in Appendix B.

The main source of difficulty in obtaining the solutions of (31) and (34) is to be found in the derivation of the quantity z. This is discussed in the next section.

D. CALCULATION OF TEMPERATURE-MODIFIED GEOPOTENTIAL HEIGHT z

It will be recalled that the quantity z is defined by

$$z\ (\theta_o, s') = \int_o^{s'} \frac{f(\theta_o, s)}{g_o} \frac{T_{eo}}{T_e(s)}\, ds \tag{47}$$

In order to evaluate z it is necessary to transform the variable of integration in the above equation from s to θ where θ is the geomagnetic latitude of the point concerned on the line of force. In Appendix A it is shown that the element of distance ds along the line of force may be written in terms of the subtended angular increment $d\theta$ by the relationship

$$ds = \frac{-r_o}{\cos^2\theta_o} \cos\theta \sqrt{1+3\sin^2\theta}\ d\theta \tag{48}$$

Substituting for ds from (48) and for f from (4) in the above expression for z and using (A4), Appendix A, we have

$$z = -\int_\theta^{\theta'} \frac{f(\theta)}{g_o} \frac{T_{eo}}{T_e(\theta)} \frac{r_o}{\cos^2\theta_o} \cos\theta \sqrt{1+3\sin^2\theta}\ d\theta$$

$$= \int_{\theta'}^{\theta_o} \frac{T_{eo}}{T_e(\theta)} r_o \sqrt{1+3\sin^2\theta} \left[\frac{\cos^2\theta_o}{\cos^3\theta} \cos\beta - \frac{\Omega^2 r_o}{g_o} \frac{\cos^4\theta}{\cos^4\theta_o} \cos\gamma\right] d\theta \tag{49}$$

where $\cos\beta$ is given by (3a) and $\cos\gamma$ by (3b) (Fig. 1) Thus

$$z = \int_{\theta'}^{\theta_o} r_o \frac{T_{eo}}{T_e(\theta)} \sqrt{\frac{1+3\sin^2\theta}{1+4\tan^2\theta}} \left[\frac{2\cos^2\theta_o}{\cos^4\theta} - \frac{3\Omega^2 r_o \cos^4\theta}{g_o \cos^4\theta_o}\right] \sin\theta d\theta$$

$$= r_o \int_{\theta'}^{\theta_o} \frac{T_{eo}}{T_e(\theta)} \sin\theta \left[\frac{2\cos^2\theta_o}{\cos^3\theta} - \frac{3\Omega^2 r_o \cos^5\theta}{g_o \cos^4\theta_o}\right] d\theta \tag{50}$$

since

$$\sqrt{\frac{1+3\sin^2\theta}{1+4\tan^2\theta}} = \cos\theta$$

This expression for z, the temperature-modified geopotential height, if substituted in Eqs. (31) and (34) will give the density distribution of electrons and ions along a line of force for any given temperature distribution along a line of force. In general, the equation will have to be computed numerically on a digital computer. It is interesting to note, however, that in the case of a constant temperature along a line of force so that $T_e(\theta) = T_{eo}$ we have

$$z(\theta_o,\theta') = 2r_o\cos^2\theta_o\int_{\theta'}^{\theta_o}\frac{\sin\theta}{\cos^3\theta}\,d\theta - \frac{3r_o^2\Omega^2}{g_o\cos^4\theta_o}\int_{\theta'}^{\theta_o}\sin\theta\cos^5\theta\,d\theta$$

$$= 2r_o\cos^2\theta_o\left[\frac{1}{2\cos^2\theta}\right]_{\theta'}^{\theta_o} + \frac{3\Omega^2 r_o^2}{g_o\cos^4\theta_o}\left[\frac{\cos^6\theta}{6}\right]_{\theta'}^{\theta_o}$$

$$= r_o\left\{\left[1-\frac{\cos^2\theta_o}{\cos^2\theta'}\right] + \frac{\Omega^2 r_o}{2g_o}\left[\cos^2\theta_o - \frac{\cos^6\theta'}{\cos^4\theta_o}\right]\right\} \qquad (51)$$

so that in the simple case of an isothermal atmosphere z has an analytical solution.

The resultant variation of z with altitude is shown in Fig. 5 for different latitudes. If the centrifugal force is disregarded, z is a function of altitude only and is independent of latitude (curve at right). It approaches a limiting value (equal to the distance from the reference level to the center of the earth) as the altitude goes to infinity. Inclusion of the centrifugal force implies a decrease in z, especially at high altitudes and low latitudes. The quantity z then has a maximum value at approximately 6 earth radii for low latitudes and approximately 8 earth radii for higher latitudes.

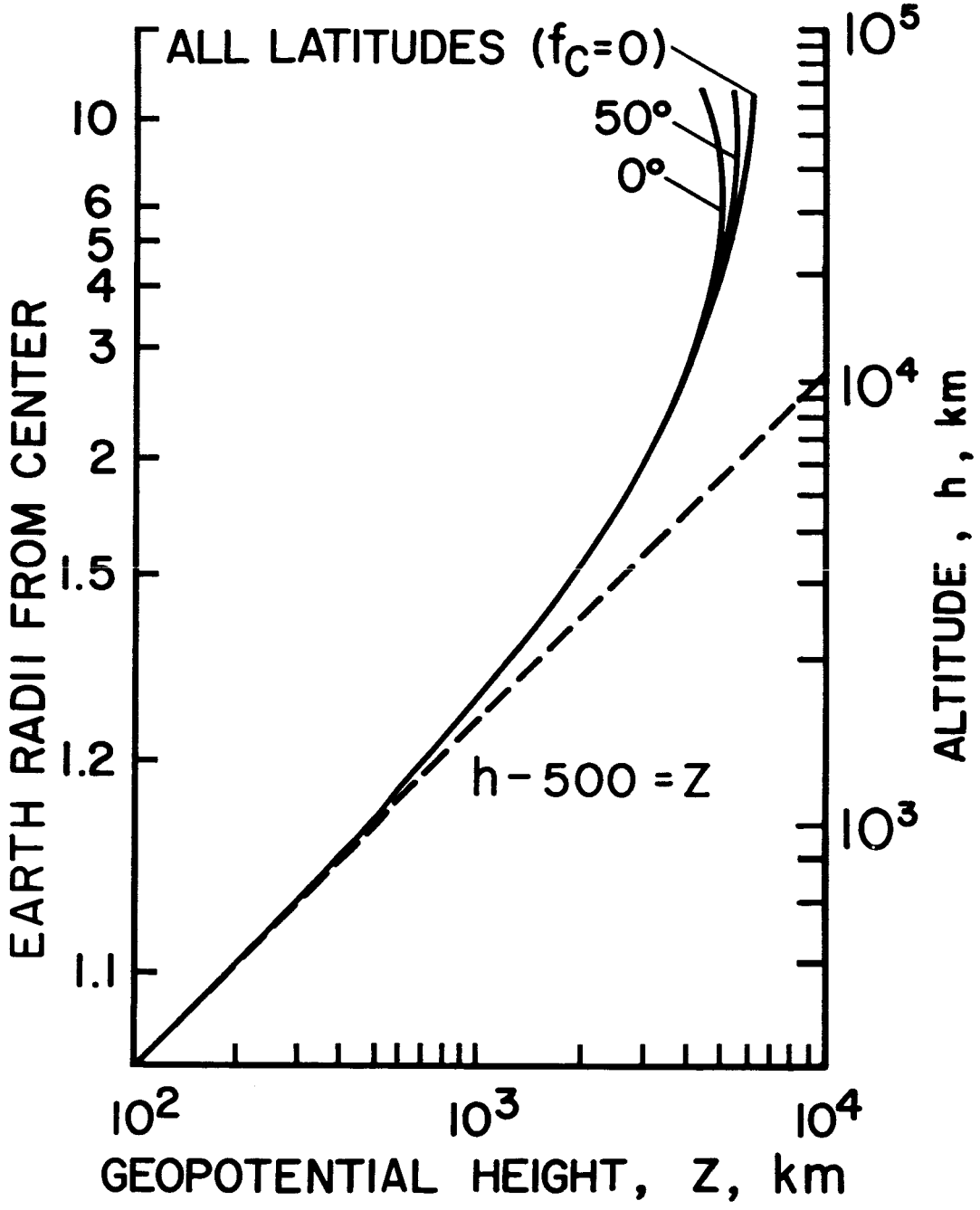

FIG. 5. VARIATION OF TEMPERATURE-MODIFIED GEOPOTENTIAL HEIGHT, z, WITH ALTITUDE, h, FOR AN ISOTHERMAL EXOSPHERE.

It should be noted, of course, that in Eqs. (31) and (34) it is possible for the temperature along different lines of force to be different and to be distributed along each line of force in a different way. As stated above, the Eqs. (31) and (34) in conjunction with the general relationship (50) may be used to compute the profile of electron density along a line of force. If, however, we require only the ratio of electron densities in the northern and southern hemispheres at the base level (see section E below), then it is useful to consider the form of Eq. (51) when θ' is small so that the point (θ_o, θ') lies near the equatorial plane. For $\theta' \tilde{=} 0$ the value z_m of z from (51) becomes

$$z\,(\theta_o,\theta') = z_m(\theta_o) = r_o \left\{ \left[1-\cos^2\theta_o\right] + \frac{\Omega^2 r_o}{2g_o}\left[\cos^2\theta_o - \frac{1}{\cos^4\theta_o}\right] \right\} \tag{52}$$

E. CALCULATION OF RATIO OF ELECTRON DENSITIES AT CONJUGATE POINTS

Attention will be given now to a rather interesting consequence of the theory presented, namely the ratio R_{eo} that must exist between the electron densities at the reference level at two magnetically conjugate points to satisfy continuity at the top of the field line.

It will be assumed that the ions and electrons have the same temperature, and hence $C=1$ in Eq. (30).

1. Temperature Constant in Each Hemisphere

As a first approximation, suppose that the average temperature in the southern (Summer) hemisphere, T_S, is greater than the average temperature in the northern (Winter) hemisphere, T_N, (Fig. 6) so that

$$T_S = KT_N \tag{53}$$

with K a constant greater than 1.

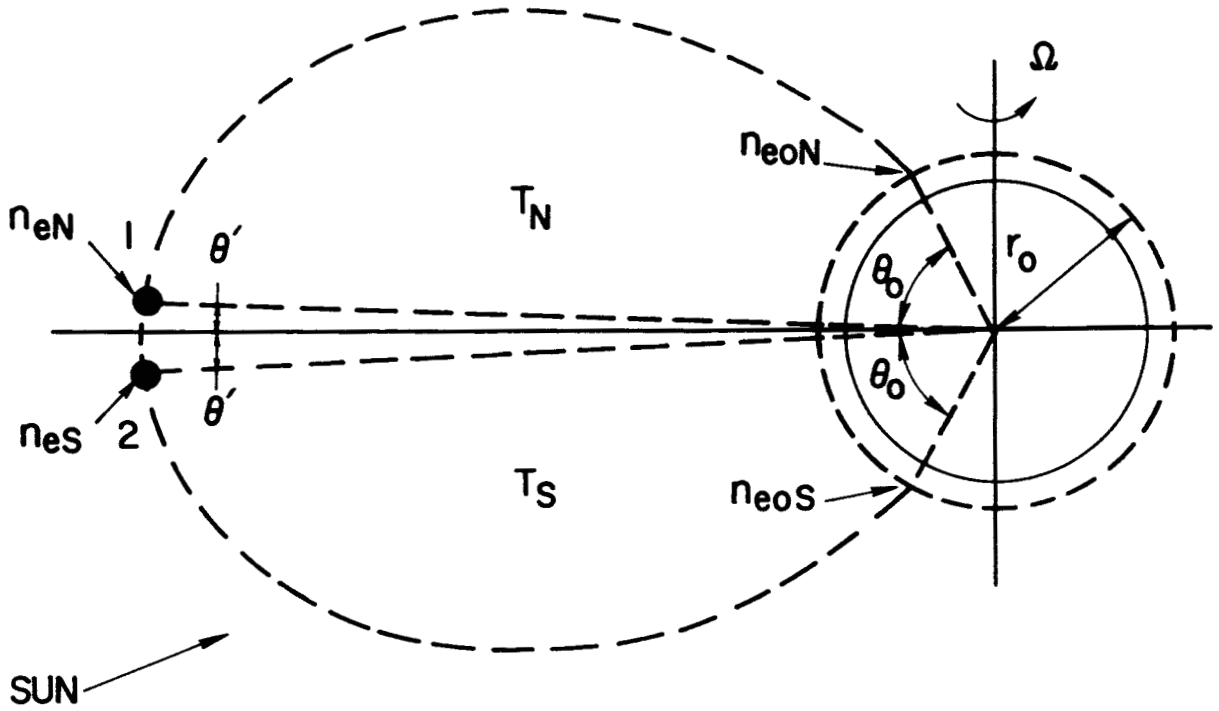

FIG. 6. PARAMETERS USED TO CALCULATE R_{eo} AT THE REFERENCE LEVEL AT TWO MAGNETICALLY CONJUGATE POINTS WHEN THE TEMPERATURE IN THE NORTHERN AND SOUTHERN HEMISPHERES ARE DIFFERENT BUT CONSTANT IN EACH HEMISPHERE.

Given the electron density n_{eo} (and ion densities, through η_2 and η_3) at a reference point on a field line, it is possible to calculate the electron density at any other point (defined by θ_o, θ') on the same field line, using Eqs. (36) and (51).

Let A be the ratio $n_e(s')/n_{eo}$ given by Eq. (36); it is clearly a function of temperature, through the values of H_i and η_i. Thus, for the northern and southern hemispheres respectively,

$$\frac{n_{eN}}{n_{eoN}} = A_N = \left[\frac{1}{\eta_N} \sum_i \eta_{iN} \exp(-z_M/H_{iN})\right]^{\frac{1}{2}}$$

$$\frac{n_{eS}}{n_{eoS}} = A_S = \left[\frac{1}{\eta_S} \sum_i \eta_{iS} \exp(-z_M/H_{iS})\right]^{\frac{1}{2}} \qquad (54)$$

where z_M is the value of z for $\theta' \simeq 0$ and is given by (52).

As the electron pressure must be the same in points 1 and 2 of Fig. 6:

$$n_{eN}kT_N = p_N = p_S = n_{eS}kT_S \tag{55}$$

From (53), (54) and (55),

$$R_{eo} = \frac{n_{eoN}(\theta_o)}{n_{eoS}(\theta_o)} = K\frac{A_S}{A_N} \tag{56}$$

This expression permits the calculation of the electron density at the reference level in the northern hemisphere if the electron density at the same level, at the conjugate point, is known. It is useful to make the following approximations.

From Fig. 4 it is seen that for z greater than about 2000 km (corresponding to z_M at $\theta_o > 35^\circ$), Eq. (46) holds so that with the present assumptions, using Eq. (20a), A_N and A_S are given by

$$\left.\begin{aligned} A_N &\approx \sqrt{\eta_{3N}/\eta_N}\,\exp(-z_M/2H_{3N}) \\ A_S &\approx \sqrt{\eta_{3S}/\eta_S}\,\exp(-z_M/2H_{3S}) \\ &= \sqrt{\eta_{3S}/\eta_S}\,\exp(-z_M/2KH_{3N}) \end{aligned}\right\} \tag{57}$$

Thus, at latitudes greater than about 35°, Eq. (56) has the approximate form

$$R_{eo} = \frac{n_{eoN}(\theta_o)}{n_{eoS}(\theta_o)} \approx K\sqrt{\frac{\eta_{3S}\eta_N}{\eta_{3N}\eta_S}}\,\exp\left(-\frac{z_M}{2H_{3N}K} + \frac{z_M}{2H_{3N}}\right)$$

$$= K\sqrt{\frac{\eta_{3S}\eta_N}{\eta_{3N}\eta_S}}\,\exp\left(\frac{z_M}{2H_{3N}}\,\frac{K-1}{K}\right) \tag{58}$$

The corresponding equation given by Rothwell (1962) may be derived as a particular case of the more general expression (58) in which the dependence of m, g and T on altitude may be properly allowed for.

2. Temperature Changing Along a Line of Force

In the preceding section, it was assumed as a convenient approximation that there was a discontinuity of temperature between two points just north and south of the equatorial plane (Fig. 6). For a complete treatment it is better to proceed as follows.

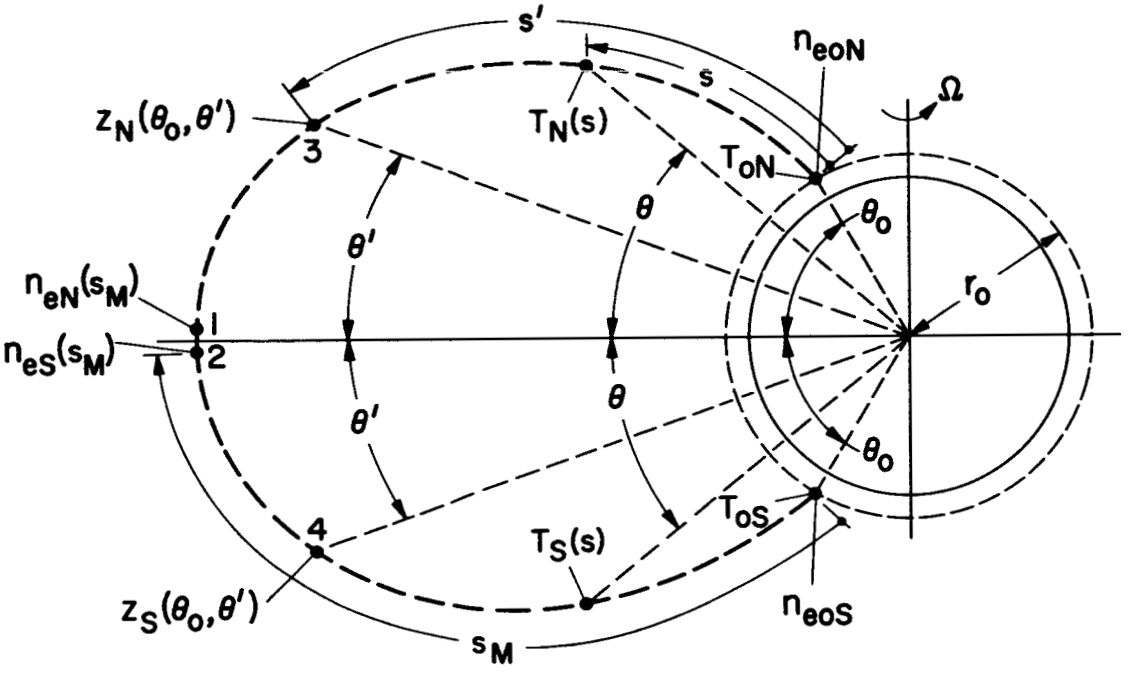

FIG. 7. PARAMETERS USED TO CALCULATE R_{eo} AT THE REFERENCE LEVEL AT TWO MAGNETICALLY CONJUGATE POINTS WHEN THE TEMPERATURE IS TAKEN AS A CONTINUOUS FUNCTION $T_N(s)$ IN THE NORTHERN HEMISPHERE, AND $T_S(s)$ IN THE SOUTHERN HEMISPHERE. At points 1 and 2, the temperatures are the same.

Figure 7 indicates the temperature as a function of distance along a line of force. The temperature must change

along the field line since it is supposed that, at the reference level, it has different values in the northern and southern hemispheres

$$T_{oS} = KT_{oN} \tag{59}$$

with K a constant greater than 1.

The distance s is clearly a function of θ_o and θ, and we call $s_M(\theta_o)$ the value of s corresponding to $\theta = 0$ (details are given in Appendix A).

The functions $T_N(s)$ and $T_S(s)$ are such that the temperature is a continuous function of s, including the point s_M, that is:

$$T_N(s_M) = T_S(s_M) \tag{60}$$

The assumed form for $T_N(s)$ and $T_S(s)$ is discussed in Section IV.

As the temperature is now a function of s, Eq. (50) must be used to calculate z, and different values will result for points 3 and 4, Fig. 7:

$$\left.\begin{aligned} z_N(\theta_o,\theta') &= r_o\int_{\theta'}^{\theta_o} \frac{T_{oN}}{T_N(s)} \sin\theta\left[\frac{2\cos^2\theta_o}{\cos^3\theta} - \frac{3\Omega^2 r_o}{g_o}\frac{\cos^5\theta}{\cos^4\theta_o}\right]d\theta \\ z_S(\theta_o,\theta') &= r_o\int_{\theta'}^{\theta_o} \frac{T_{oS}}{T_S(s)} \sin\theta\left[\frac{2\cos^2\theta_o}{\cos^3\theta} - \frac{3\Omega^2 r_o}{g_o}\frac{\cos^5\theta}{\cos^4\theta_o}\right]d\theta \end{aligned}\right\} \tag{61}$$

These equations, together with Eq. (35), give the electron density distributions in the northern and southern hemispheres.

$$\left.\frac{n_{eN}(s')}{n_{eoN}} = \frac{T_{oN}}{T_N(s')}\left[\frac{1}{\eta_N}\sum_i\left\{\eta_{iN}\exp\left(-\frac{z_N}{H_{iN}}\right)\right\}\right]^{\frac{1}{2}}\right\} \tag{62}$$

$$\frac{n_{eS}(s')}{n_{eoS}} = \frac{T_{oS}}{T_S(s')} \left[\frac{1}{\eta_S} \sum_i \left\{ \eta_{iS} \exp\left(-\frac{z_S}{H_{iS}}\right) \right\} \right]^{\frac{1}{2}} \tag{62}$$

For $s' = s_M$ the electron densities are the same in the northern and southern hemispheres (points 1 and 2, Fig. 7), and so are the temperatures. Thus, the last equations, together with (60) give

$$R_{eo} = K\left[\frac{\eta_N}{\eta_S} \frac{\sum_i \left\{ \eta_{iS} \exp(-z_{MS}/H_{iS}) \right\}}{\sum_i \left\{ \eta_{iN} \exp(-z_{MN}/H_{iN}) \right\}} \right]^{\frac{1}{2}} \tag{63}$$

where z_{MN} and z_{MS} are given by the corresponding Eqs. (61) with $\theta' = 0$. For sufficiently large values of z_{MS} and z_{MN}, such that Eq. (46) holds, Eq. (63) may be written as

$$R_{eo} \simeq K\left[\frac{\eta_N}{\eta_S} \frac{\eta_{3S}}{\eta_{3N}} \right]^{\frac{1}{2}} \exp\left[\frac{z_{MN} - z_{MS}/K}{2H_{3N}} \right] \tag{64}$$

in which use has been made of Eq. (20a) and (59).

IV. RESULTS OF THE THEORY

A. INTRODUCTION

In this section, relative electron and ion density distributions calculated on the basis of the theory outlined in the previous sections are presented. The results are given as distributions calculated as functions of the temperature modified geopotential height z, as functions of the distance s measured along a line of force and also as functions of the altitude, h. These distributions are referred to as N(z), N(s) and N(h) curves respectively. The computations are based on a number of different assumptions about the exospheric temperature and about the ionic composition of the atmosphere at 500 kilometers. In particular, the distributions are derived

A) when a constant temperature is assumed along a line of force

B) when the temperature is assumed to vary with distance, s, along a line of force.

In addition, two sets of assumptions are made about the composition at the base level usually taken to be 500 kilometers above the earth's surface. These are

1. that the composition at 500 kilometers is independent of the temperature at that level, and

2. that the composition at 500 kilometers is a strong function of the temperature at that level.

The N(h) calculations referred to above were carried out both when a proper allowance was made for the effect of the centrifugal force arising from the earth's rotation and also when this force was neglected. Subsequently, use is made of

observational data from the Alouette satellite (Thomas and Sader 1963) to convert the relative electron density profiles into absolute profiles based on the electron density observed at approximately 1000 kilometers. This leads to a set of theoretical profiles calculated using reasonable experimentally observed magnitudes for ion composition (Bauer 1963), temperature (Harris and Preister 1962), and electron density at 1000 km (Alouette observations). These theoretical profiles are then compared with a number of whistler and other observations of electron density in the earth's exosphere. Tables 1 and 2, pg. 61,62,give a summary of the way in which the calculations were developed and in which the results are presented. Further details are noted in the ensuing sections.

B. THE ELECTRON AND ION DISTRIBUTIONS

The electron and ion distributions presented below were calculated using a digital computer program. The N(z) curves were computed from equation (35) using the assumption that the temperature was constant, the N(s) curves were computed from equations (35), (51) and (A4), the N(h) profiles being subsequently computed from the N(s) profiles using electron density observations at 1000 kilometers as measured by the Alouette satellite.

The calculations in which the temperature is assumed constant along the line of force of the earth's magnetic field are denoted by the letter A (Table 1, pg. 61). For each value of the temperature assumed, it is necessary to specify the composition at the base level at 500 kilometers. This was taken from the data presented by Bauer (1963) for the helium and hydrogen ion densities relative to the oxygen ion density as a function of the temperature. The relevant equations are

$$\eta_2(T_o) = 0.2 \times 10^{-T_o/1000}$$

$$\eta_3(T_o) = 0.16 \times 10^{-T_o/500} \qquad (65)$$

In this equation, T_o is the temperature assumed at the reference level. The variation of η_2 and η_3 with temperature as given by equations (65) is shown in Fig. 8.

The exospheric temperature enters the calculations in two ways. Firstly, via the temperature modified geopotential height z, and secondly, via its effect on the composition assumed at the base level through equations (65). It is, however, interesting to carry out computations in which the composition at 500 kilometers is held constant nevertheless allowing the temperature to vary. In this case the values for η_2 and η_3 were taken from equations (65) using $T_o = 1000°K$ and these results are referred to as "Composition 1," Table 1.

The calculations in which equations (65) were applied to give the relative densities at 500 kilometers are referred to as "Compositions 2a,b,c," etc. depending on the value of the temperature at 500 kilometers (see Table 1). In other words, in "Compositions 2," once the temperature at the base level is specified, the relative ion densities are automatically specified at that level by equations (65). Some calculations are also performed using the assumption that the temperature is changing along the field line. These results are denoted by the letter B (Table 1) and will be described later.

Details relating to the curves shown in Figs. 9 - 18 are summarized in Tables 1 and 2 which precede the figures (pg. 61).

In Figures 9a - e (see Tables 1 and 2), electron and ion densities are plotted as functions of the temperature-modified geopotential height z for different values of the (constant) temperature (assumed independent of s) and for different compositions. The distributions shown in Figs. 9a - e, do not show marked "kinks" or cusps and the ion transition levels do not show up clearly in the electron density curves. These curves are discussed in greater detail in Appendix B.

The electron densities of Figs. 9a - e are summarized in Fig. 10, where the relative effects of temperature and composition changes can be seen. At low values of z, where O^+ is predominant for all curves, the slopes are proportional to temperature. As we go to higher values of z the effect of the ion composition at the base becomes relatively more important and the slopes are no longer simply proportional to temperature. For instance, at z = 3000 km, the slope of curve e (2000°K) is less than the slope of curve b (1000°K). This is so because, although for curve b at z = 3000 km, the H^+ is strongly predominant (Fig. 9b); this is not the case for curve e (Fig. 9e).

It is seen from the curves of Figs. 9a - e that the ion transition levels (the levels at which $n(O^+) = n(He^+)$, etc.), change with temperature. The variation of the ion transition levels with temperature is shown in Fig. 11 for two different assumptions about the composition at the base level, namely, that the composition is independent of temperature (continuous lines) and that the composition is temperature-dependent as indicated by equations (65) (broken lines). An important conclusion which can be drawn from an examination of Figs. 9a - e, and 11 is that the transition levels approach nearer the earth at night. These curves agree with those given by Bauer (1963).

The N(z) curves may be transformed using equation (51) into curves giving N as a function of θ and θ_o where θ is the angle between the equatorial plane and a point at a distance s measured along a field line. The field line is assumed to intersect the base level (500 km above the earth) at a point making an angle θ_o with the equatorial plane (Fig. 1). The use of equation (A4) (Appendix A) converts the $N(\theta,\theta_o)$ curves to distributions of electron density along a line of force ($N(s,\theta_o)$ curves). Curves of this kind are given in Figs. 12a,b,c, for θ_o= 45°, 55° and 65° respectively. In each diagram the results corresponding to the case in which proper allowance has been made for centrifugal force are shown as continuous lines. The corresponding results for the cases in which the centrifugal force was neglected are shown by broken lines. As expected, the effect of the centrifugal force is largest at the higher latitudes, and tends to increase the electron density at the high levels. The increase is never greater than about 20% over the range of heights considered. It is found also that along the field line at 45° the centrifugal force has no appreciable effect (Fig. 12a). The effects of changes in temperature and composition are seen very clearly in Fig. 12a in which the distance scale is expanded.

Similar calculations (denoted by the letter B, Tables 1 and 2) were carried out in which the temperature varied along a line of force. The temperature distribution assumed along a line of force in the cases labelled B is given by the formula

$$T(s) = T_o + (T_T - T_o)\,\frac{1 - \exp(-s/D)}{1 - \exp(-s_M/D)} \qquad (66)$$

where T_o is the temperature at the reference level (500 kilometers), T_T is the temperature at the top of the field

line, D is a variable distance along the line of force (taken to be 10^4 km), and the distances s and s_M are defined along the line of force as indicated in Fig. 7, page 29.

In order to be able to calculate the ratios of electron densities at magnetically conjugate points when a difference of temperature exists between hemispheres, it is convenient to apply equation (66) separately for the two hemispheres. Thus for the northern (winter) hemisphere, T_o and T_T were taken to be 1000°K and 1800°K respectively and the resulting temperature distribution along the line of force as given by (66) for the northern hemisphere is denoted by $T_1(s)$. For the southern (summer) hemisphere T_o = 1400°K and T_T = 1800°K and equation (66) is again used to give $T_2(s)$. The distributions $T_1(s)$ and $T_2(s)$ are sketched in Fig. 13.

Electron densities along lines of force were calculated for a variable temperature along the line of force using equations (35), (50), and (A4). The results are shown in Figs. 14a - d, for θ_o = 35°, 45°, 55°, and 65°, respectively. The general behaviour of the curves in Figs. 14 is similar to that of the curves in Figs. 12. For instance, an increase in temperature, keeping the base level composition constant, increases the electron densities in both cases, and a contrary effect is produced if the composition is supposed to vary as given by equations (65). Also, the effect of neglecting the centrifugal force is negligible below θ_o = 45°.

It is important to note that the calculated electron distributions depend strongly on the assumed base temperature but do not depend appreciably on the small temperature changes assumed along a line of force, and, that to a first order, vertical profiles and distributions along the line of force computed assuming a constant temperature are adequate.

The ratios R_e (subsequently referred to as R) of the electron densities at conjugate points in the two hemispheres predicted by the theory were calculated for a series of heights (Fig. 15a,b). The temperature distribution along a line of force was assumed to be as shown in Fig. 13, the temperature T_{o1} corresponding to that at the base level in the northern (winter) hemisphere. If it is supposed that the compositions at the base level are the same in winter and summer, the ratio, R = N(winter)/N(summer) is slightly greater than unity and tends to increase with increasing latitude (Fig.15a). If, instead, the ionic composition at 500 km is assumed to depend on the temperature as given by Bauer (1963) (Fig. 8 and Equation (65)) then the curves of Fig. 15b are obtained and the ratio R is still about unity except for the 1000 km level for which it decreases from 1 at the equator to approximately 0.5 at high latitudes.

Fig. 16a,b,c shows N(h) profiles computed assuming base composition 1 for the two assumed temperature models (see Fig. 13 and Equation (66)). It was assumed that the electron density at 1000 km was 10^4/cc. Fig. 16a corresponds to an equatorial profile ($\theta = 0°$), and Figs. 16b, c correspond to $\theta = 30°$ and $60°$ respectively. The differences in the profiles shown in Figs. 16a,b,c arise only because of the effect of the centrifugal force.

In order to convert the relative electron density distributions to absolute values, electron density data for 1000 km obtained from the Alouette satellite were used (Thomas and Sader 1963). Fig. 17, based on the results of Thomas and Sader (1963) shows the mean variation of the electron density at 1000 km for a series of magnetically quiet days and nights in summer and winter as a function of dip latitude. The broken lines are extrapolated values. N(h) profiles were computed for a variety of conditions

using the data of Fig. 17 at 1000 km. These profiles are shown in Figs. 18a - d. If the assumptions about temperature and base compositions indicated are correct, then the theory outlined in this report predicts that the electron profiles in summer (day and night) and winter (day and night) are as shown in Figs. 18a - d, respectively.

The differences between the curves shown in Fig. 18a - d arise firstly because of the different assumptions about temperature and composition, and secondly because of changes in the electron density at 1000 km from summer to winter and from day to night used in converting from relative distributions to absolute distributions. In particular, the rapid fall off of electron density with height in the summer night curves is mainly attributable to the rapid decrease in the electron density at 1000 km with dip latitude over the range 50° - 65°. Typical diurnal and seasonal changes depicted in these curves are illustrated for a given temperature and base composition in Fig. 18e which shows also the value of the latitude θ_o corresponding to the foot of the field line (at 1000 km above the earth) which extends to a given distance from the center of the earth in the equatorial plane.

A number of theoretical N(h) distributions have been predicted for the exospheric plasma and these are discussed in Section IV.C. Some typical examples are reproduced in Fig. 19a (Bates and Patterson 1961; Dungey 1954; Johnson 1960) and these may be compared with the curves predicted by the theory presented in this report.

No detailed comparison of the predicted N(h) profiles with experimentally observed data for any given day is possible at the present time. However, a number of whistler mean exospheric electron density profiles have been published covering a wide range of observational conditions. A number

of these are reproduced in Fig. 19b and are labelled a to h in that diagram (Storey 1953; Allcock 1959; Carpenter and Angerami (quoted by Carpenter 1963); Smith 1960, 1961; Pope 1961, 1962; Schmelovsky 1960; Schoute-Vanneck and Muir 1963). It should be noted that the observation of Storey (1953), quoted above, refers to a single point only. The incoherent scatter observations of Bowles (1962) lie within the arrow indicated in Fig. 19b.

In Fig. 20 the experimental data of Fig. 19b are superposed on the theoretical curves of Fig. 19a. The experimental curves of Fig. 19b cover a wide variety of observed conditions and include results for different times of day, different seasons and different solar epochs. In general, however, all these results lie within the approximate region indicated by the diagonally shaded area in Fig. 20. The values of electron density measured by Alouette lie within the approximate zone indicated by the vertically shaded area.

It is clear from Fig. 20 that when the values of electron density given by the Alouette data for summer nights are used, the theory outlined in this report gives reasonably good agreement with the observations (curves c and d) whereas the curves a, f, e, b, g indicate too small a decrease of electron density with height. Furthermore the present theory provides a better agreement with the observed slope of the N(h) profile near the level of the Alouette orbit. It should be noted that the curve labelled e represents a probable extreme value indicated by the present work since it corresponds to summer daytime conditions when the assumption that there is no production of ionization near the base level is most likely to be invalid.

Until further information is available concerning the exospheric temperature and composition, it is probably unfruitful to consider detailed comparison of theory with experiment. However, the number of reasonable choices is not unlimited and for example (Fig. 21), the N(h) curve of Smith (1960, 1961) is well matched by the present theory if the temperature is assumed to be 1000°K and the starting electron density at 1000 km is assumed to be roughly that corresponding to the curve labelled "summer night" in Fig. 17. Thus, quite good agreement can be obtained with values which might be reasonally expected to apply at the time when the whistler observations were made.

The general agreement between theory and experiment is illustrated in another way in Fig. 22 which shows the theoretically predicted values of the ratio R as a function of geomagnetic latitude, together with observations of R at 1000 km measured by the Alouette satellite. The shaded area corresponds to values within which all the observed values of the ratio R lie and thus allows for changes from night to night, etc. The circled points give the values for magnetically quiet days.

V. COMPARISON WITH OTHER WORK AND SUMMARY OF RESULTS

A. DISCUSSION

The basic concepts which govern the distributions of ions and electrons in the exosphere have been discussed in a number of important papers in the scientific literature. It is generally agreed that the main constituent of the atmosphere at great heights above the earth (above approximately 1500 kilometers) is hydrogen. Hydrogen ions are formed by the reaction

$$O^+ + H \rightleftarrows H^+ + O$$

as was first pointed out by Dungey. The relative equilibrium concentrations in the exosphere are determined largely by the importance of this reaction near the base of the neutral particle exosphere where the cross-section for collisions between ions and neutral particles is relatively high. The base of the exosphere at approximately 550 kilometers is believed to be the most probable level of origin for protons entering the exosphere from below after formation in the charge exchange reaction referred to above (Johnson 1960). Thus, the relative abundances of O^+ and H^+ (and also of the He^+ ions) at the base of the exosphere controls the electron and ion distributions throughout the exosphere. The charge exchange reaction referred to above proceeds very rapidly near the peak of the F2 layer and the proton number density is given by the chemical equilibrium expression (Hanson and Ortenburger 1961)

$$[H^+] = \frac{9}{8} \frac{[H]\ [O^+]}{[O]}$$

where the square brackets denote the concentrations of the constituents bracketed.

It has also been shown by Hanson and Ortenburger (1961) that the oxygen ions near the F2 peak are only weakly coupled with the protons in the protonosphere and it seems likely that the time constant for the establishment of equilibrium between the two hemispheres near the F region peak is greater than one day. The results of Hanson and Patterson (1963) and of Hanson, et al (1963) provide an estimate of the proton fluxes likely to be involved as the result of the diurnal variation of the abundance of the atomic hydrogen in the exosphere. They considered the flow of hydrogen into and out of the protonosphere by the charge exchange process referred to above, the escape of hydrogen from the daytime exosphere associated with higher daytime temperatures and also the lateral flow of hydrogen around the earth due to any asymmetry in the distribution of hydrogen around the earth.

It is clear from this work and from other considerations that some modifications to a simple equilibrium theory are probably required to describe completely the physics of the exosphere in terms of diurnal and other changes. However, before a non-equilibrium theory is properly applied, it is valuable to explore the extent to which an equilibrium theory is adequate to explain the observational data and this has been the purpose of the work reported herein. In particular, it seems likely that an equilibrium theory might be applicable for explaining seasonal variations which are likely to occur in a given hemisphere as well as other changes involving time constants greater than one day.

The structure of the lower exosphere has been discussed in some detail by Hanson (1962), Bauer (1962, 1963) and by Gliddon (1962) who considered the distributions of the O^+, He^+, and H^+ ions together with the electrons under diffusive equilibrium. The corresponding distributions at much greater altitudes have been discussed by Dungey (1954), Johnson (1960) and by Bates and Patterson (1961).

The main differences between the work presented in this report and the earlier work referred to above relate to the following points:

1. Under the circumstances where diffusive equilibrium applies, it is well known that whereas in a non-ionized atmosphere each constituent is distributed independently of the other constituents, the distribution of a light ionic constituent in diffusive equilibrium is dependent upon the presence of the others because of the electric field, E, which arises from the slight charge separation between electrons and positive ions (Dungey 1954, Mange 1960, Hanson and Ortenburger 1961). In the present work, it has been assumed that the electrons and ions can diffuse only along the geomagnetic field lines and, therefore, the direction of the electric field, E, has been assumed to be along the particular field line concerned.

2. It is shown that it is convenient to work in terms of a parameter, z, called the temperature-modified geopotential height. The equations have been developed to allow for the possibility that the electron and ion temperatures may be different and that a temperature gradient may exist along a line of force.

3. As was first pointed out by Bates and Patterson (1961), up to the present time, the theories of electron and ion distributions in the earth's exosphere have not taken into account conditions in the upper part of the earth's ionosphere which may be strongly dependent on latitude. Such a latitude dependence would influence the electron density distribution in the equatorial plane since the diffusion of charged particles in the earth's exosphere is appreciable only along geomagnetic field lines. Since our N(h) profiles have been deduced from the theoretically computed N(s) distributions (i. e., the calculated equilibrium distributions along a line of force when diffusion

along the field lines is operative), the starting electron density assumed at the base level and, in particular, its variation with latitude, is an extremely important factor.

An examination of the results of Thomas and Sader (1963) shows that the electron density at 1000 km as observed by the Alouette satellite does vary quite strongly with latitude and, in particular, there is an important minimum in the curve under certain circumstances near a dip latitude of 65°. This latitude dependence was inserted into the theory so that the actual observed electron densities at 1000 km were used. The computed N(h) curves in the equatorial plane at great distances from the earth were then compared with observations from whistler data. It was found that the disagreement between theory and observations of the exospheric plasma electron density distribution in the vicinity of the Alouette orbit (see Fig. 20) was removed. Under certain circumstances, the disagreement at greater distances from the earth was also removed when reasonable assumptions about the exospheric temperature and about the relative ion densities at 500 km were made and the Alouette data for summer nights used. It is possible that at the times when the N(h) slopes far out do not agree with theory, that some of the assumptions made in the theory were invalid. In particular, it might be the case that composition and temperature changes at 1000 km were inapplicable, or that the level above which diffusive equilibrium occurs varies with time.

The slope of the N(h) profile in the lower exosphere (approximately 600 - 1000 km).

It has been assumed in the theory that the production of electrons by the sun's ionizing radiations and the loss of electrons by recombination are both non-existent. Thus no attempt is made to discuss the N(h) distributions at or near the peak of the F2 layer, though a great deal of

observational and theoretical data are available (see for example Thomas 1963, Rishbeth, Lyon and Peart 1963 and references quoted therein). Instead, the discussion has been confined to consideration of the theory which might apply above the critical level (Johnson 1960) at about 500 km above the earth's surface.

Bauer (1962), (1963), assumed that in the vicinity of the Alouette orbit there is diffusive equilibrium with O^+, He^+ and H^+ as the main constituents and later was able to fit a topside profile from the Alouette satellite on the basis of an equilibrium theory down to quite low altitudes. The results of the theory outlined in the present work in the vicinity of the Alouette orbit agree with Bauer's slopes.

The main differences between the work presented in the report and that referred to above is that Bauer considered an isothermal case and does not allow for centrifugal force: both assumptions being justified for the cases which Bauer considers since he restricts his theory to distances which do not exceed about one earth radii above the F2 region peak. Bauer, however, considers equilibrium in a vertical column rather than in a column confined by a tube of force. In the approach outlined in this report, a vertical profile is very strongly influenced by a north-south gradient in the temperature and ionic composition at the base level or by a north-south gradient in the electron density at the base level.

Since the calculations described in this report were carried out, a number of N(h) profiles deduced from the Alouette satellite data have been circulated.* The available

* Radio Research Station, Slough, England, Topside N(h) Profiles, Vol. I, Dec. 1963; King, J. W., et al, Radio Research Report No. IM 94, July 1963; and King, J. W., et al, Report No. IM 112, Dec. 1963.

profiles correspond to equatorial crossings of the satellite and were observed at the telemetry station at Singapore. From the N(z) plots of King, et al (1963) (see footnote, pg. 46), measurements were made of the scale height for electrons at 1000 km for one daytime and one nighttime revolution: 26 November 1962, 14:58 local time, and 15 April 1963, 20:28 local time, respectively.

For the daytime pass, the scale height at 1000 km varies between 170 km at 14°N latitude (consistent with O^+ at 1380°K) and 260 km at 12°S latitude (consistent with a mixture of O^+ and He^+ at 1380°K). Around the latitude 14°N the electron distribution is a pure exponential down to 350 km, supporting the idea that O^+ is indeed strongly predominant.

For the nighttime pass, the scale height at 1000 km varies between 380 km at 20°N (consistent with strongly predominant He^+ at 780°K--or a mixture of the He^+ with a significant amount of O^+, at a slightly higher temperature) and 620 km at 9°S (consistent with strongly predominant He^+ at 1270°K--or a mixture of He^+ and a significant amount of H^+ at a slightly lower temperature). The preceding measurements show then that the lower boundary of the helium layer is lower at night than during the day.

From the above it appears that the scale height for electrons at 1000 km varies strongly from day to night (by a factor 2.4 in the above measurements) and also varies with latitude. It is apparent that, at 1000 km, both the ionic composition and the temperature must vary diurnally and also with latitude, at least in the equatorial regions. Also, it is important to note that the assumption that H^+ strongly predominates at 1000 km would lead to extremely low temperatures in order to explain scale heights as low as 170 km (T less than 100°K).

The slope of the N(h) profile in the upper exosphere.

An examination of the theoretical profiles of Fig. 20 shows that at very great heights the rate at which the electron density decreases with height is often less than the experimental observations indicate. Furthermore, the slopes of the profiles near 1000 km for curves a, b, f, g, Fig. 19a, are not in agreement with those observed from electron density profiles deduced in the vicinity of the Alouette orbit. The theoretical profiles of Dungey (1954), Bates and Patterson (1961) and Johnson (1960) allow only for the presence of H^+ and not for helium. Thus, the slopes are small even at low altitudes. The present work produces slopes in agreement with those observed by the Alouette satellite near its orbit in conformity with the results of Bauer.

At the present time, until more information is available about the positive ion abundances at 1000 km, it is not known to what extent profiles observed at all times can be fitted by a simple equilibrium theory. However, it is clear that the main features of the seasonal variations will probably, to a large extent, be governed by the broad precepts dictated by an equilibrium theory, although there will be diurnal changes superimposed on the broad seasonal changes. The theory outlined in the present paper does, under certain circumstances, lead to electron density profiles which fall off at great altitudes at a rate which is in agreement with the experimental data obtained from whistlers and at the same time gives the correct slope near the Alouette orbit.

B. CONCLUSIONS

1. The equilibrium distributions of electrons and ions in the earth's exosphere have been computed for a wide variety of conditions on the assumption that diffusive equilibrium applies.

2. The theory assumes that diffusion of electrons and ions is possible only along the geomagnetic field lines.

3. The presence of He^+ ions near the base of the exosphere has been allowed for in the calculations. This is vital for an understanding of the changes accompanying the transition from day to night conditions.

4. The most crucial factors governing the form of these distributions are the exospheric temperature and the ionic composition at the base level assumed to be at 500 kilometers above the earth's surface.

5. The strong latitude dependence of electron density at 1000 km as observed by the Alouette satellite has been taken into consideration in the calculations. As a result, it is clear that the discrepancy previously observed between theory and experiment, namely, that the electron density gradient at great heights predicted by the theories turned out to be much smaller than that indicated by the whistler observations, is now removed under certain circumstances.

6. The effect of the earth's centrifugal force is included in the calculations--its neglect would, at the high altitudes lead to electron density values which are too low at a given height by an amount which does not exceed 20 percent, for altitudes less than about 7 earth radii.

Although it is not suggested that an equilibrium theory is adequate to describe the entire properties of the plasma distribution in the exosphere, it is quite clear that a first order agreement can be obtained, at any rate, in terms of

seasonal dependencies. The basic question of why the electron density at the Alouette orbit varies with latitude in the way that it does, remains unsolved. Further work is needed to determine the nature and the relative abundances of the positive ions at the base of the exosphere and the dependence of these relative abundances on the exospheric temperature. Measurements of the relative abundances on a daily routine basis through satellite observations will probably be necessary before it is possible to determine accurately the circumstances in which an equilibrium theory becomes inapplicable.

ACKNOWLEDGMENTS

The authors wish to acknowledge valuable discussions with Professors R. A. Helliwell and O. K. Garriott and with colleagues in the Radioscience Laboratory, Stanford Electronics Laboratories, Stanford University.

The work was financed in part by a grant, NsG 30-60 from the National Aeronautics and Space Administration, and in part by the Air Force Office of Scientific Research under grant AF-AFOSR-62-370.

APPENDIX A. GEOMETRY OF THE DIPOLE FIELD

It was assumed in this report that the actual magnetic field of the earth could be approximated by a centered dipole field, as indicated in Mlodnosky and Helliwell (1962). Most of the equations quoted in this appendix appear in Fig. 1 of that paper, to which reference should be made. Thus, the equation of a line of force in a dipole field is

$$\frac{r}{r_o} = \frac{\cos^2\theta}{\cos^2\theta_o} \tag{A1}$$

in which the quantities are as shown in Fig. 1, page 4, of this report. In this figure, the distance s_1 along the line of force with feet at θ_o, from the equatorial plane to the latitude θ is

$$s_1(\theta_o,\theta) = \frac{r_o}{2\sqrt{3}\ \cos^2\theta_o}\ (x + \sinh x.\cosh x) \tag{A2}$$

$$= \frac{r_o}{2\sqrt{3}\ \cos^2\theta_o}\ [\ln\ (y + \sqrt{1 + y^2}) + y\sqrt{1 + y^2}]$$

where

$$y = \sinh x = \sqrt{3}\ \sin\theta$$

We called $s_M(\theta_o)$ the value of s_1 corresponding to $\theta = \theta_o$, as shown in Fig. 7, page 29:

$$s_M(\theta_o) = \frac{r_o}{2\sqrt{3}\cos^2\theta_o}\ [\ln\ (y_o + \sqrt{1 + y_o^2}) + y_o\sqrt{1 + y_o^2}] \tag{A3}$$

with

$$y_o = \sqrt{3}\,\sin\theta_o$$

For convenience, the distance $s(\theta_o,\theta)$ between a base level (θ_o) and a latitude θ was used (see Fig. 1, page 4):

$$s(\theta_o,\theta) = s_M(\theta_o) - s_1(\theta_o,\theta) \qquad (A4)$$

The increment of distance ds, corresponding to an increment $d\theta$ (keeping θ_o constant) is easily shown to be

$$ds = -\frac{r_o}{\cos^2\theta_o}\sqrt{1 + 3\sin^2\theta}\,\cos\theta\,d\theta \qquad (A5)$$

It is clear that by means of eq. (A1) the distances s_1, s_M and s can be written as functions of (θ_o,r), and this is convenient for electron and ion density calculations in which the exospheric temperature is assumed constant. This procedure was used in the computations leading to Figs. 12 and 18.

It should be noted that the inversion of eq. (A2) [or (A4)] to give θ as a function of θ_o and s_1 (or s) is only possible numerically. Thus, in the computations leading to Figs. 14 - 16, in which the temperature is assumed a function of the distance s, the numerical integrations to get z (from eq.(50)) were made using θ as the independent variable.

APPENDIX B. NOTE ON THE ION DISTRIBUTION CURVES

For an isothermal exosphere, the relative electron and ion densities can be conveniently plotted as functions of z. Assuming that the electrons and ions all have the same temperature (i. e., C = 1), their relative densities are obtained from equations (31) - (33) respectively (pages 16 - 17):

$$\frac{n_e(z)}{n_{eo}} = \left\{ \frac{\exp(-z/H_1) + \eta_2 \exp(-z/H_2) + \eta_3 \exp(-z/H_3)}{\eta} \right\}^{\frac{1}{2}} \quad \text{(B1)}$$

$$\frac{n_i(z)}{n_{io}} = \exp\left[-\frac{z}{H_i}\right]\left[\frac{n_{eo}}{n_e(z)}\right] \quad \text{(B2)}$$

$$\frac{n_i(z)}{n_{eo}} = \frac{\eta_i}{\eta} \exp\left[-\frac{z}{H_i}\right]\left[\frac{n_{eo}}{n_e(z)}\right] \quad \text{(B3)}$$

If one ion is strongly predominant, so that only the term for this particular ion is important on the right-hand side of equation (B1), then,

$$\frac{n_e(z)}{n_{eo}} \simeq \sqrt{\frac{\eta_i}{\eta}} \exp\left[-\frac{z}{2H_i}\right] \quad \text{(B4)}$$

where the suffix i refers to the strongly predominant ion. Equation (B4) is a simple exponential and is represented by a straight line on semi-logarithmic paper, with slope $2H_i$, (twice the scale height of the non-ionized specimen). These straight lines are drawn in Figs. 9a - d for O^+, He^+, H^+, (c.f. Hanson (1962)) and are labelled $2H_1$, $2H_2$ and $2H_3$ respectively.

Reference to the N(z) curve of Fig. 9b shows that the simple exponential behaviour of electron density referred to above is exhibited below 100 km where O^+ is strongly predominant (note that the ordinate is z not h) and is also exhibited above 1500 km where H^+ is strongly predominant. Around 500 km, although He^+ is predominant, it is not sufficiently strongly predominant and a straight line distribution is not achieved.

Comparison of Figs. 9c and d shows the effect in the slope of the N(z) curve of changing the composition at the base level. According to Table 1, Fig. 9d corresponds to a smaller percentage of He^+ and H^+ at the base level, so that the O^+ is predominant over a greater height range. Thus, the electron density maintains a high rate of decrease over a greater height range so that the electron density turns out to be smaller for the same z, in curve d than in curve c (Fig. 10). As a result, one sees that a change in composition is far more important than a change in temperature in determining the value of the relative electron density as a function of z (Fig. 10).

In equation (B2), the term $\exp(-z/H_i)$ decreases with increasing z, whereas the term $n_{eo}/n_e(z)$ increases with increasing z. It is therefore possible for the ion density to increase with z, since it is made up of the product of these two factors.

The ratio of densities of two different ions as function of z may be obtained from equation (B3):

$$\frac{n_i(z)}{n_j(z)} = \frac{\eta_i}{\eta_j} \exp\left[\frac{z}{H_j} - \frac{z}{H_i}\right] \qquad (B5)$$

which, in the logarithmic plot of Figs. 9a - e, is a straight line with (positive) slope $H_j H_i/(H_i - H_j)$ passing through the

point η_i/η_j at $z = 0$. These lines are not shown in Figs. 9a - e but may readily be included.

Equation (B3) may be written in a more convenient form:

$$\left\{\frac{n_i(z)}{n_{eo}}\right\}\left\{\frac{n_e(z)}{n_{eo}}\right\} = \frac{\eta_i}{\eta} \exp\left[-\frac{z}{H_i}\right] \qquad (B6)$$

so that the geometric mean of the electron and ith ion densities relative to the electron density at the base level is

$$\sqrt{\frac{\eta_i}{\eta}} \exp\left[\frac{-z}{2H_i}\right]$$

which is our previous equation (B4) giving the asymptotic behaviour for the relative electron density curve when the ith ion is strongly predominant. Thus from (B6)

$$\frac{1}{2}\left\{\log\left[\frac{n_i(z)}{n_{eo}}\right] + \log\left[\frac{n_e(z)}{n_{eo}}\right]\right\} = \log\left\{\sqrt{\frac{\eta_i}{\eta}} \exp\left[\frac{-z}{2H_i}\right]\right\} \qquad (B7)$$

The left-hand side of this equation is the arithmetic mean of the logarithms of the electron density and the density of the ith ion relative to the electron density at the base level.

Thus, if relative electron density curves are plotted using a logarithmic scale in density (as in Figs. 9a - e) then the distribution curve for the ion i may be derived from a simple geometric construction as follows. First the straight line (B4) is plotted (slope $2H_i$, crossing the abscissa at a value $\sqrt{\eta_i/\eta}$) then the relative electron distribution (B1) is plotted. For each value of z, a point is plotted such that the horizontal distance from the point to the straight line is the same as that from the straight line to the electron

distribution. The locus of these points is the ion distribution curve (Fig. 9b). This procedure may be repeated for each ion.

It is clear from this construction that the ionic transition levels (the values of z at which two ions have the same density, i. e., the intersection point of two ionic distribution curves) may be alternatively identified as the intersection of the corresponding asymptotic straight lines.

REFERENCES

Allcock, G. M., "The Electron Density Distribution in the Outer Ionosphere Derived from Whistler Data," J. Atmos. Terr. Phys., 14, 185, 1959.

Bates, D. R., and T. N. L. Patterson, "Hydrogen Atoms and Ions in the Thermosphere and Exosphere," Planet. Space Sci., 5, 257, 1961.

Bauer, S. J., "On the Structure of the Topside Ionosphere," J. Atmos. Sci., 19, 276, 1962.

Bauer, S. J., "Helium Ion Belt in the Upper Atmosphere," Nature, 197, 36, 1963.

Bordeau, R. E., "Rocket and Satellite Investigations of the Ionosphere, Trans. Am. Geophys. Union, 44, 443, 1963.

Bowles, K. L., "Profiles of Electron Density over the Magnetic Equator Obtained Using the Incoherent Scatter Technique," NBS Report 7633, 1962.

Carpenter, D. L., "Whistler Measurements of the Equatorial Profile of Magnetospheric Electron Density," presented at the XIVth General Assembly of URSI, Tokyo, 1963 (to be published by Elsevier, Amsterdam).

Dungey, J. W., "Electrodynamics of the Outer Atmosphere," Scientific Report No. 69, Contract No. AF 19(122)-44, Ionospheric Research Lab., Penn. State Univ., 1954.

Gliddon, J. E. C., "The Distribution of Ions in the Exosphere," J. Atmos. Terr. Phys., 25, 175, 1963.

Hanson, W. B., "Upper Atmosphere Helium Ions," J. Geophys. Res., 67, 183, 1962.

Hanson, W. B., and T. N. L. Patterson, "Diurnal Variation of the Hydrogen Concentration in the Exosphere," Planet. Space Sci., 11, 1035, 1963.

Hanson, W. B., T. N. L. Patterson, and S. S. Degaonkar, "Some Deductions from a Measurement of the Hydrogen Ion Distribution in the High Atmosphere," J. Geophys. Res., 68, 6203, 1963.

Hanson, W. B., and I. B. Ortenburger, "The Coupling Between the Protonosphere and the Normal F Region," J. Geophys. Res., 66, 1425, 1961.

Harris, Isadore and Wolfgang Priester, "Theoretical Models for the Solar-Cycle Variation of the Upper Atmosphere," NASA, Goddard Space Flight Center X-640-62-70, June, 1962.

Johnson, F.S., "The Ion Distribution Above the F_2 Maximum," J. Geophys. Res., 65, 577, 1960.

Jackson, J. E., "NASA Investigation of the Topside Ionosphere," NASA Report X-615-63-105, 1963.

King, J. W., P. A. Smith, D. Eccles, and H. Helm, "The Structure of the Upper Ionosphere as Observed by the Topside Sounder Satellite, Alouette," D.S.I.R., Radio Research Station, Slough, England, 1963.

King-Hele, D. G. and D. M. C. Walker, "Variation of Upper Atmosphere Density with Altitude and Season: Further Evidence from Satellite Orbits," Nature, 185, 727, 1960.

Lockwood, G. E. K., and G. L. Nelms, "Topside Sounder Observations of the Equatorial Anomaly, Part I: 75° W Longitude," J. Atmos. Terr. Phys., in press.

Mange, P., "The Distribution of Minor Ions in Electrostatic Equilibrium in the High Atmosphere," J. Geophys. Res., 65, 3833, 1960.

Mlodnosky, R. F., and R. A. Helliwell, "Graphic Data on the Earth's Main Magnetic Field in Space," J. Geophys. Res., 67, 2207, 1962.

Nicolet, M., "Helium, an Important Constituent in the Lower Exosphere," J. Geophys. Res., 66, 2263, 1961.

Pope, J. H., "An Estimate of Electron Densities in the Exosphere by Means of Nose Whistlers," J. Geophys. Res., 66, 67, 1961.

Pope, J. H., "A Correction to the Exospheric Electron Density Estimate Using the Nose Whistlers of March 19, 1959 " J. Geophys. Res., 67, 412, 1962.

Rishbeth, H., A. J. Lyon, and M. Peart, "Diffusion in the Equatorial F Layer," J. Geophys. Res., 68, 2559, 1963.

Rothwell, P., "Diffusion of Ions Between F Layers at Magnetic Conjugate Points," Proc. of the Int. Conf. on the Ionosphere, The Inst. of Physics and The Physical Society, 217, 1962.

Schmelovsky, K. H., "The Electron Density Distribution Derived from Whistler Data and Faraday-fading Observations," J. Atmos. Terr. Phys., 19, 68, 1960.

Schoute-Vanneck, C. A., and M. S. Muir, "The Electron Density Distribution in the Magnetosphere Derived from Whistling Atmospheric Data," J. Geophys. Res., 68, 6079, 1963.

Smith, R. L., "Properties of the Outer Ionosphere Deduced from Nose Whistlers," J. Geophys. Res., 66, 3709, 1961.

Smith, R. L., The Use of Nose Whistlers in the Study of the Outer Ionosphere," Stanford Electronics Labs. Technical Report No. 6, Contract AF18(603)-126, Stanford University, 1960.

Storey, L. R. O., "An Investigation of Whistling Atmospherics," Phil. Trans. Royal Soc. A (London), 246, 113, 1953.

Thomas, J. O., "The Electron Density Distributions in the F_2 Layer of the Ionosphere in Winter," J. Geophys. Res., 68, 2707, 1963.

Thomas, J. O., and A. Y. Sader, "Alouette Topside Soundings Monitored at Stanford University," Stanford Electronics Laboratories Technical Report No. 6, NASA Grant NsG 30-60, Radioscience Laboratory, Stanford University, 1963.

ASSUMPTIONS ABOUT TEMPERATURE		ASSUMPTIONS ABOUT COMPOSITION AT 500 KM				
		COMPOSITION 1	COMPOSITIONS 2			
				T °(K)	η_2	η_3
	A [T = constant]	$\eta_2 = 2.0 \times 10^{-2}$ $\eta_3 = 1.6 \times 10^{-3}$	2a	500	6.3×10^{-2}	1.6×10^{-2}
			2b	750	3.6×10^{-2}	5.1×10^{-3}
			2c	1250	1.1×10^{-2}	5.1×10^{-4}
			2d	1500	6.3×10^{-3}	1.6×10^{-4}
			2e	2000	2.0×10^{-3}	1.6×10^{-5}
				T_o °(K)	η_2	η_3
	B [T = T(s)]	$\eta_2 = 2.0 \times 10^{-2}$ $\eta_3 = 1.6 \times 10^{-3}$	2f	1400	8.0×10^{-3}	2.6×10^{-4}

TABLE 1

TEMPERATURE AND COMPOSITION ASSUMPTIONS

TABLE 2. SUMMARY OF PRESENTATION OF RESULTS

ASSUMPTIONS ABOUT TEMPERATURE		ASSUMPTIONS ABOUT COMPOSITION AT 500 KILOMETERS		Quantity Plotted
		COMPOSITION 1 $[\eta_{2,3}\ (1000)]$	COMPOSITIONS 2 $[\eta_{2,3}\ (T_o)]$	
A [T = constant]		T = 1000 Fig. 9b T = 1500 Fig. 9c	Fig. 10 → Fig. 9a T = 500; Fig. 9d T = 1500; Fig. 9e T = 2000	N(Z)
		T = 1000, 1500	Fig. 12 → a. $\theta_o = 45°$; b. $\theta_o = 55°$; c. $\theta_o = 65°$	N(s)
B [T = T(s)]		$T_1(s)$, $T_2(s)$	Fig. 14 → a. $\theta_o = 35°$; b. $\theta_o = 45°$; c. $\theta_o = 55°$; d. $\theta_o = 65°$	N(s)
		$T_{winter} = T_1(s)$; $T_{summer} = T_2(s)$	Fig. 15a / Fig. 15b	R(θ,h)
		$T_1(s)$, $T_2(s)$	Fig. 16 → a. $\theta = 0°$; b. $\theta = 30°$; c. $\theta = 60°$	N(h)
A [T = constant]		T = 750, 1000, 2000	Fig. 18 → a. summer day; c. winter day	N(h)
		T = 500, 750, 1000, 1500	Fig. 18 → b. summer night; d. winter night	

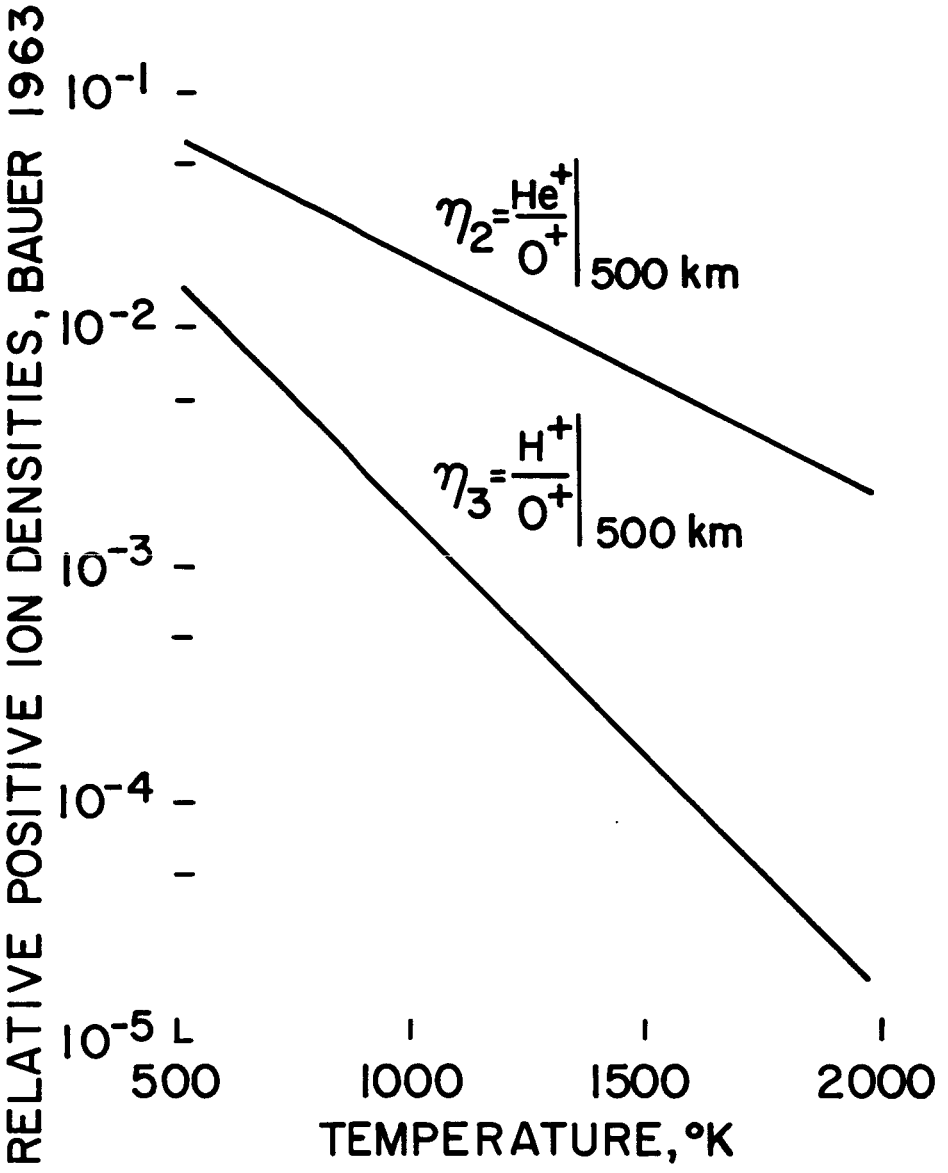

FIG. 8. VARIATION OF THE ION COMPOSITION AT 500 KM WITH THE TEMPERATURE AT THAT LEVEL (BAUER 1963).

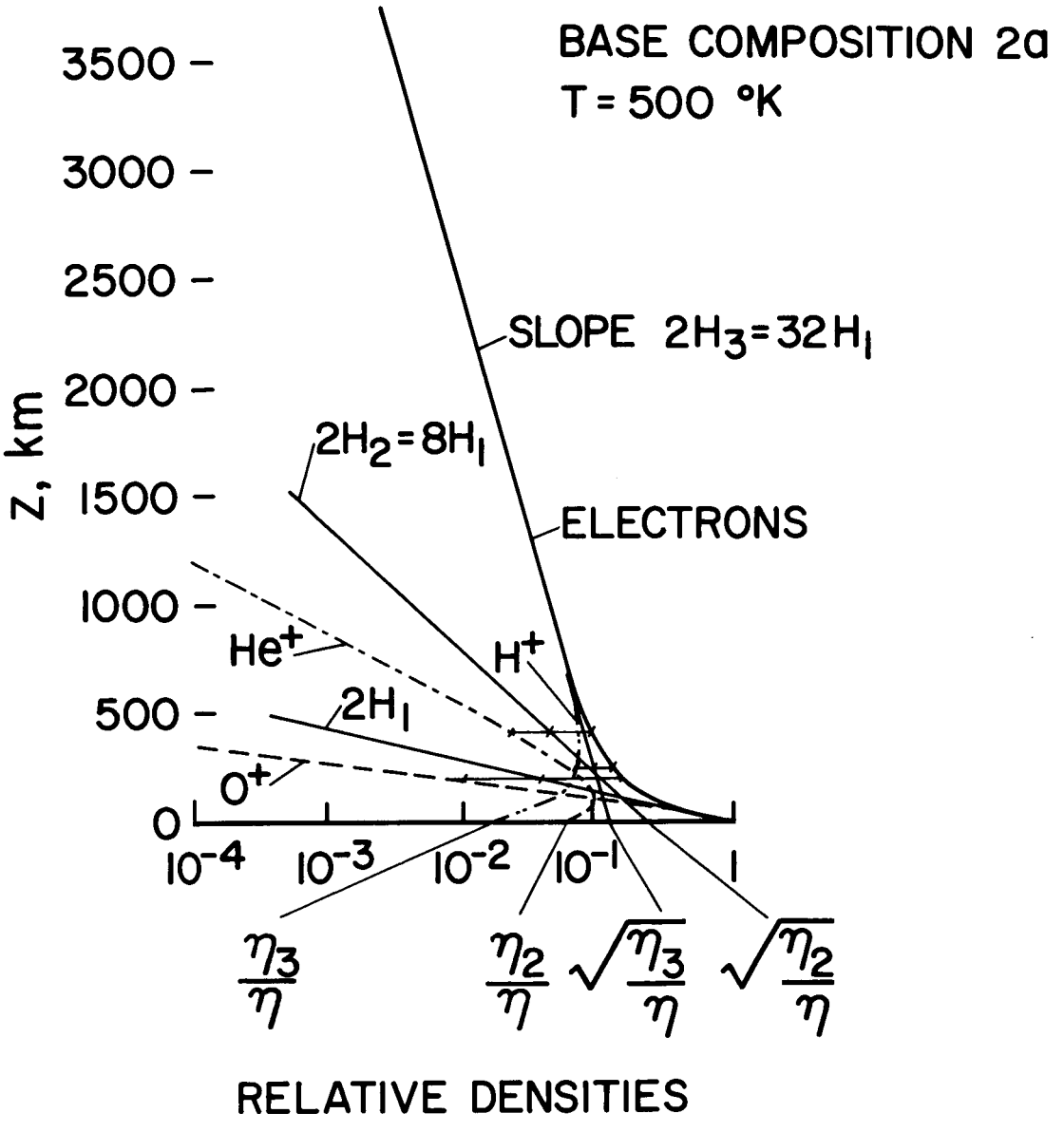

FIG. 9a. RELATIVE ELECTRON AND ION DENSITIES AS A FUNCTION OF THE GEOPOTENTIAL HEIGHT, z, FOR AN ISOTHERMAL EXOSPHERE. The form of the distributions depends strongly on the assumed base level composition and the assumed temperature as may be seen by comparing the above with the subsequent figures.

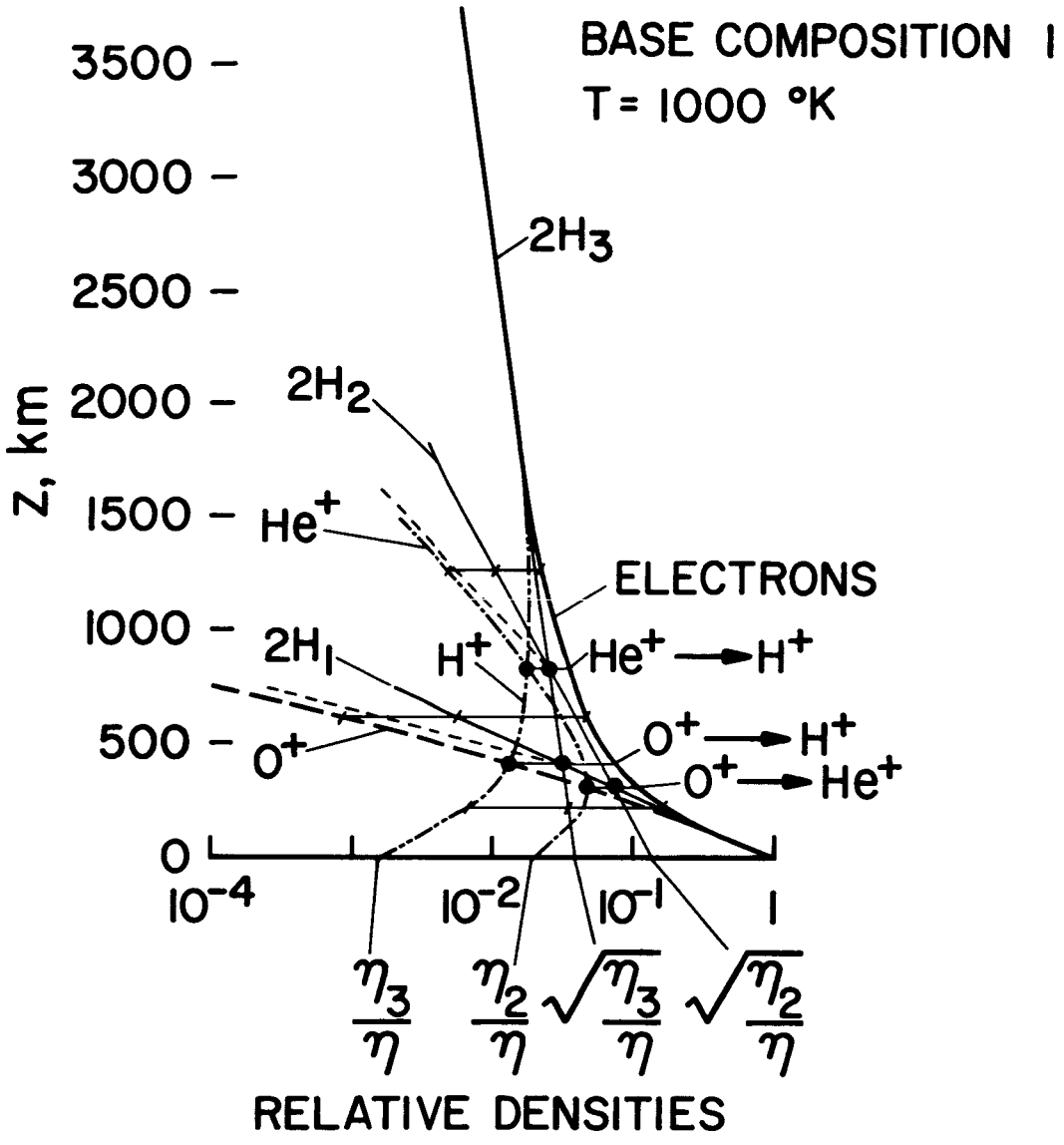

FIG. 9b. RELATIVE ELECTRON AND ION DENSITIES AS A FUNCTION OF THE GEOPOTENTIAL HEIGHT, z, FOR AN ISOTHERMAL EXOSPHERE. Comparison with Fig. 9c indicates the effect on the distributions of changing the temperature only.

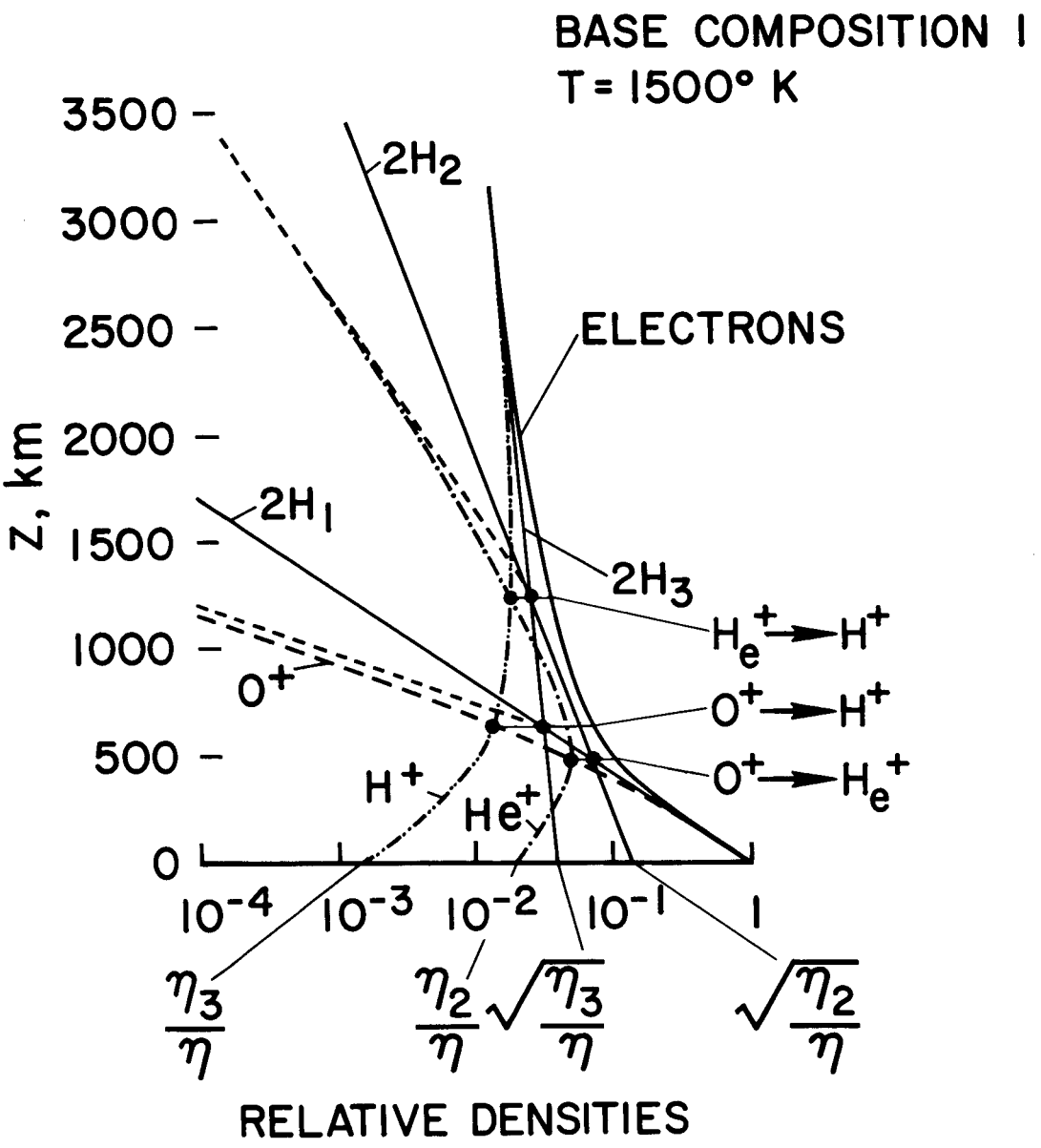

FIG. 9c. RELATIVE ELECTRON AND ION DENSITIES AS A FUNCTION OF THE GEOPOTENTIAL HEIGHT, z, FOR AN ISOTHERMAL EXOSPHERE. Comparison with Fig. 9b indicates the effect on the distributions of changing the temperature only. Comparison with Fig. 9d reveals the effect of changing the base composition only.

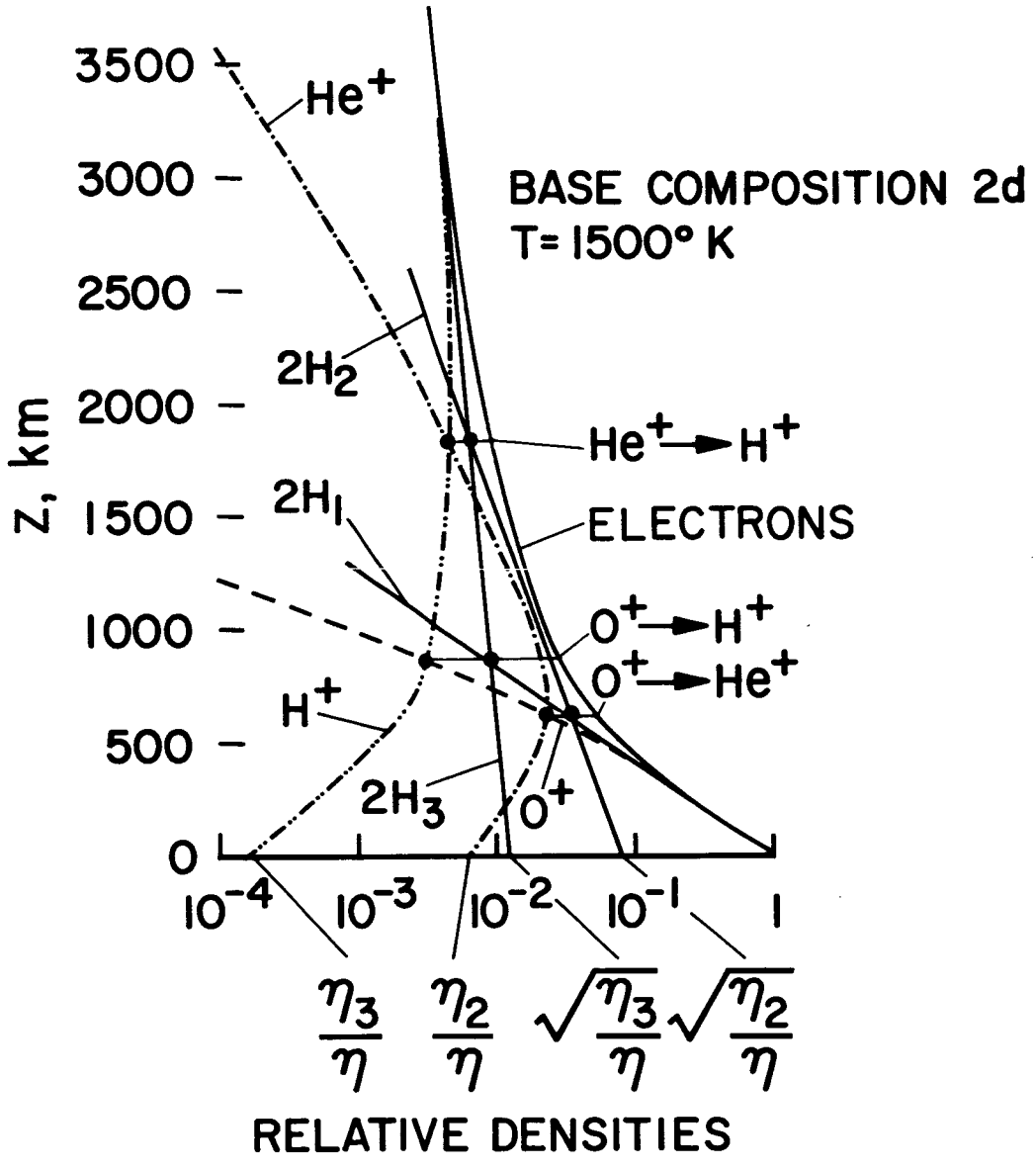

FIG. 9d. RELATIVE ELECTRON AND ION DENSITIES AS A FUNCTION OF THE GEOPOTENTIAL HEIGHT, z, FOR AN ISOTHERMAL EXOSPHERE. Comparison with Fig. 9c reveals the effect of changing the base composition only.

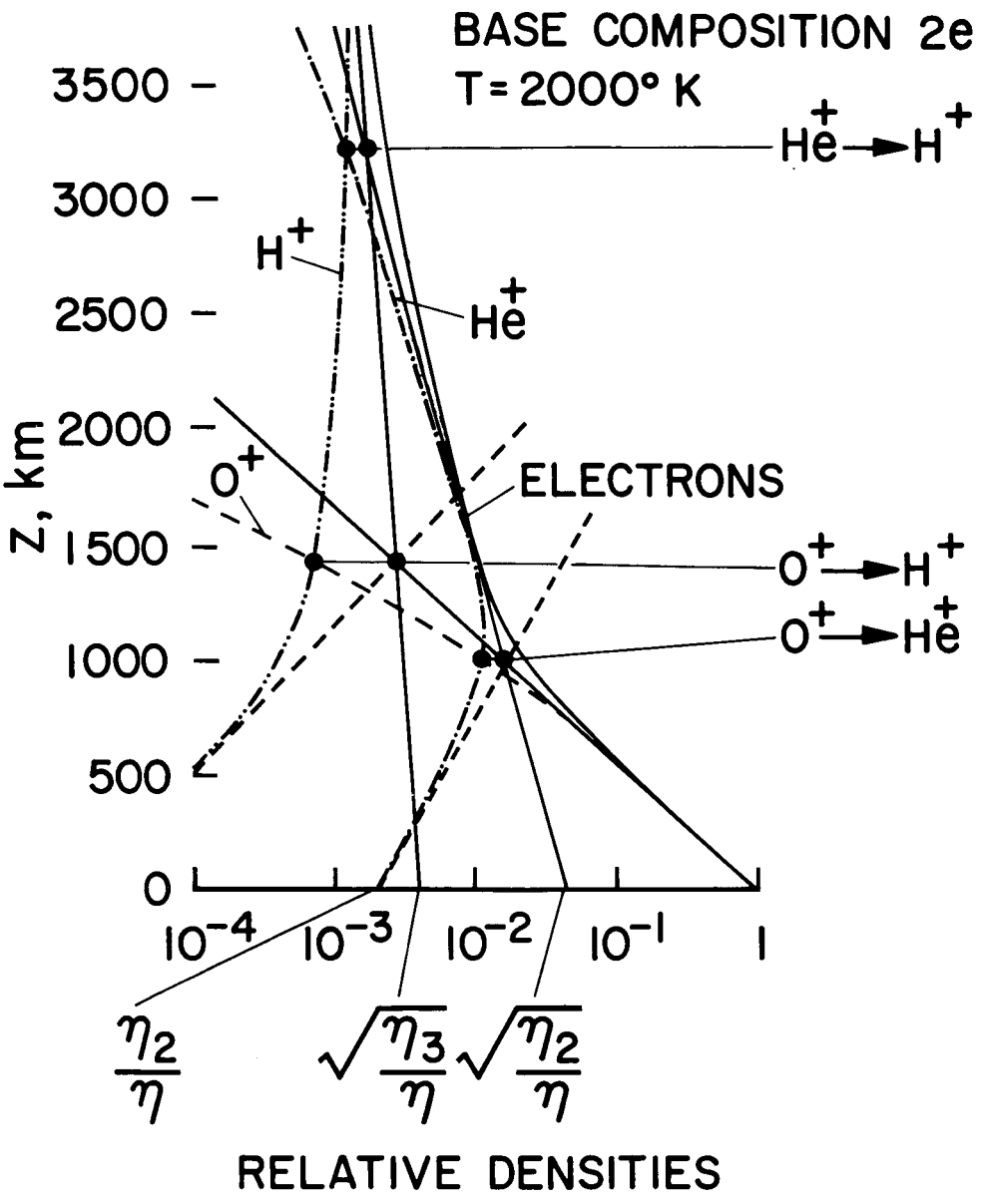

FIG. 9e. RELATIVE ELECTRON AND ION DENSITIES AS A FUNCTION OF THE GEOPOTENTIAL HEIGHT, z, FOR AN ISOTHERMAL EXOSPHERE WITH A RELATIVELY HIGH TEMPERATURE.

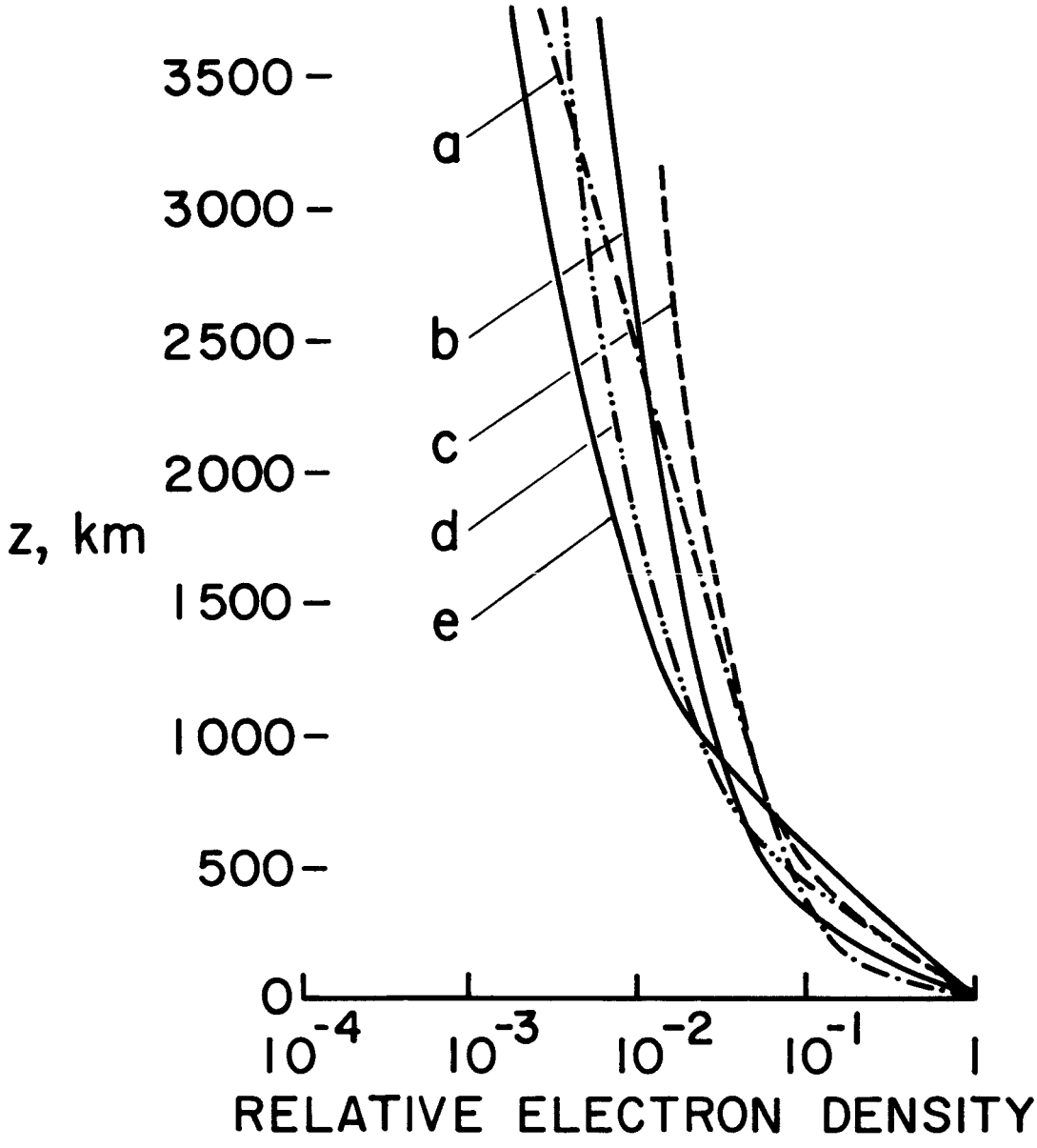

FIG. 10. SUMMARY OF THE RESULTS OF FIGS. 9a - e FOR THE RELATIVE ELECTRON DENSITY DISTRIBUTIONS IN THE EXOSPHERE OVER A WIDE RANGE OF CONDITIONS.

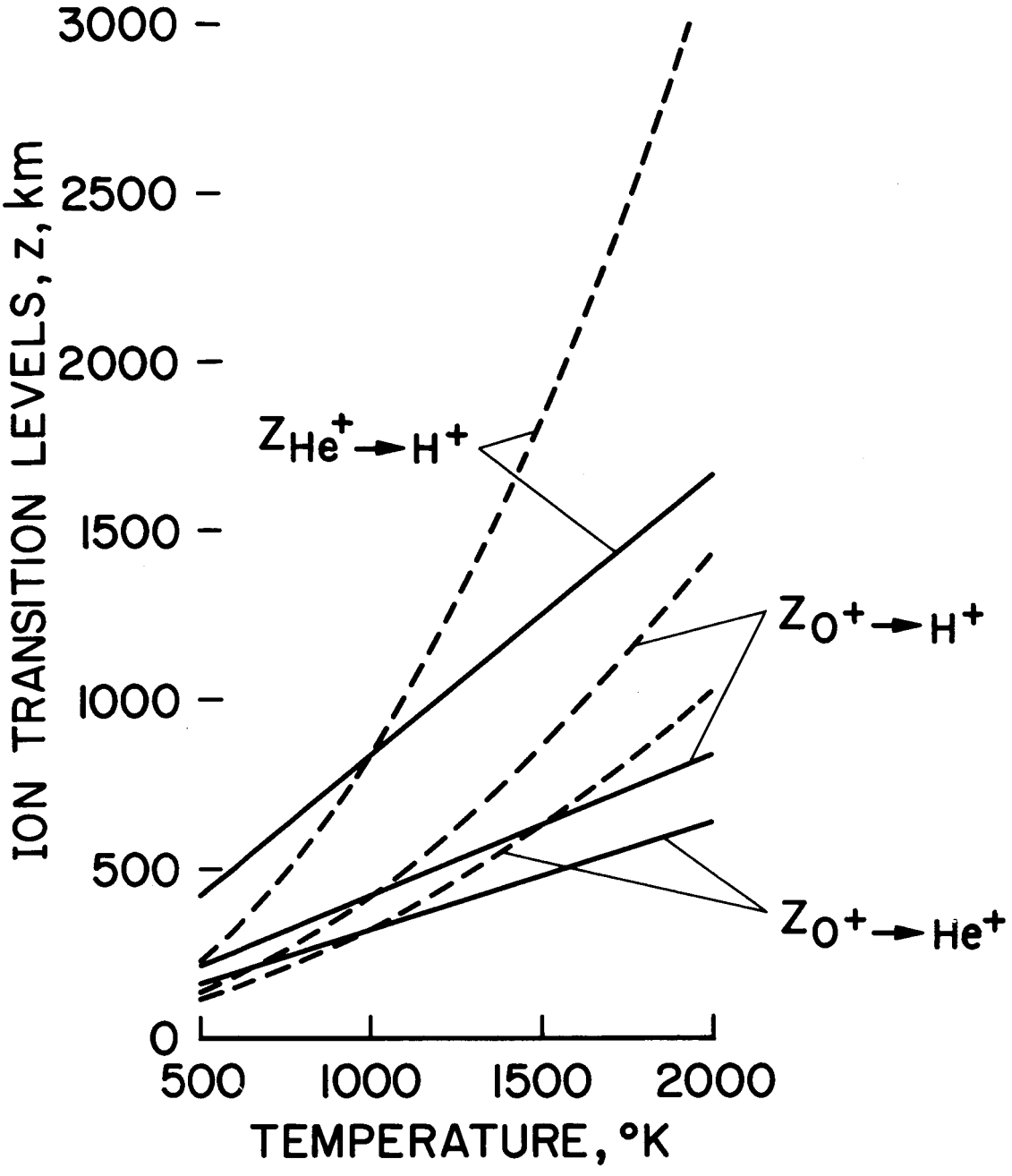

FIG. 11. THE VARIATION WITH TEMPERATURE OF THE LEVELS AT WHICH THE IONS INDICATED HAVE EQUAL ABUNDANCES. The broken lines correspond to the cases when the composition at the base level depends on the temperature there (through equations (65)). The continuous lines correspond to the case when the composition at the base level is independent of temperature (Composition 1). These results are in agreement with those presented earlier by Bauer (1962).

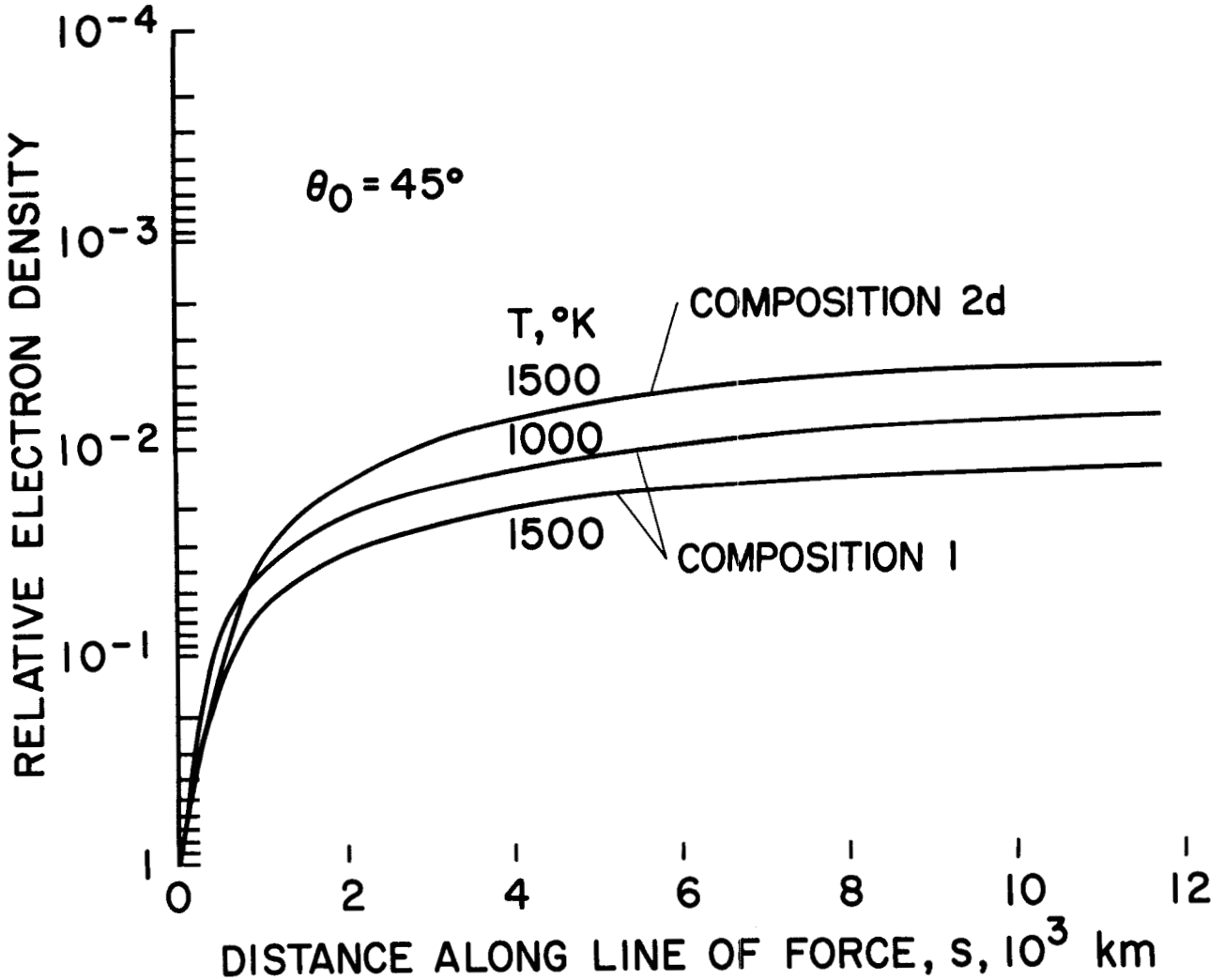

FIG. 12a. TO ILLUSTRATE, FOR AN ISOTHERMAL EXOSPHERE, THE RELATIVE ELECTRON DENSITY DISTRIBUTIONS ALONG A FIELD LINE WITH FEET (AT 500 KM ABOVE THE EARTH) AT GEOMAGNETIC LATITUDE 45° (SEE TABLES 1 AND 2).

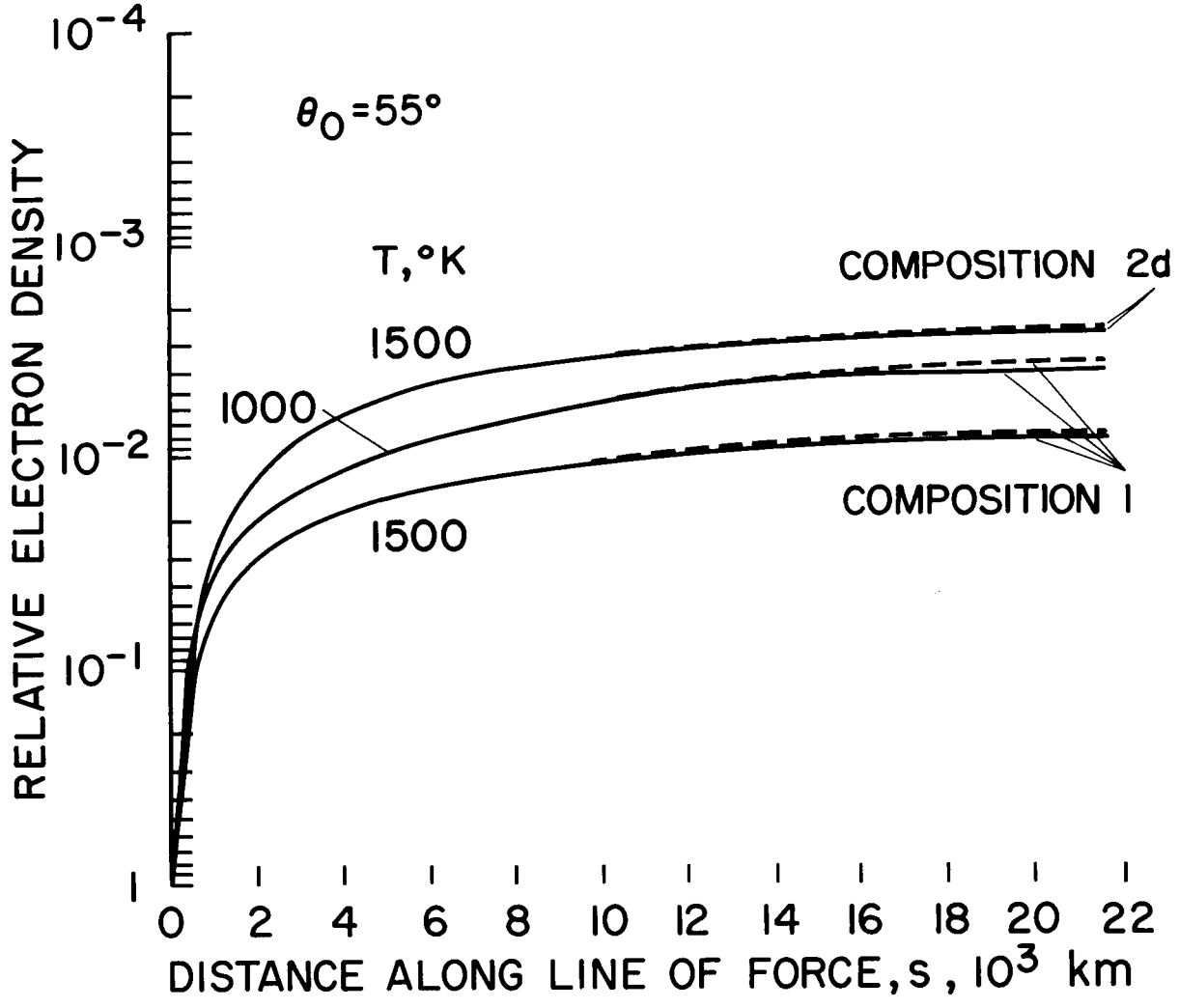

FIG. 12b. TO ILLUSTRATE, FOR AN ISOTHERMAL EXOSPHERE, THE RELATIVE ELECTRON DENSITY DISTRIBUTIONS ALONG A FIELD LINE WITH FEET (AT 500 KM ABOVE THE EARTH) AT GEOMAGNETIC LATITUDE 55° (SEE TABLES 1 AND 2). The broken lines indicate the distributions which would have been obtained if the centrifugal force had been neglected.

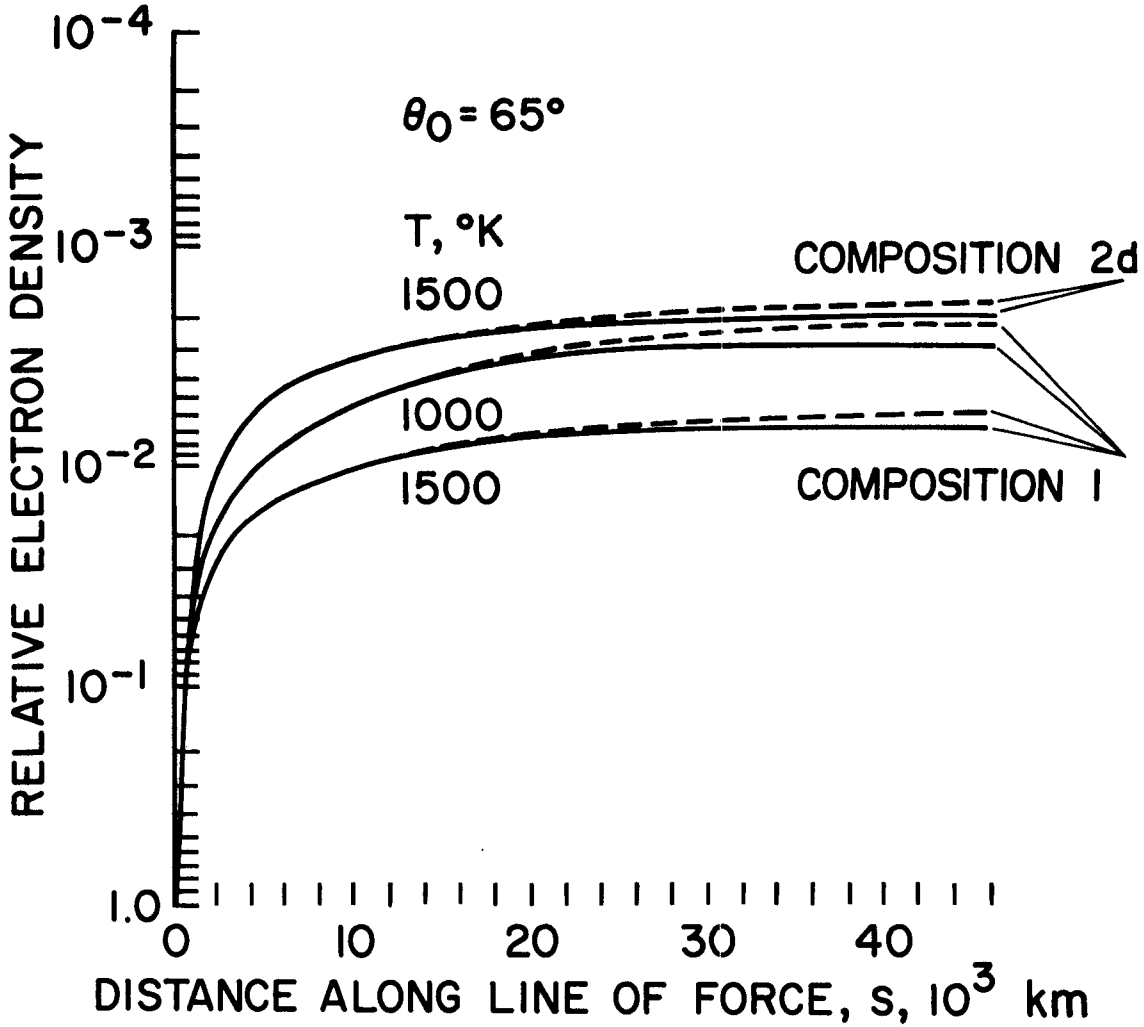

FIG. 12c. TO ILLUSTRATE, FOR AN ISOTHERMAL EXOSPHERE, THE RELATIVE ELECTRON DENSITY DISTRIBUTIONS ALONG A FIELD LINE WITH FEET (AT 500 KM ABOVE THE EARTH) AT GEOMAGNETIC LATITUDE 65° (SEE TABLES 1 AND 2). The broken lines indicate the distribution which would have been obtained if the centrifugal force had been neglected.

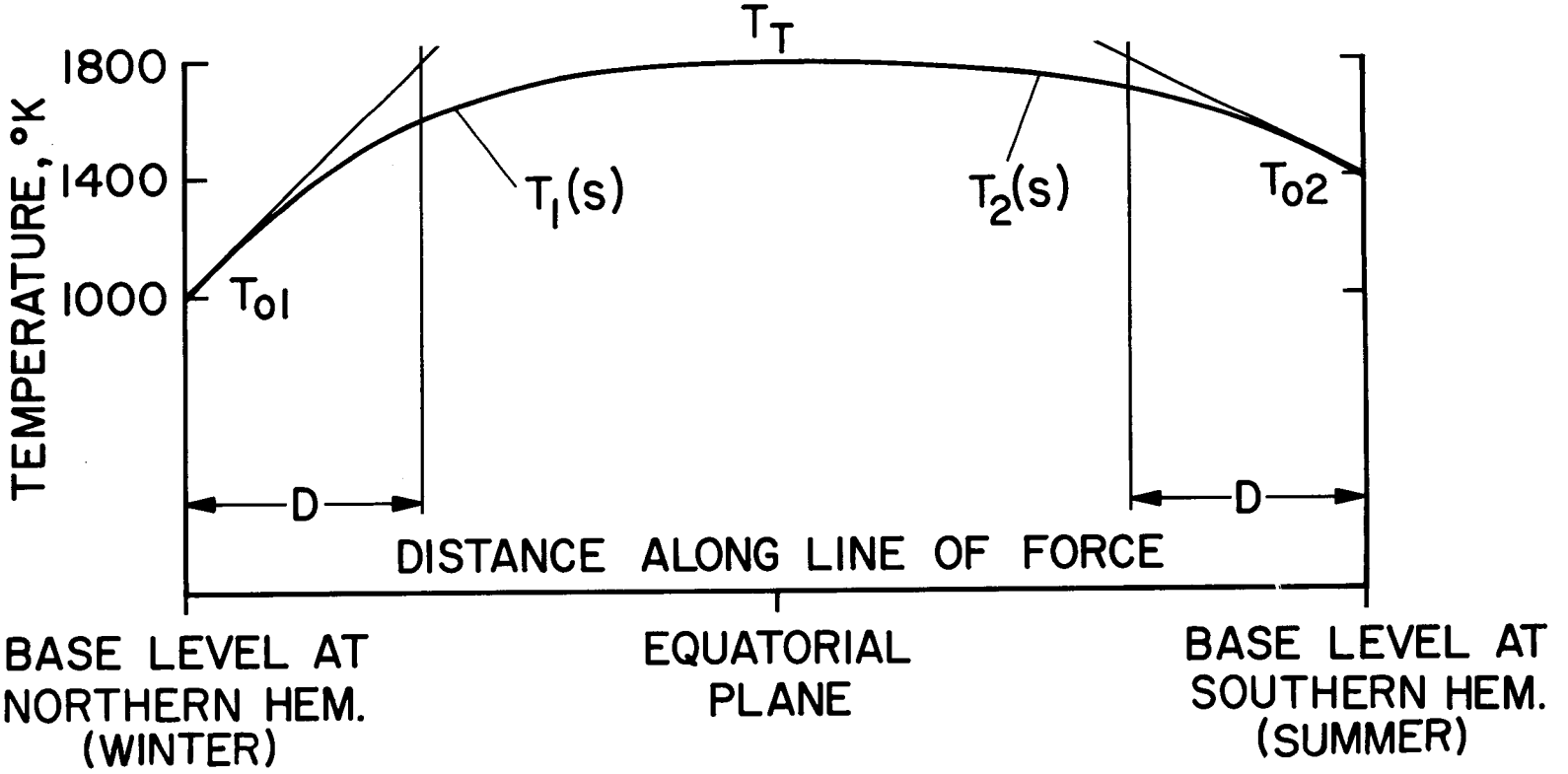

FIG. 13. SCHEMATIC DIAGRAM TO ILLUSTRATE THE VARIATION OF TEMPERATURE ALONG A LINE OF FORCE. T_1 (s) is used for the temperature distributions in the northern (winter) hemisphere and T_2(s) for the southern (summer) hemisphere.

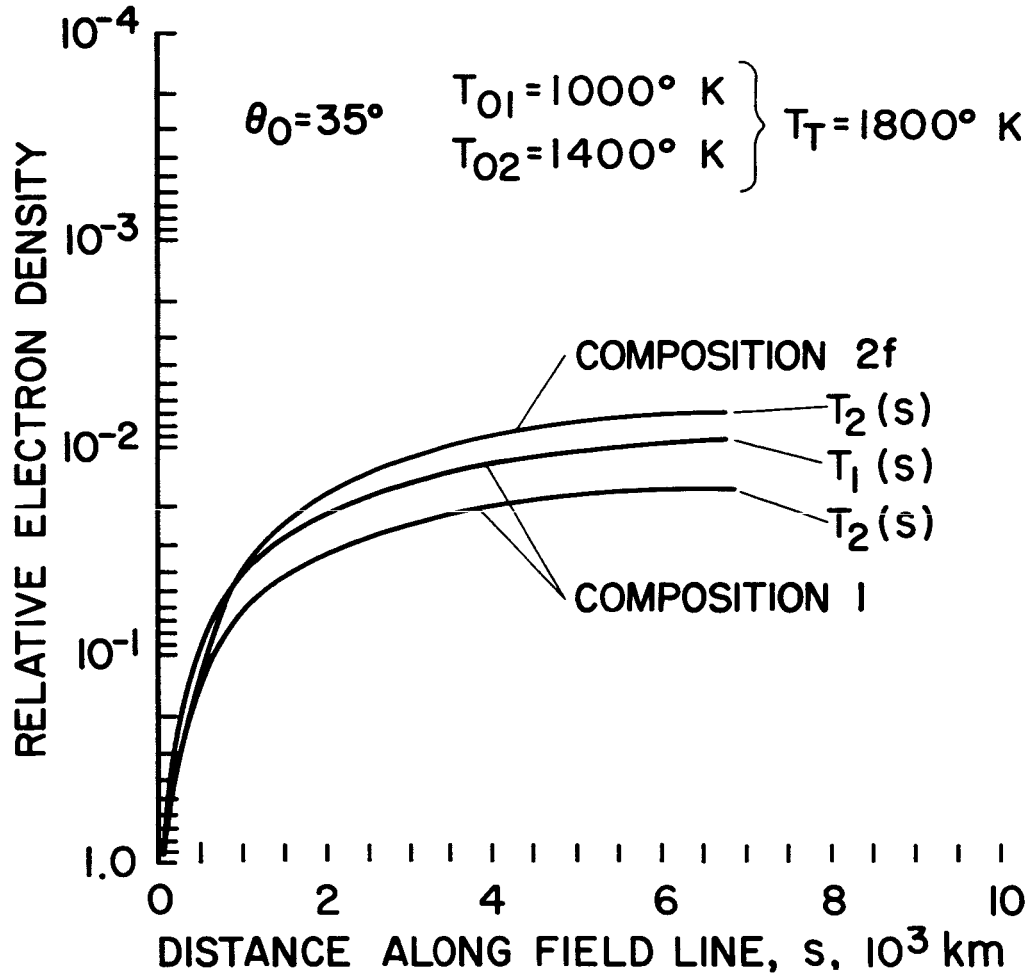

FIG. 14a. TO ILLUSTRATE, FOR A NON-ISOTHERMAL EXOSPHERE (SEE FIG. 13), THE RELATIVE ELECTRON DENSITY DISTRIBUTION ALONG A FIELD LINE WITH FEET (AT 500 KM ABOVE THE EARTH) AT GEOMAGNETIC LATITUDE 35° (SEE TABLES 1 AND 2).

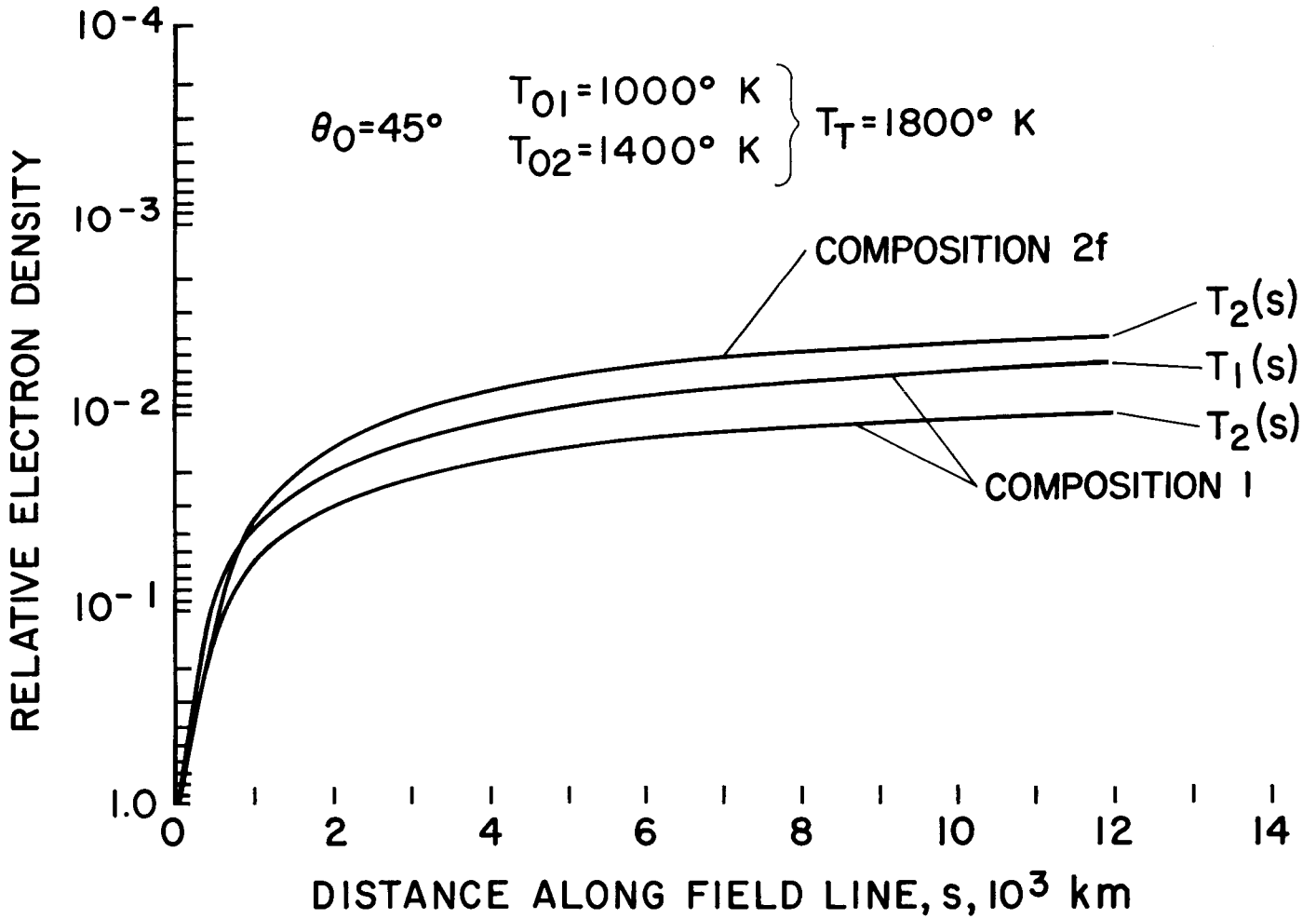

FIG. 14b. TO ILLUSTRATE, FOR A NON-ISOTHERMAL EXOSPHERE (SEE FIG. 13), THE RELATIVE ELECTRON DENSITY DISTRIBUTION ALONG A FIELD LINE WITH FEET (AT 500 KM ABOVE THE EARTH) AT GEOMAGNETIC LATITUDE 45° (SEE TABLES 1 AND 2).

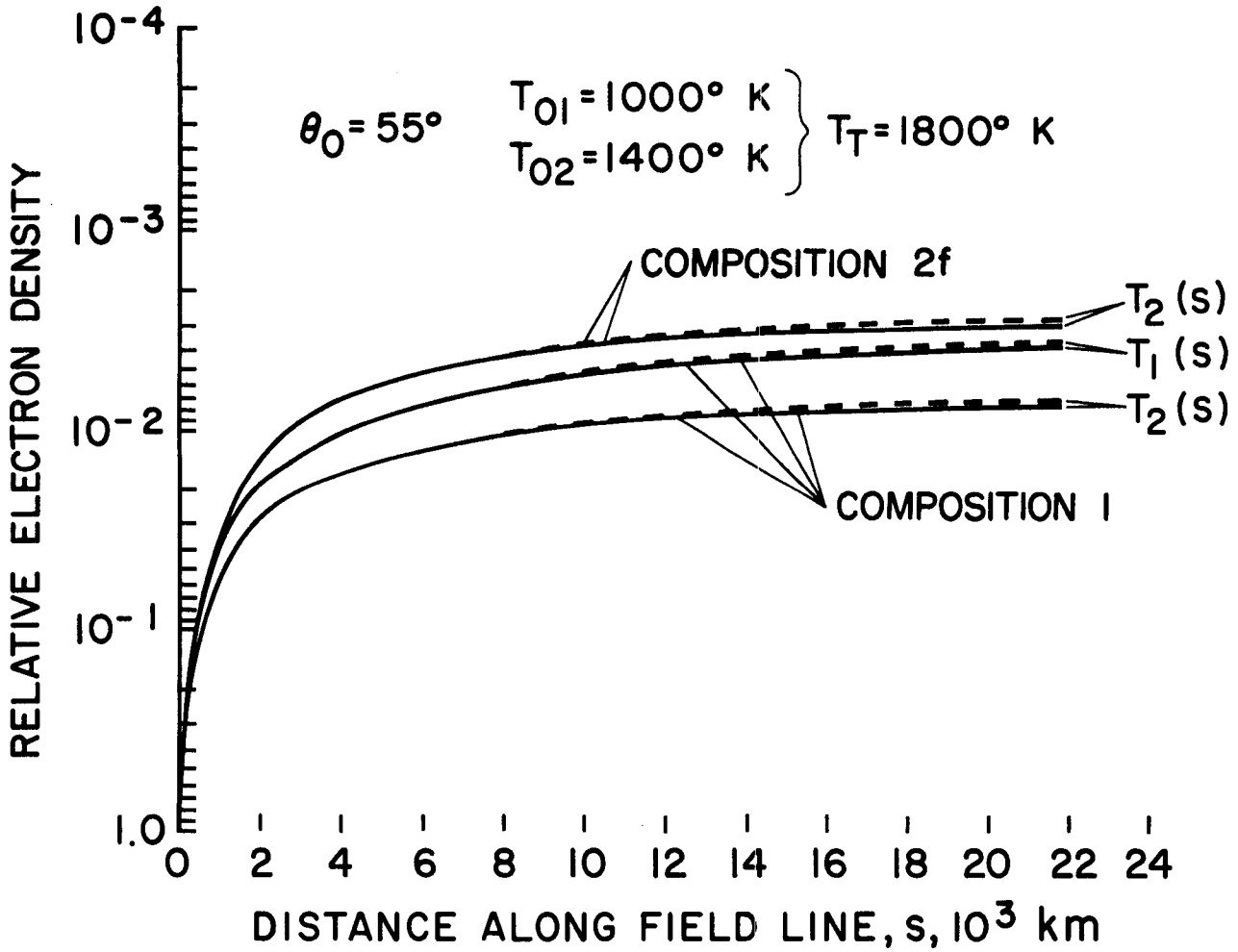

FIG. 14c. TO ILLUSTRATE, FOR A NON-ISOTHERMAL EXOSPHERE (SEE FIG. 13), THE RELATIVE ELECTRON DENSITY DISTRIBUTION ALONG A FIELD LINE WITH FEET (AT 500 KM ABOVE THE EARTH) AT GEOMAGNETIC LATITUDE 55° (SEE TABLES 1 AND 2). The broken lines indicate the distributions which would have been obtained if the centrifugal force had been neglected.

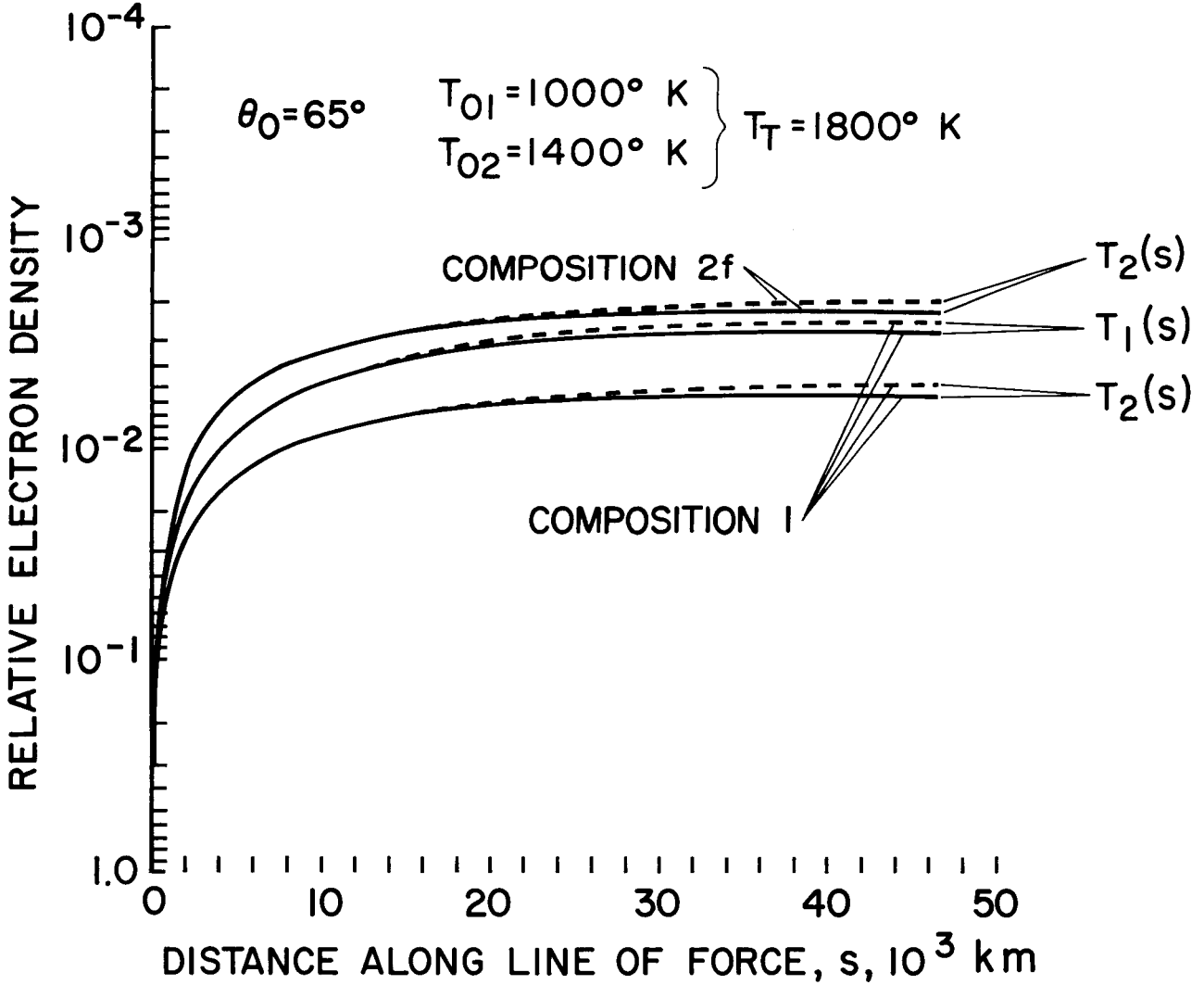

FIG. 14d. TO ILLUSTRATE, FOR A NON-ISOTHERMAL EXOSPHERE (SEE FIG. 13), THE RELATIVE ELECTRON DENSITY DISTRIBUTION ALONG A FIELD LINE WITH FEET (AT 500 KM ABOVE THE EARTH) AT GEOMAGNETIC LATITUDE 65° (SEE TABLES 1 AND 2). The broken lines indicate the distributions which would have been obtained if the centrifugal force had been neglected.

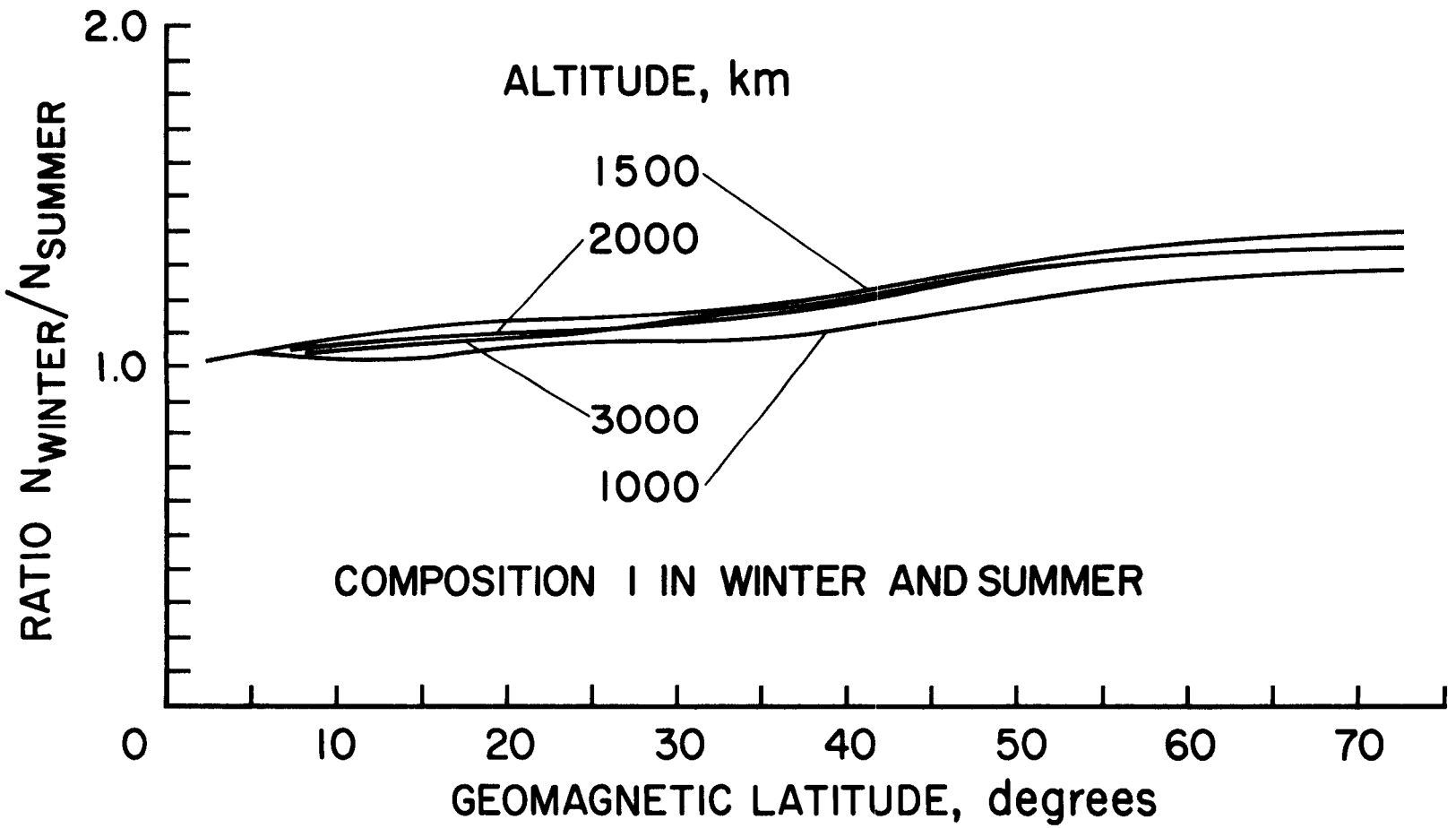

FIG. 15a. THE PREDICTED RATIO OF THE ELECTRON DENSITY IN WINTER TO THAT AT THE SAME LOCATION AND ALTITUDE IN SUMMER FOR A NUMBER OF DIFFERENT ALTITUDES. Composition 1 (See Table 1) is used at 500 km, as was done previously. The assumed temperature distribution is illustrated in Fig. 13.

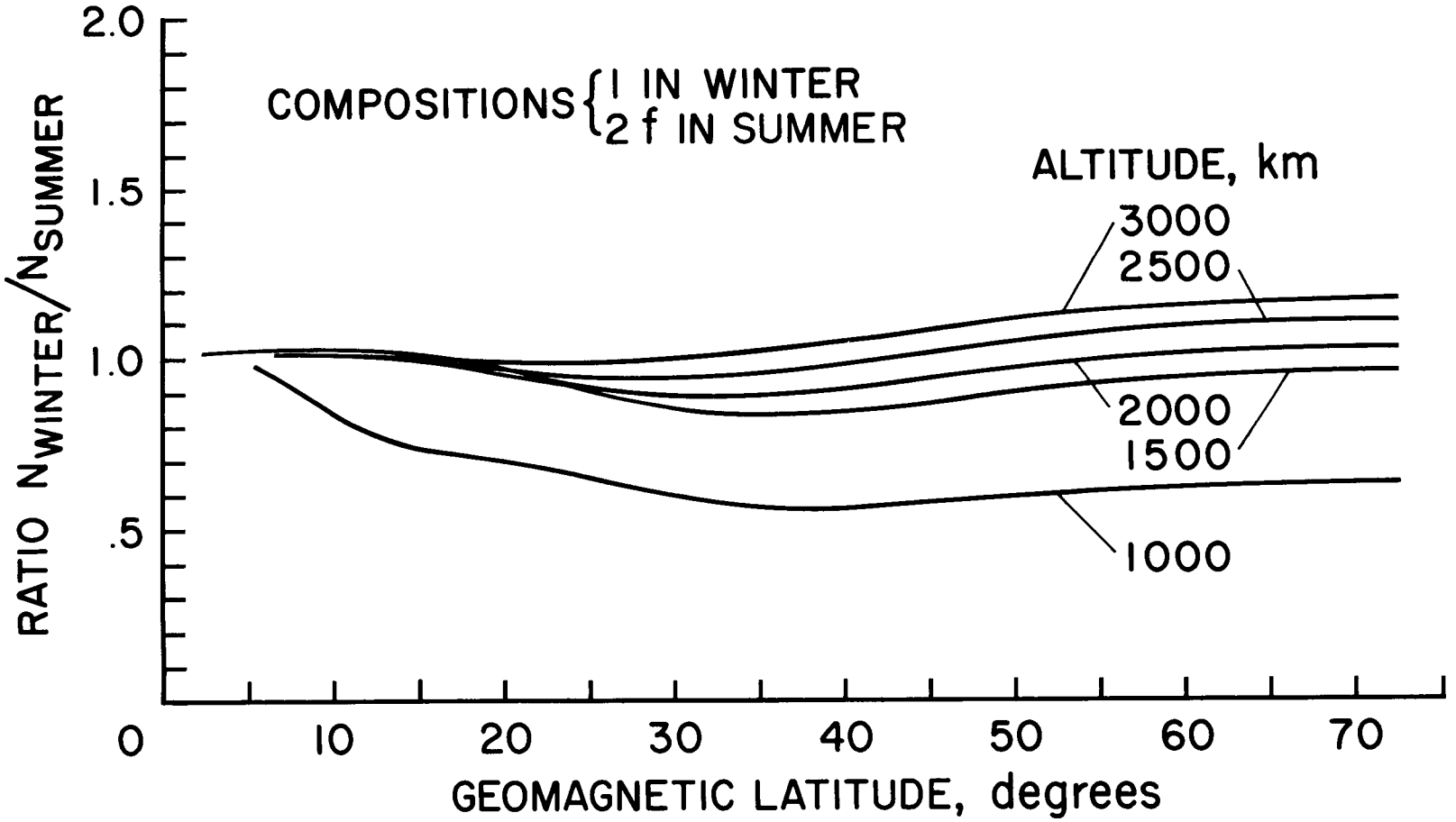

FIG. 15b. THE PREDICTED RATIO OF THE ELECTRON DENSITY IN WINTER TO THAT AT THE SAME LOCATION AND ALTITUDE IN SUMMER FOR A NUMBER OF DIFFERENT ALTITUDES. Compositions 1 and 2f (See Table 1) are used at 500 km, as was done previously. The assumed temperature distribution is illustrated in Fig. 13.

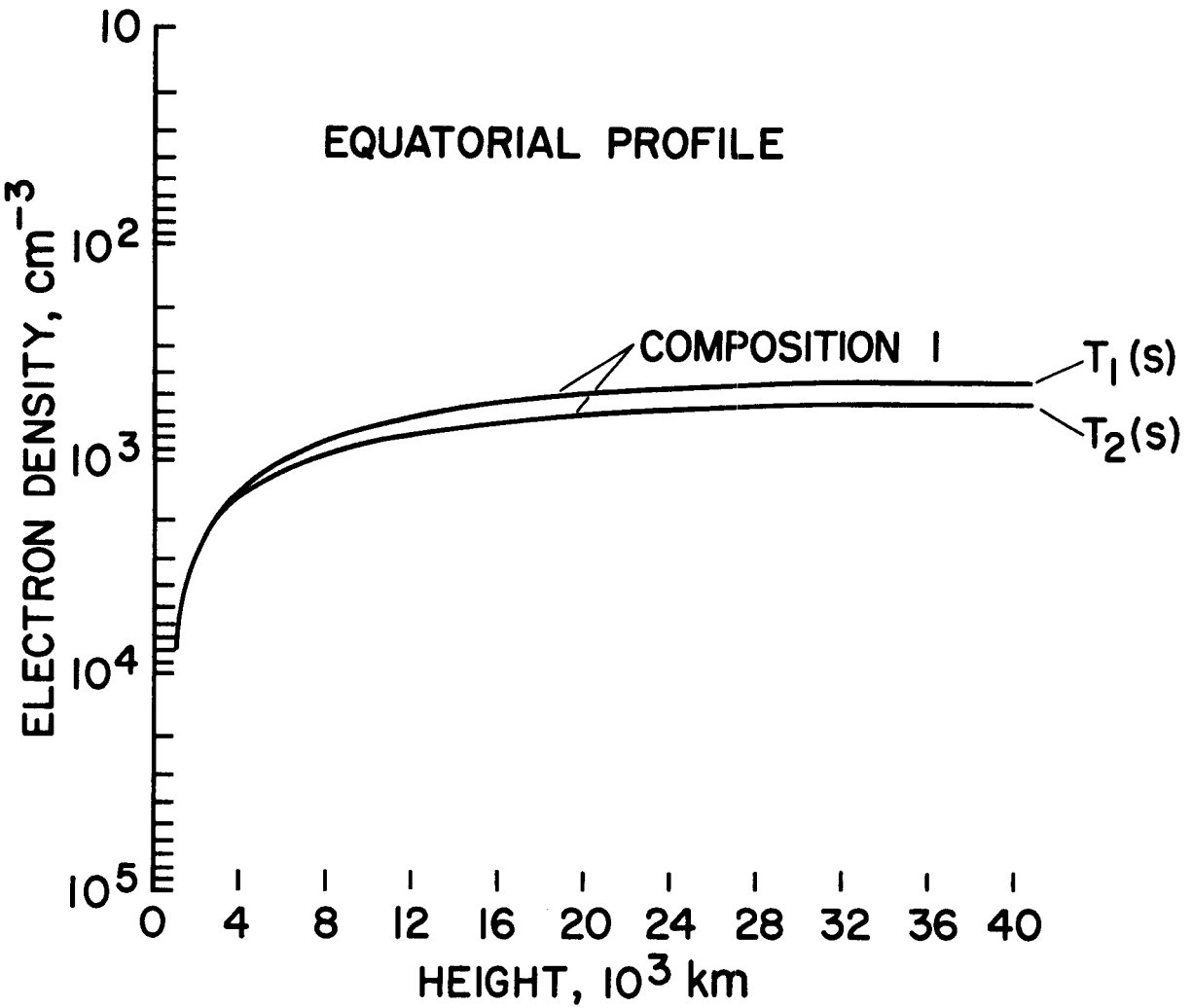

FIG. 16a. EQUATORIAL N(h) PROFILE. The electron density at 1000 km was assumed to be 10^4/cc (See Tables 1 and 2). The temperature distributions along a field line are given by equation (66) and are illustrated schematically in Fig. 13.

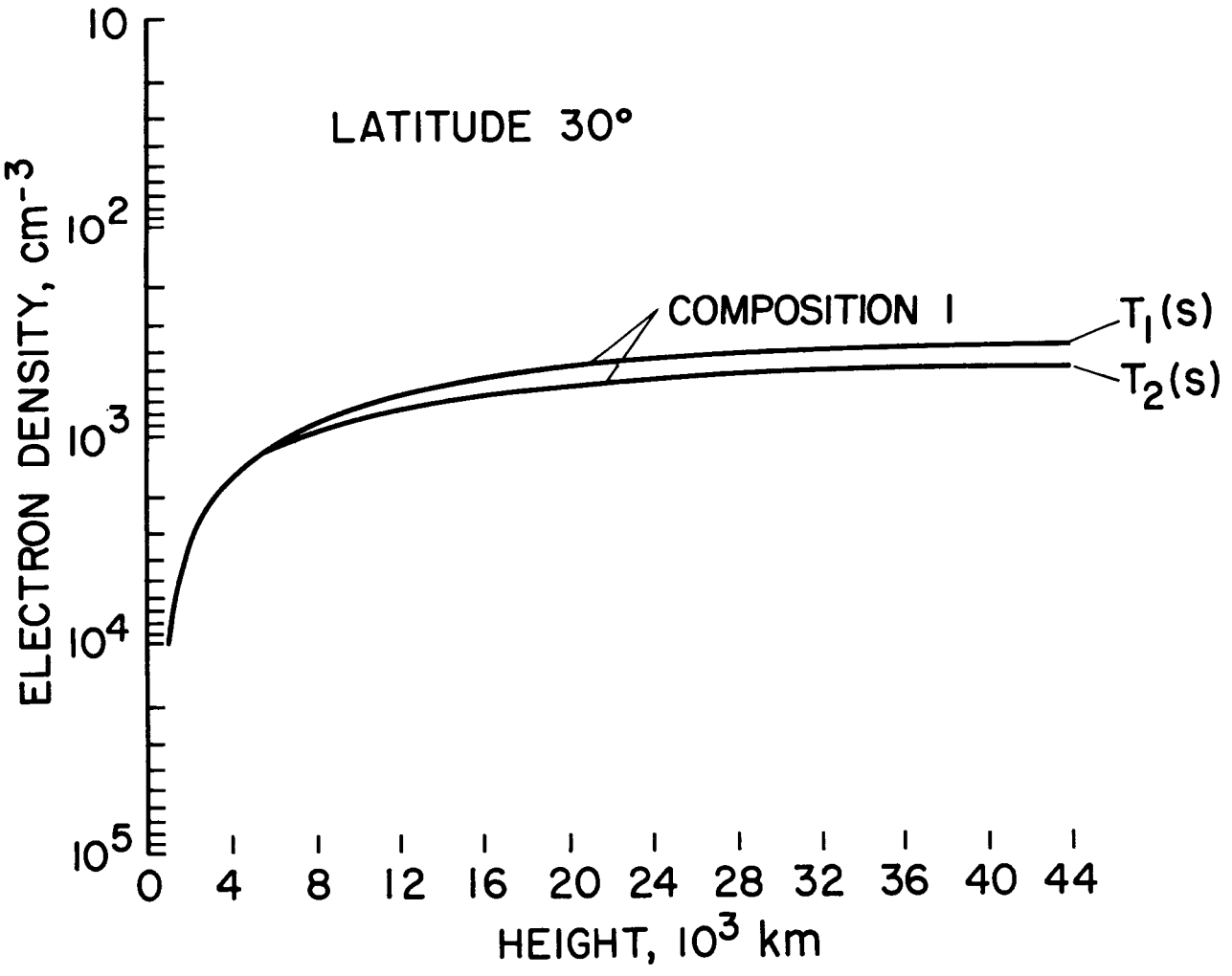

FIG. 16b. N(h) PROFILE AT GEOMAGNETIC LATITUDE 30°. The electron density at 1000 km was assumed to be 10^4/cc (See Tables 1 and 2). The temperature distributions along a field line are given by equation (66) and are illustrated schematically in Fig. 13.

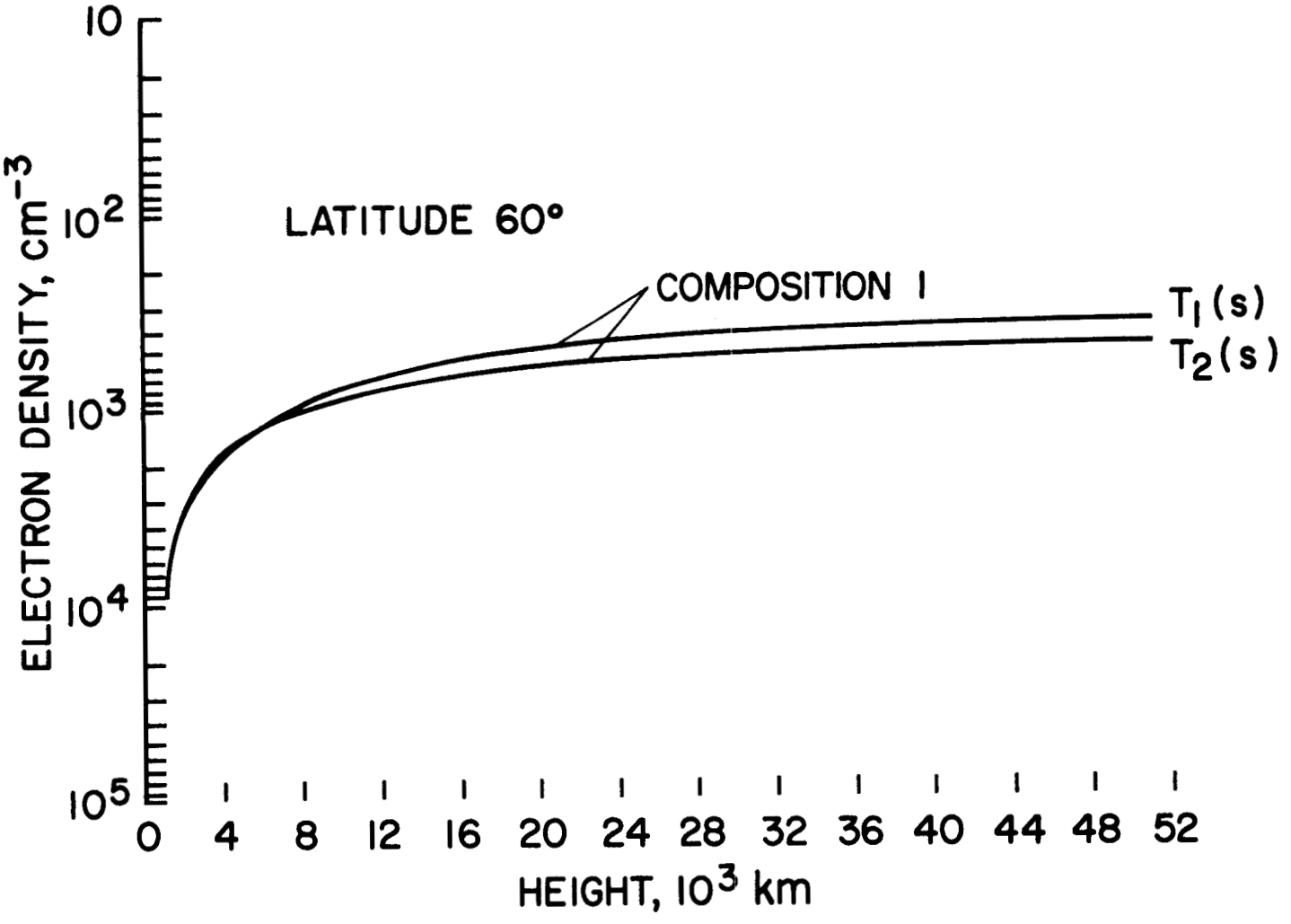

FIG. 16c. N(h) PROFILE AT GEOMAGNETIC LATITUDE 60°. The electron density at 1000 km was assumed to be 10^4/cc (See Tables 1 and 2). The temperature distributions along a field line are given by equation (66) and are illustrated schematically in Fig. 13.

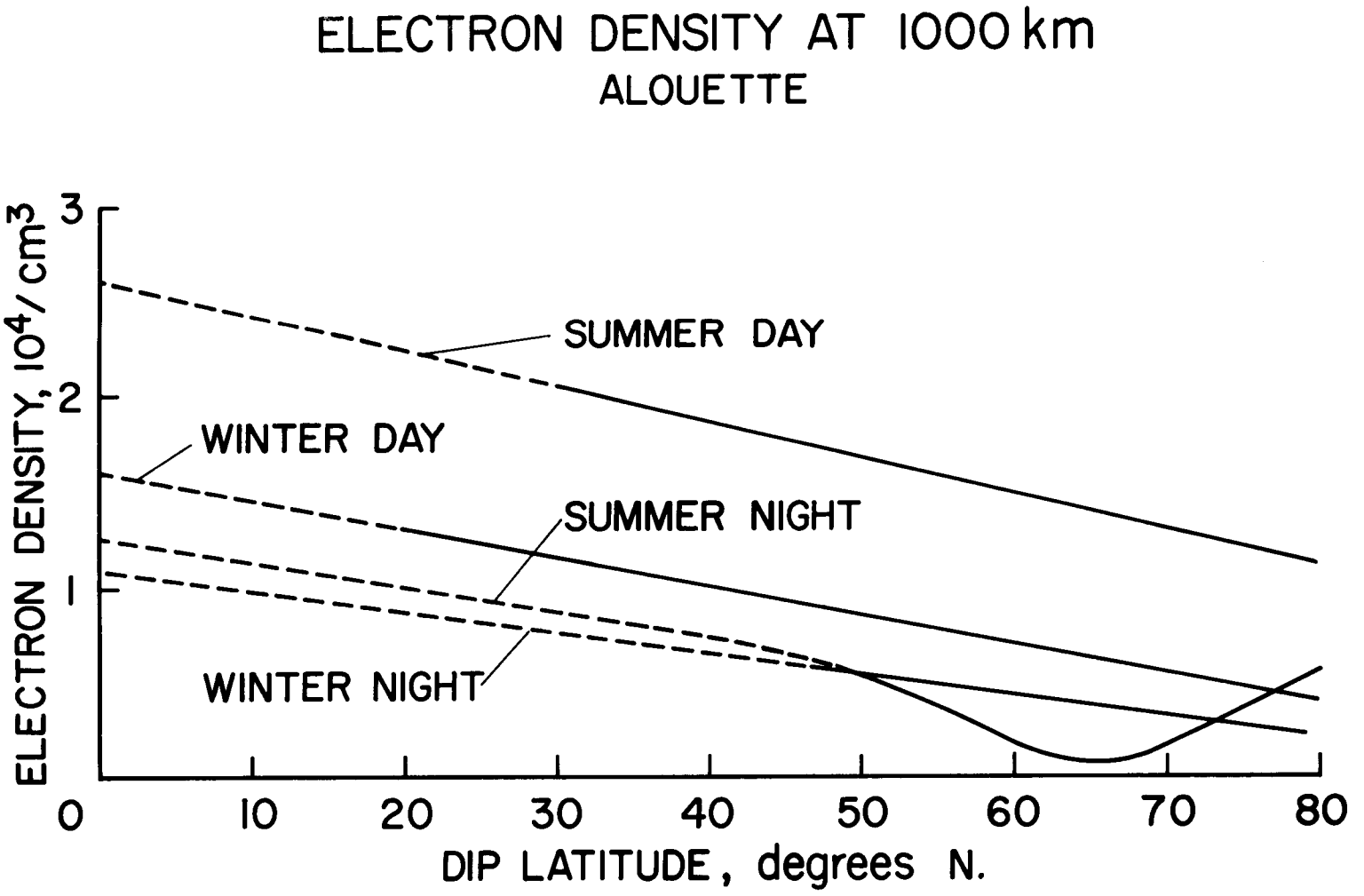

FIG. 17. THE AVERAGE QUIET DAY ELECTRON DENSITY AT 1000 KM (BASED ON THE RESULTS OF THOMAS AND SADER 1963). The continuous lines are observed values and the broken lines are extrapolations which are roughly consistent with equatorial Alouette data.

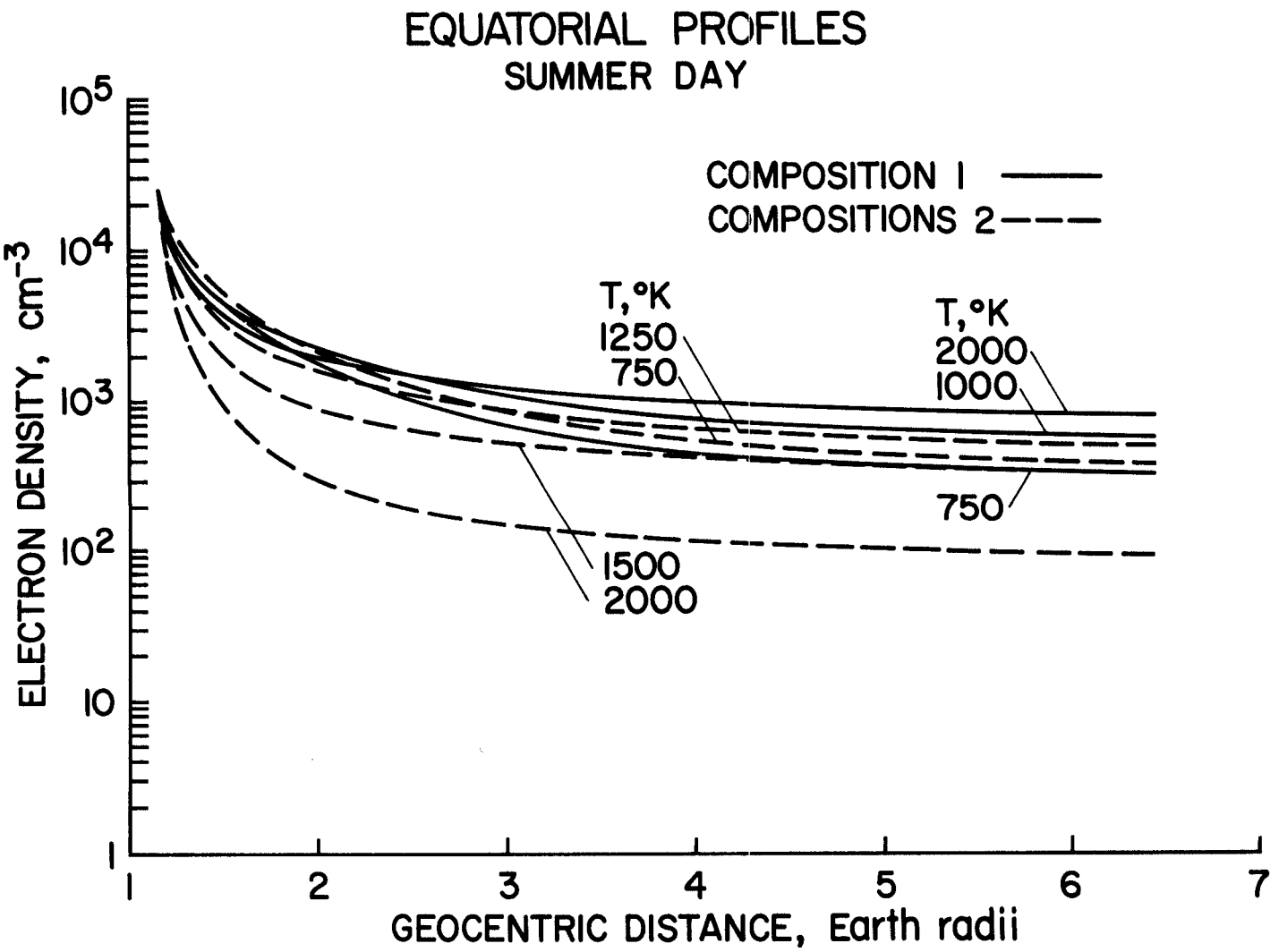

FIG. 18a. THEORETICALLY PREDICTED EQUATORIAL N(h) PROFILES BASED ON OBSERVED ALOUETTE DATA FOR THE ELECTRON DENSITY AT 1000 KM FOR SUMMER DAYS. Curves for a wide variety of isothermal exospheric temperatures and compositions are illustrated (See Tables 1 and 2).

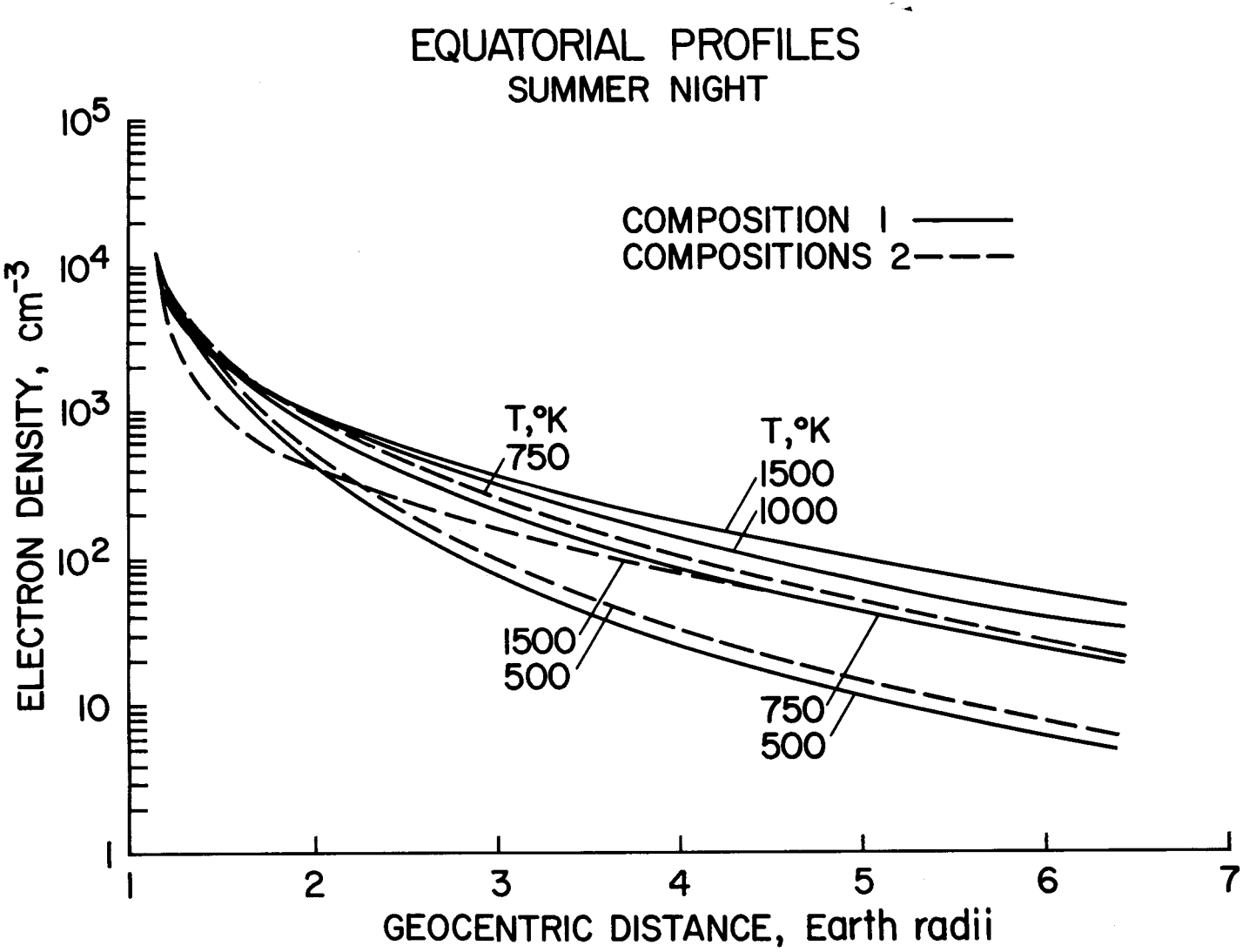

FIG. 18b. THEORETICALLY PREDICTED EQUATORIAL N(h) PROFILES BASED ON OBSERVED ALOUETTE DATA FOR THE ELECTRON DENSITY AT 1000 KM FOR SUMMER NIGHTS. Curves for a wide variety of isothermal exospheric temperatures and compositions are illustrated (See Tables 1 and 2). Note the marked increase in the rate of fall off of electron density with height at great distances from the earth.

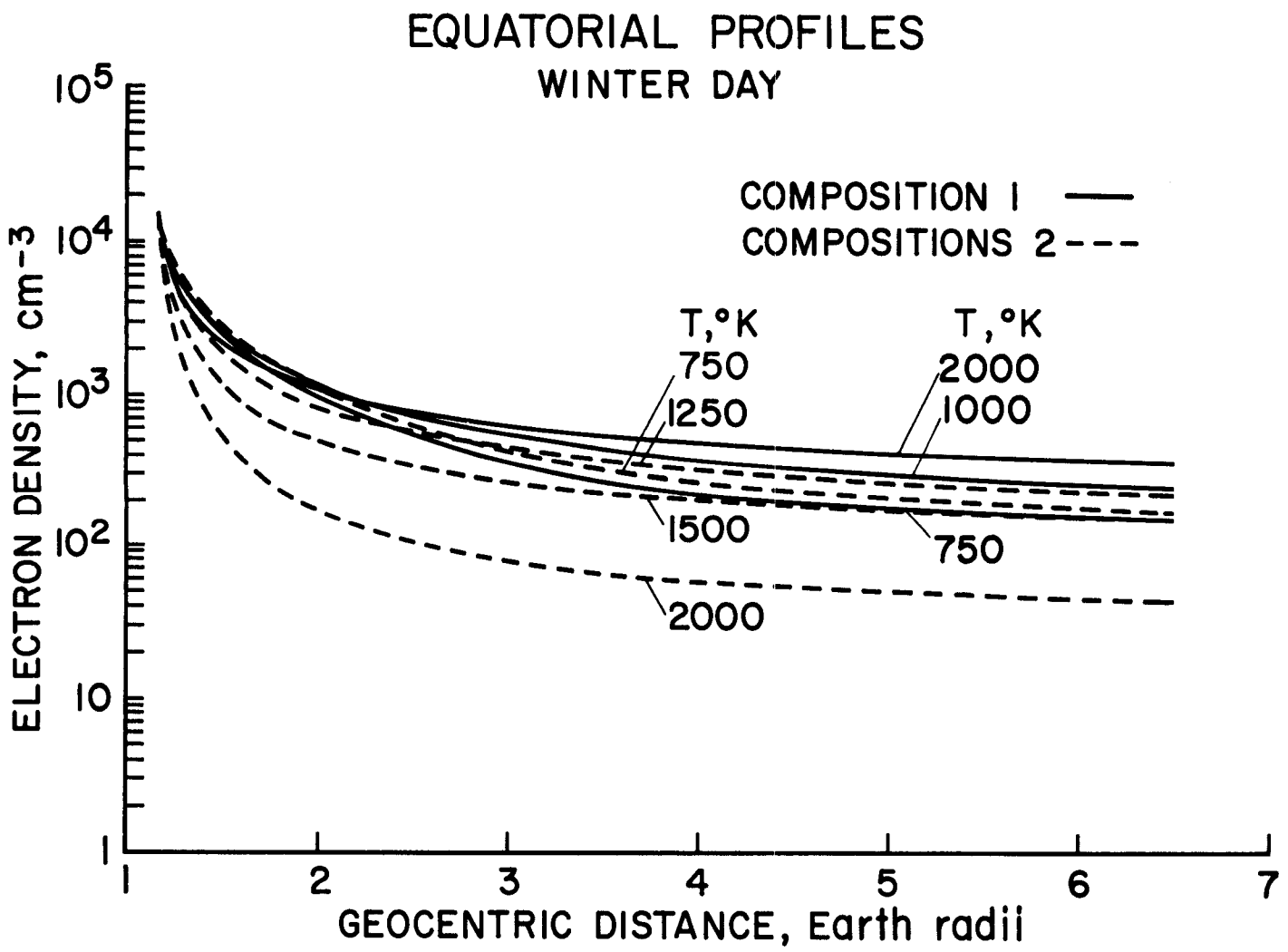

FIG. 18c. THEORETICALLY PREDICTED EQUATORIAL N(h) PROFILES BASED ON OBSERVED ALOUETTE DATA FOR THE ELECTRON DENSITY AT 1000 KM FOR WINTER DAYS. Curves for a wide variety of isothermal exospheric temperatures and compositions are illustrated (See Tables 1 and 2).

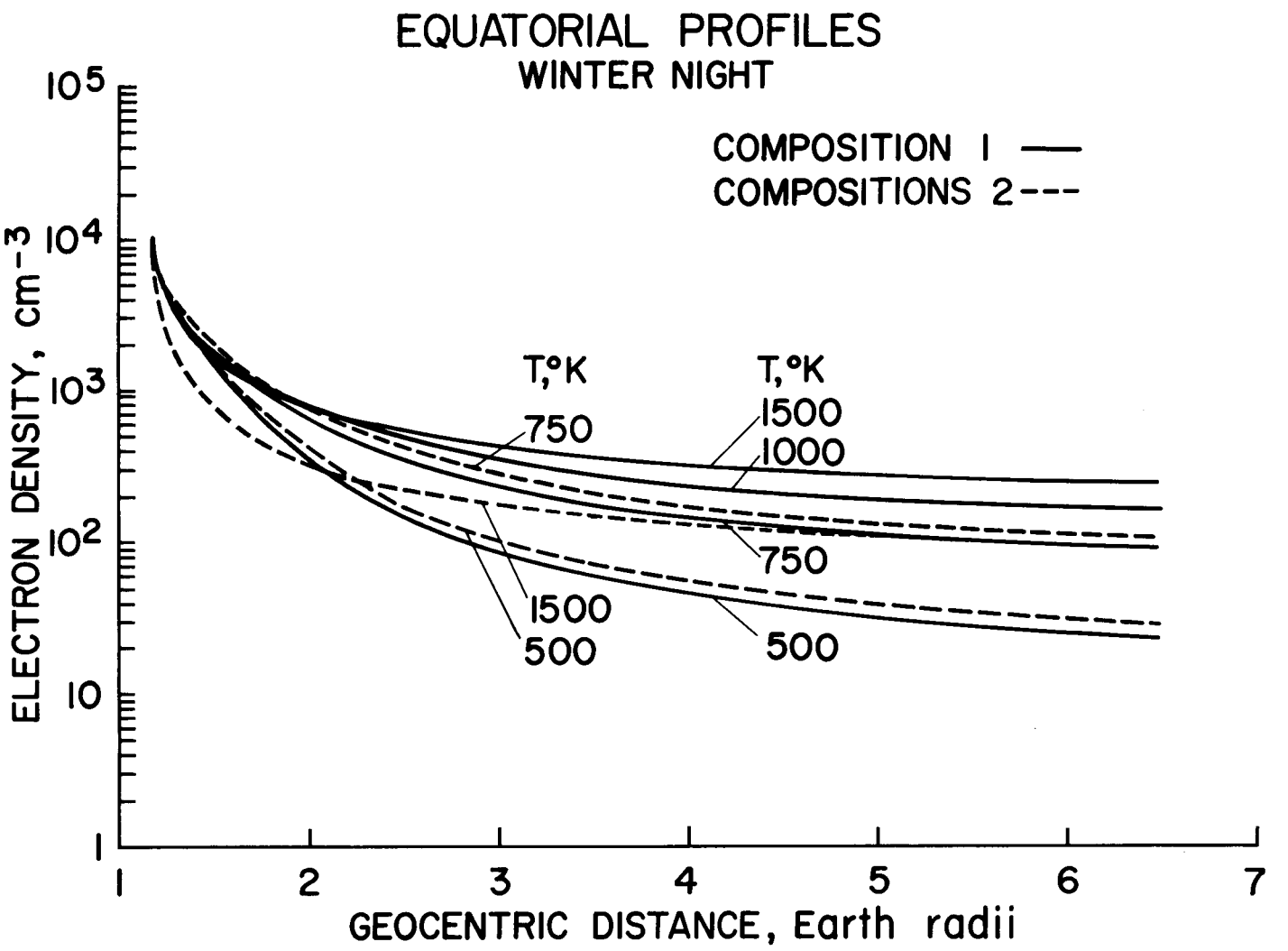

FIG. 18d. THEORETICALLY PREDICTED EQUATORIAL N(h) PROFILES BASED ON OBSERVED ALOUETTE DATA FOR THE ELECTRON DENSITY AT 1000 KM FOR WINTER NIGHTS. Curves for a wide variety of isothermal exospheric temperatures and compositions are illustrated (See Tables 1 and 2).

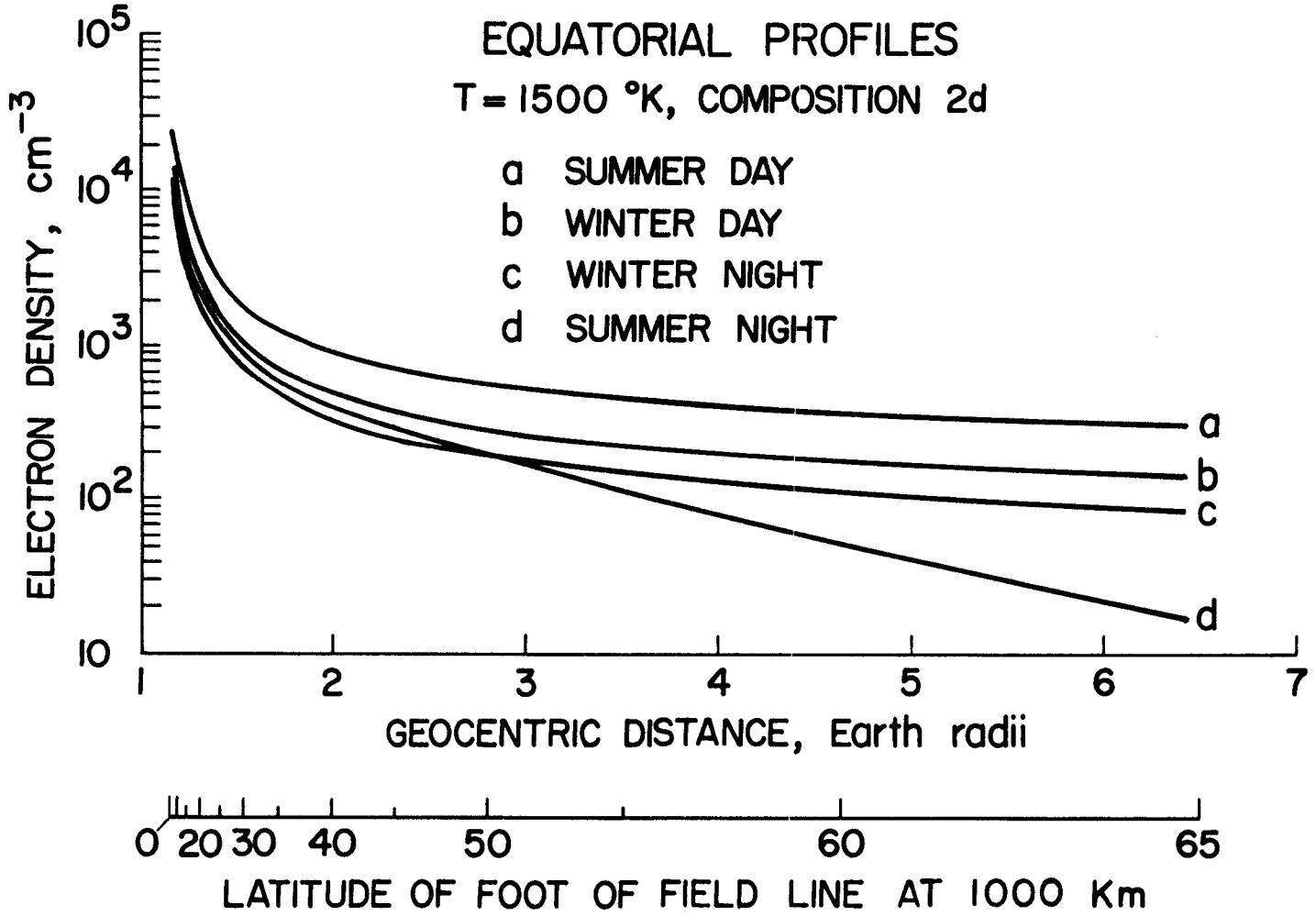

FIG. 18e. SUMMARY OF THE RESULTS OF FIGS. 18a - d. The curves shown are the predicted theoretical N(h) distributions.

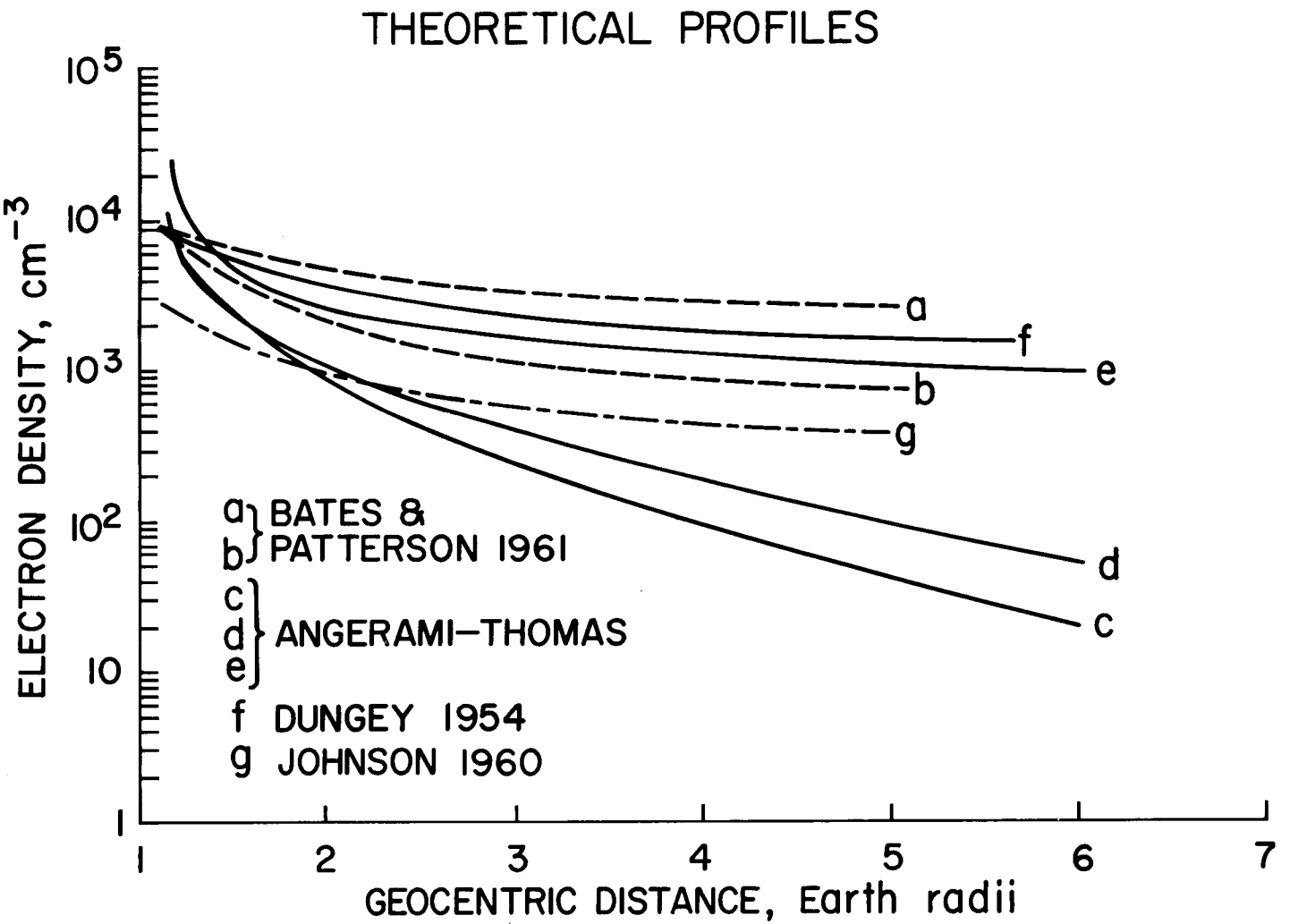

FIG. 19a. THEORETICAL N(h) PROFILES PREDICTED BY A NUMBER OF WORKERS. The temperatures for curves a - e are 2000, 1000, 750, 1500, 1500 °K respectively. Composition 1 (Table 1) has been used for curves c, d and e. Curves c and d are based on Alouette data for summer nights and curve e for Alouette data for summer days. Note that the slopes of curves c, d and e are substantially different from the others near 1000 km. Also, the slopes of curves c and d at great distances from the earth are different from the others.

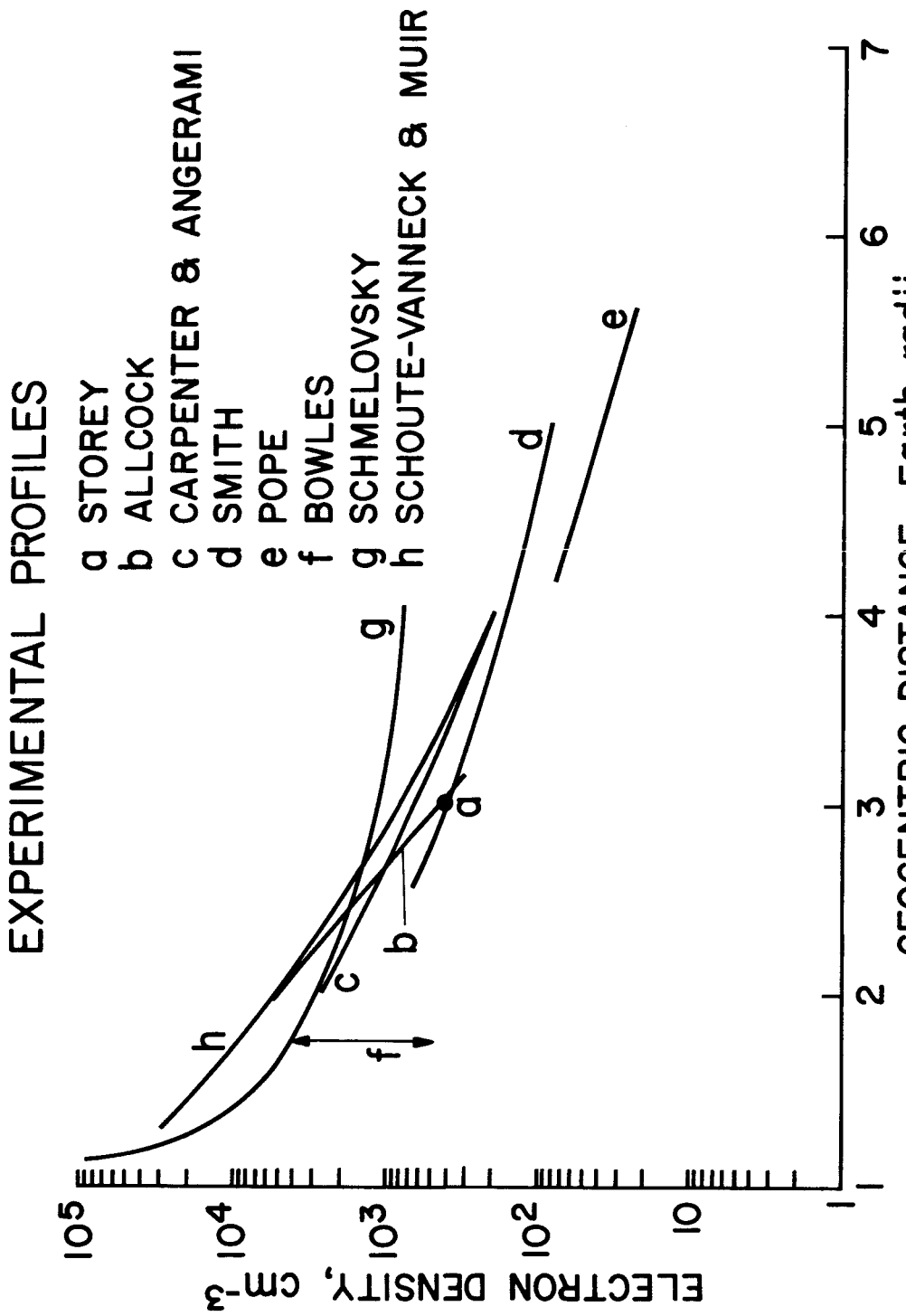

FIG. 19b. EXAMPLES OF EXPERIMENTAL OBSERVATIONS OF EXOSPHERIC ELECTRON DENSITY (EQUATORIAL PROFILES).

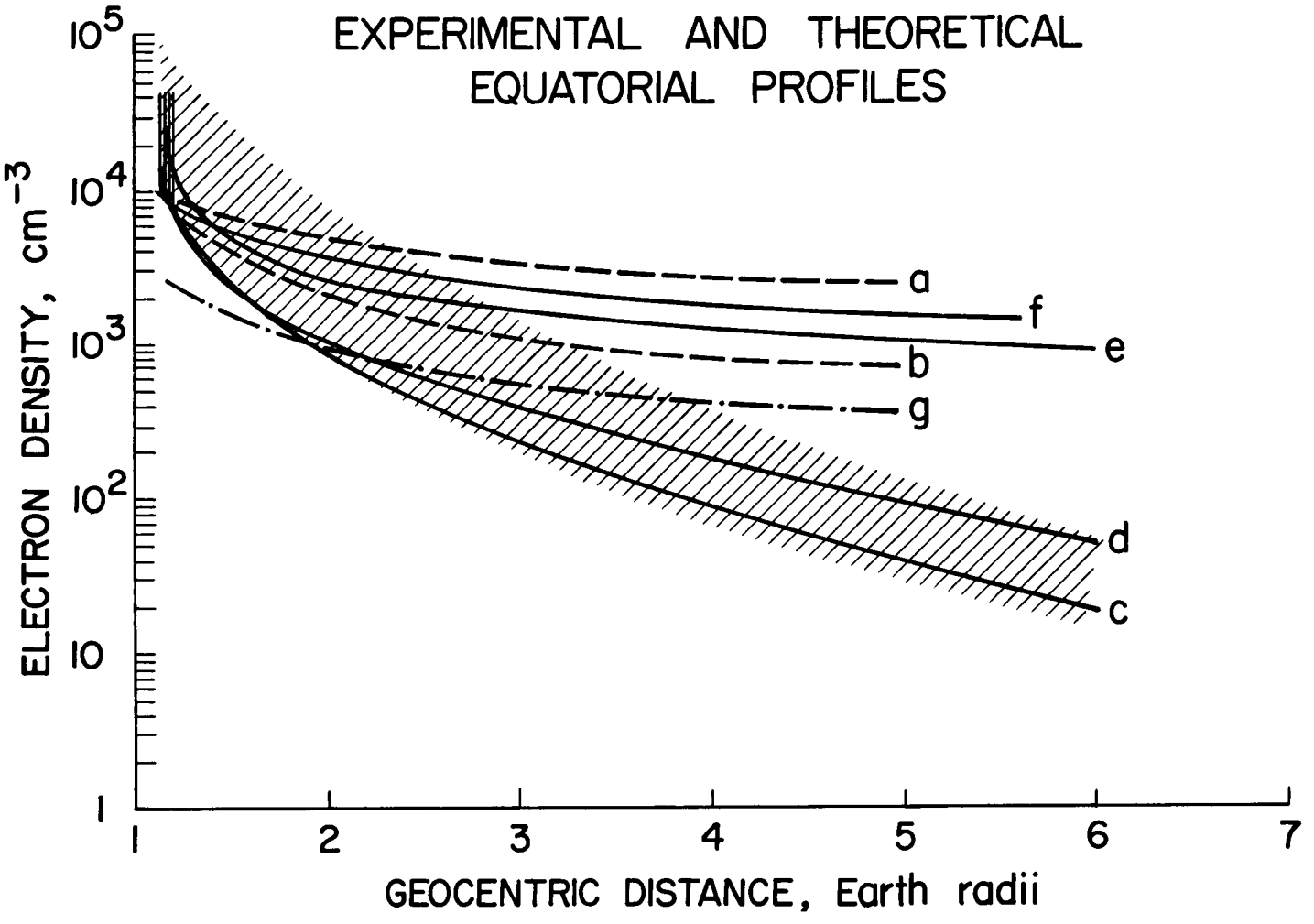

FIG. 20. COMPARISON OF EXPERIMENTAL AND THEORETICAL EXOSPHERIC N(h) PROFILES IN THE EQUATORIAL PLANE. The curves a - g are those described in Fig. 19a. The diagonally shaded area defines approximately the region within which the experimental profiles of Fig. 19b are observed to lie. The vertical shading near 1000 km indicates the approximate region in which the Alouette observations for 1000 km lie.

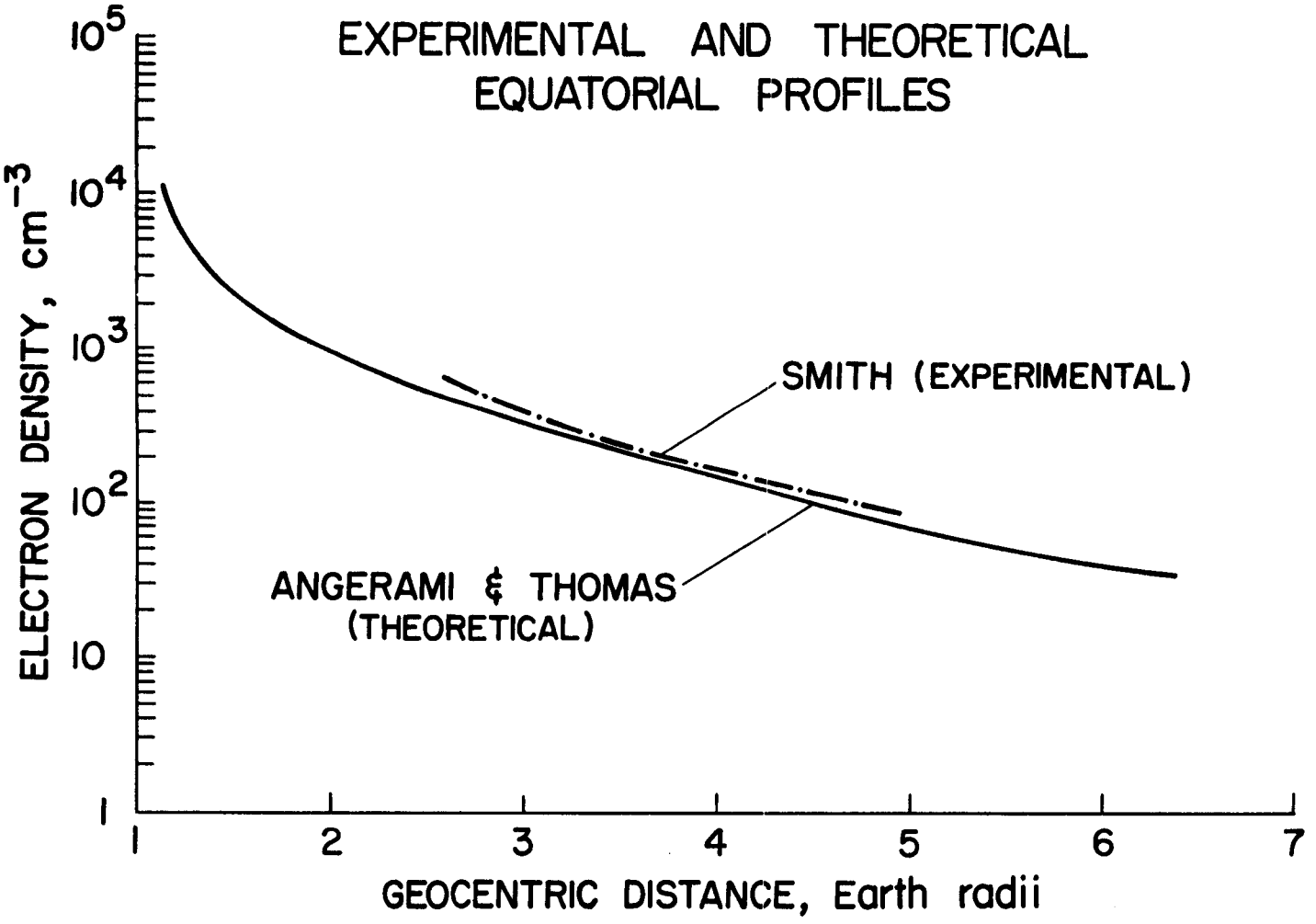

FIG. 21. COMPARISON OF THEORY AND EXPERIMENT. The theoretical curve was computed assuming a constant exospheric temperature of 1000 °K and ionic Composition 1 (Table 1) at the base level. The electron density at 1000 km was taken to be that given by Alouette for summer night conditions (Fig. 17).

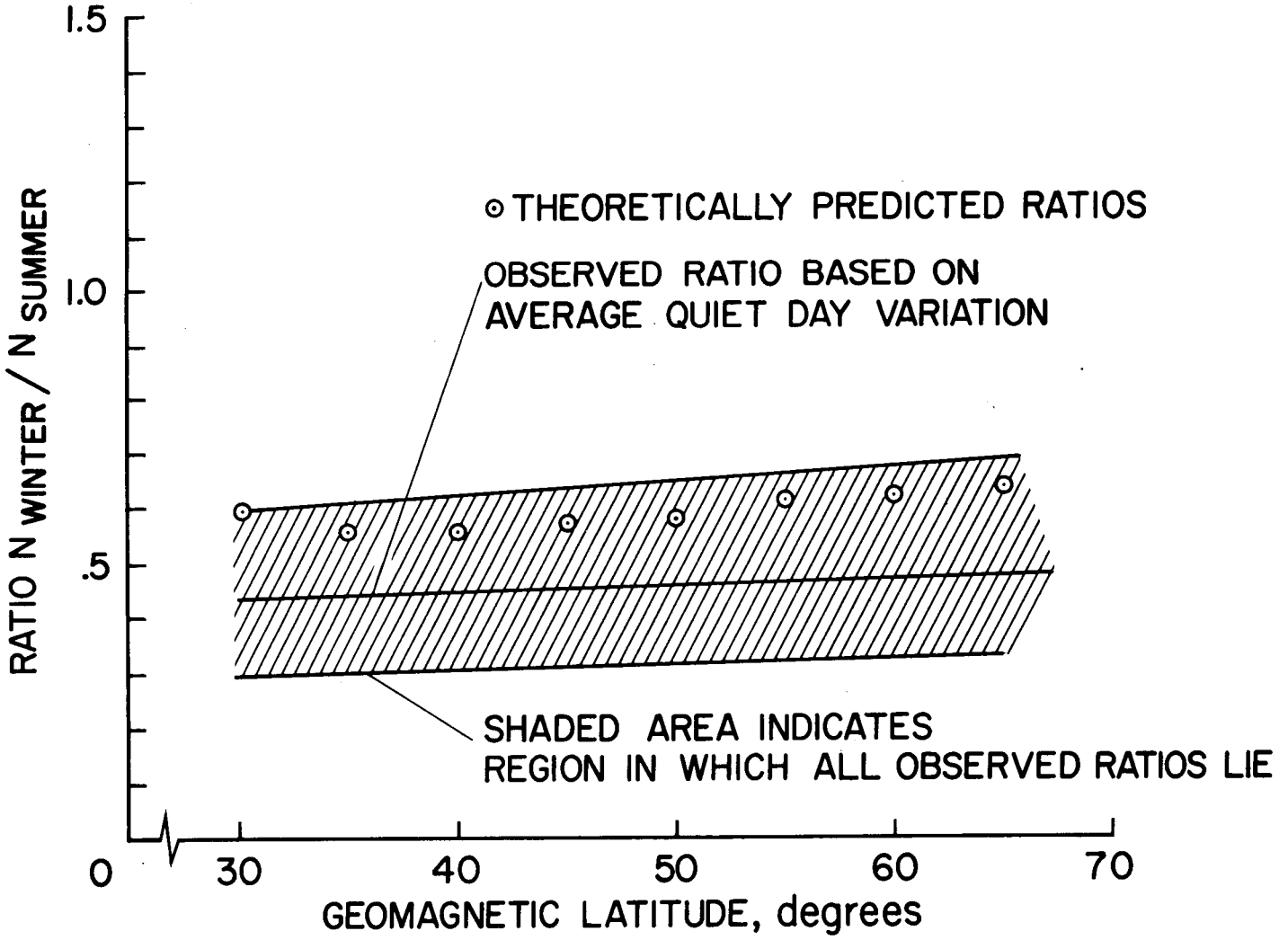

FIG. 22. OBSERVED AND PREDICTED RATIOS OF THE ELECTRON DENSITY AT 1000 KM AT CONJUGATE POINTS IN THE WINTER AND SUMMER HEMISPHERES. The middle line giving the observed average quiet day ratios is based on summer and winter Alouette observations at Stanford. The ratio is approximately 0.5 over the latitude range considered. The theoretically predicted ratios are in reasonably good agreement.